Stimuli-Responsive Microgel-Based Materials and Their Assembly for Controlled Drug
Delivery and Sensing Systems

by

Yingnan Zhang

A thesis submitted in partial fulfillment of the requirements for the degree of

Doctor of Philosophy

Department of Chemistry
University of Alberta

Abstract

Conventional drug delivery methods result in a burst of drug concentration in plasma, followed by a decline, which leads to issues with maintaining drug concentrations in the therapeutic range. Furthermore, this high plasma concentration can lead to undesirable (and dangerous) side effects that minimizes patient compliance with such treatments. As a result, novel controlled drug delivery systems are being developed that can maintain the drug within the desired therapeutic range for longer times with a single dose, leading to enhanced clinical outcomes. Drug delivery systems that respond to endogenous or exogenous cues inherently present in living systems, provides possibilities to develop novel drug delivery and tissue engineering strategies. This thesis covers the general scope of stimuli-responsive polymers on a basis of temperature-responsive poly (*N*-isopropylacrylamide) (pNIPAm) microgels, their co-functional polymers, their assemblies and their applications in controlled/triggered drug delivery and sensing systems, which can solve problems related to human health and the environment. Firstly, I give a brief introduction of stimuli-responsive polymers, their assemblies and applications, and also discusses background of controlled drug delivery especially for smart drug delivery systems (Chapter 1). After that, we fabricated microgel-based stretchable reservoir devices for elongation enhanced small molecule release rate. Such release rate could be tuned by varying the Au layer thickness coating the microgels and

device elongation. Importantly, the release process of small molecules could be turned on/off simply by stretching and relaxing the etalons (Chapter 2). Futhermore, by tuning the chemistry of microgels, we were able to develop novel temperature/light-responsive poly(*N*-isopropylacrylamide-*co*-nitrobenzyl methacrylate) (pNIPAm-*co*-NBMA) microgels for the use of delivering a model drug (fluorescein). Moreover, we proved that either UV irradiation or heat can promote the on-demand release of preloaded drug into the aqueous solution (Chapter 3). On the basis of such novel temperature/light-responsive microgels, we described the study of utilizing pNIPAm-*co*-NBMA microgels in the field of controlled osteogenic differentiation of human mesenchymal stem cells (hMSCs). Dexamethasone (DEX), a synthetic glucocorticoid, has been found to be the earliest and more readily small molecule osteogenic inducers for hMSCs, which can be loaded into pNIPAm-*co*-NBMA microgels, and released in a light-controlled manner. Such DEX-loaded photo-responsive microgels were able to control hMSCs osteogenic differentiation upon light exposure (Chapter 4). Subsequently, since chitosan is an attractive non-toxic, biocompatible and biodegradable polymer, we tried to develop a system of doxorubicin-hydrochloride (Dox-HCl) encapsulated chitosan-based supramolecular nanogels for the use of pH and ATP competitive drug release (Chapter 5). Moreover, pNIPAm-based sensing system related to human health have also attracted more attention to date. An optical sensor assembled by poly(N-isopropylacrylamide) (pNIPAm)-microgels for analysis of volatile organic compounds (VOC) such as hexane,

cyclohexane, chloroform, petroleum ether and tetrahydrofuran (THF) were fabricated. The sensitivity, selectivity, response time and limit of detection of our sensors are investigated in details (Chapter 6). In Chapter 7, conclusion and future outlook are expressed to discuss. Ultimately, the appendix A and B have been included in the end of this dissertation, which consists of preliminary experimental results on related research projects during my Ph.D. program.

Preface

This thesis is an original work by Yingnan Zhang (Y. Zhang) under the supervision of Dr. Michael J. Serpe (M. J. Serpe)

Chapter 2 of this thesis has been published as Y. Zhang, Y. Gao, W.S.P. Carvalho, C. Fang and M. J. Serpe, Microgel-Based Stretchable Reservoir Devices for Elongation Enhanced Small Molecule Release Rate. *ACS Appl. Mater. Interfaces* 2020, 12, 19062-19068. I was responsible for designing and executing experiments, data collection and analysis, and manuscript composition. Y. Gao participated in important discussions, and W.S.P. Carvalho, and C. Fang assisted with the data collection. M. J. Serpe was the supervisory author and was involved in the concept formation and manuscript composition

Chapter 3 of this thesis has been submitted as Y. Zhang, C. Fang, W.S.P. Carvalho, Y. Gao, and M. J. Serpe, Triggered Small Molecule Release from Dual-Stimuli Responsive Microgels. *J Mater Chem B*. 2020. I was responsible for the experimental design, execution of experiments, data collection and analysis and manuscript composition. C. Fang assisted with the data collection as well as the manuscript composition and contributes equally with me. W.S.P. Carvalho, and Y. Gao took part in useful discussions. M. J. Serpe was the supervisory author and was involved in the research design and manuscript composition.

In Chapter 4 and 5, I already completed these two manuscripts that are ready to be submitted as soon as possible. I was again responsible for the experimental design, execution of experiments, data collection and analysis and manuscript composition. In Chapter 4, C. Fang and S. Zhang also participated in the data collection, and W.S.P. Carvalho participated in useful discussions while in Chapter 5, Y. Chang assisted with the data collection and X. Zhang was involved with experimental design and important discussions. M. J. Serpe was the supervisory author and was involved in the research design and manuscript composition of Chapter 4 and 5.

Chapter 6 of this thesis has been published as Y. Zhang, W.S.P. Carvalho, C. Fang and M. J. Serpe, Volatile Organic Compound Vapor Detection with Responsive Microgel-Based Etalons. *Sensors and Actuators B: Chemical* 2019, 290, 520-526. I was responsible for the experimental design, execution of experiments, data collection and analysis and manuscript composition. W.S.P. Carvalho assisted with the data analysis and manuscript composition as well. C. Fang took part in the data collection. M. J. Serpe was the supervisory author and was involved in the research design and manuscript composition,

Acknowledgement

Foremost, I would like to express my deep and sincere gratitude to my supervisor, Dr. Michael J. Serpe, for giving me the opportunity to take this wonderful journey of exploiting diverse topics in polymer materials at University of Alberta, and providing invaluable guidance throughout my research projects. As a great supervisor, he is enthusiastic and motivated in science, quite considerate and friendly in guiding us to pursue our goals. During his spare time, he always hangs out playing basketball with me, hosts various great holiday parties, and enjoys helping me in my daily life. It seems to me that he is not only my supervisor, but also a rich friend or a family member. Without his endless encouragements and advice, I cannot have been capable of achieving my Ph.D. degree. In a word, I am extremely grateful for his support, friendship, life suggestions, and for the greatest times we shared.

I cannot express enough thanks to my supervisory committee members, Dr. Mark T. McDermott and Dr. Liang Li for their insightful comments, valuable suggestions, and constructive criticism on my research projects. I am also grateful to Dr. Ran Zhao and Dr. Hyun-Joong Chung for participating in my candidacy examination and Dr. Ravin Narain and Dr. Jose Moran-Mirabal for agreeing to serve as the arm's length examiners for my final doctoral examination. I also would like to thank Prof. Xi Zhang, who provided me with a wonderful project when I was visiting Tsinghua University.

I would like to express my gratitude to all the past and current Serpe group members and all the undergraduate students who worked with me. A special thanks to Yongfeng Gao, Wildemar Carvalho and Changhao Fang, you guys definitely made my journey meaningful, and gave me lots of encouragements during my research. I feel so happy to be one of this big family over the past five years.

I would like to extend my gratitude to Gareth Lambkin from Biological Service for helping me during my project involving the cultivation of human mesenchymal stem cells and Anita Weiler for answering my questions about the requirements of graduate program and the applications of scholarship. I am also grateful to Norman Gee, Yoram Apelblat, and Gregory Kiema for their guidance during my TA duties.

Many thanks to the financial support provided by Alberta Innovates (AI) in Alberta, and Department of Chemistry at University of Alberta.

Finally, I would like to thank my family and friends for their love, support, and encouragements. A deepest gratitude to my girlfriends Jianing Li, who has sacrificed so much to make my life go this far, and who shares her unconditional love, and spiritual support with me. I really appreciate your support and encouragement when times get rough. I love you.

Table of Content

List of Figures

List of Videos

List of Tables

List of Schemes

List of Abbreviations

βGP: β-glycerophosphate

ΔG: free energy of dissolution

ΔH: dissolution of enthalpy change

ΔS: dissolution of entropy change

1D: one dimensional

2D: two dimensional

3D: three dimensional

AA: ascorbic acid

AAc: acrylic acid

ALP: alkaline phosphatase

APBA: 3-aminophenylboronic acid

APS: ammonium persulfate

ATP: adenosine-5'-triphosphate

BIS: *N,N'*-methylene(bisacrylamide)

BM: basal medium

BMPs: bone morphogenetic proteins

CCK-8: cell counting kit-8 assay

CV: crystal violet

DEX: Dexamethasone

DLS: dynamic light scattering

DMEM: dulbecco's modified eagle medium

Dox-HCl: doxorubicin-hydrochloride

DSC: differential scanning calorimetry

ECM: extracellular matrix

EE: encapsulation efficiency

FBS: fetal bovine serum

FTIR: fourier-transform infrared spectroscopy

GA: glutaraldehyde

HCl: hydrochloric acid

HepG2: human hepatic cancer cells

hMSCs: human mesenchymal stem cells

HPMA: *N*-(2-Hydroxypropyl) methacrylamide

KPS: potassium persulfate

LC-MS: liquid chromatography-mass spectrometry

LCST: lower critical solution temperature

LOD: limit of detection

MB: methylene blue

MC: merocyanine

NaOH: sodium hydroxide

NIPAm: *N*-isopropylacrylamide

NIR: near-infrared

NMR: nuclear magnetic resonance spectroscopy

OM: osteogenic medium

o-NBE: *o*-nitrobenzyl ester

P2VP: poly(2-vinyl- pyridine)

P4VP: poly (4-vinylpyridine)

PAAc: poly (acrylic acid)

PAMPS: poly (2-acrylamido-2-methylpropane sulfonic acid)

PCL: polycaprolactone

PDEA: poly (*N,N*□-diethylacrylamide)

PDI: polydispersity index

PDMA: poly (*N,N*- diethyl aminoethyl methacrylate)

PDMAEMA: poly (*N,N*-dimethylaminoethyl methacrylate)

PDMAPS-MA: poly(2-dimethyl[methacryloxyethyl] ammonium propane sulfonate)

PDMS: polydimethylsiloxane

PEGDA: poly (ethylene glycol) diacrylate

PGC-C_{18}: poly (glycerol monostearate carbonate-co-caprolactone)

pH_{en}: endosome pH

pH$_{ex}$: extracellular pH

PLGA: poly (lactic-*co*-glycolic acid)

PMAAc: poly (methacrylic acid)

PMAm: poly(methacrylamide)

PMVE: poly (methyl vinyl ether)

PNAAGA: poly(*N*-acryloylasparaginamide)

pNIPAm: poly (*N*-isopropylacrylamide)

pNIPAm-*co*-AAc: poly (*N*-isopropylacrylamide-*co*-acrylic acid)

pNIPAm-co-AAc: poly (N-isopropylacrylamide-co-acrylic acid)

pNIPAm-co-APBA: poly (N-isopropyl-acrylamide-3-(acrylamido)phenylboronic acid)

pNIPAm-*co*-NBMA: poly (*N*-isopropylacrylamide-*co*-nitrobenzyl methacrylate)

pNP: p-nitrophenol

pNPP: p-nitrophenol phosphate

PNVCL: poly (*N*-vinylcaprolactam)

POEGMA: poly (oligo ethylene glycol methacrylate)

PSSA: poly (4-styrenesulfonic acid)

SP: spiropyran

SRP: stimuli-responsive polymers

TEM: transmission electron microscopic

TGF-β: transforming growth factor-beta

THF: tetrahydrofuran

TPyP5: 5-tetra(4-pyridyl) porphyrin

TPyP5-MGs: 5-tetra(4-pyridyl) porphyrin contained microgels

UCST: upper critical solution temperature

UV: ultraviolet

VEGF: vascular endothelial growth factor

VOCs: volatile organic compounds

VPTT: volume phase transition temperature

Chapter 1

1. Introduction

1.1 Stimuli-responsive polymer

Stimuli-responsive polymers (SRP) include natural polymers and synthetic polymers that are capable of changing their physical and/or chemical properties in response to changes in their environment (external stimuli).[1] In nature, stimuli-responsive materials could endow organisms with competitiveness and survival skills. For example, desert-dwelling Namaqua chameleons change the space between guanine crystals under their skin, which are sensitive to the intensity of the sun,[2] and the Mimosa pudica plant undergoes changes in its leaf orientation in response to physical disturbances.[3] Inspired by nature, synthetic SRPs that are called 'smart polymers' also can change their polymeric size, conformation, solubility, and color in response to a variety of external stimuli, which have been developed to mimic the naturally responsive system. Thus, such stimuli-responsive polymers are an excellent applicant to design smart materials, providing a tremendous convenience in the development of intelligent systems.

There are many different types of stimuli that can be applied to generate a response such as physical, chemical and biological stimuli. The conformation, properties and

intramolecular or intermolecular interactions of polymeric chains can be altered in response to such stimuli, including temperature, magnetic field, electric potential, pressure, light, pH, oxygen levels, enzymes, and other biological molecules.[4-14] Herein, various stimuli-responsive polymers will be introduced and illustrated, including temperature, pH, and light responsive polymers.

1.1.1 Temperature-responsive polymer

By far, the most well-studied and understood response is temperature. Temperature-responsive polymers have seen an upsurge attention due to their external stimuli in a noninvasive manner. Moreover, spontaneous temperature variations, such as the increased temperature of inflamed tissue, also easily occur in our body.[15] Therefore, temperature-responsive polymers play an indispensable role in the development of a diverse range of applications, e.g., for sensing, biosensing, and on-demand drug delivery as well.[16-18]

Temperature-responsive polymers exhibit a low critical solution temperature (LCST) or upper critical solution temperature (UCST), which depend on their transition manner from monophasic to biphasic or on the contrary, from biphasic to monophasic when the temperature is raised, respectively.[19] LCST polymers have been investigated widely, whereas UCST polymers are quite rare. Among all the LCST based polymers, poly(*N*-isopropylacrylamide) (pNIPAm) is one of the most extensively studied

temperature responsive polymer that exhibits a coil to globule transition at 32 °C. That is, pNIPAm is fully water soluble at temperatures below 32 °C, existing as a random coil, and transitions to a collapsed, "water insoluble" globule when the temperature of the solution is above 32 °C. This transition is fully reversible and can be repeated many times.[20] To further demonstrate this temperature-dependent phase transition, Gibbs free energy can be used to explain the behavior of pNIPAm single chains:

$$\Delta G = \Delta H - \text{T}\Delta S \tag{1-1}$$

Where ΔG is the change in the Gibbs free energy of dissolution, ΔH is the change in the enthalpy of dissolution, ΔS is the change in the entropy of dissolution, and T is the environmental temperature in K. The changes in S are mainly due to the interaction between water and polymer chains. Based on this equation, a positive ΔG means that polymer dissolution is not spontaneous and the polymer solution is biphasic, that is, heterogeneous, and phase separation will occur; a negative ΔG means that polymer dissolution is spontaneous, and the polymer is homogenous and soluble in a solvent. As shown in Figure 1-1, the interactions between water and segments of pNIPAm chain have an effect on such transitions. When the temperature is below the LCST, the water and pNIPAm segments have two different ways to bind together: one is the clathrate-like water, with main hydrocarbon chains and ordered structures surrounding the hydrophobic isopropyl groups, and the other one is water binding around the pNIPAm amide groups.[21] Thus, negative ΔH and ΔS can be observed from the above hydration process, resulting in

a negative ΔG and a spontaneous polymer dissolution process due to the enthalpy effect at low temperatures. However, at temperatures above the LCST, the entropy effect is dominant, leading to a positive ΔG and an unspontaneous dissolution process of the polymer. Based on such a phenomenon, the polymer could transition from soluble (extended coil) to an insoluble (globule) state via temperature variations.
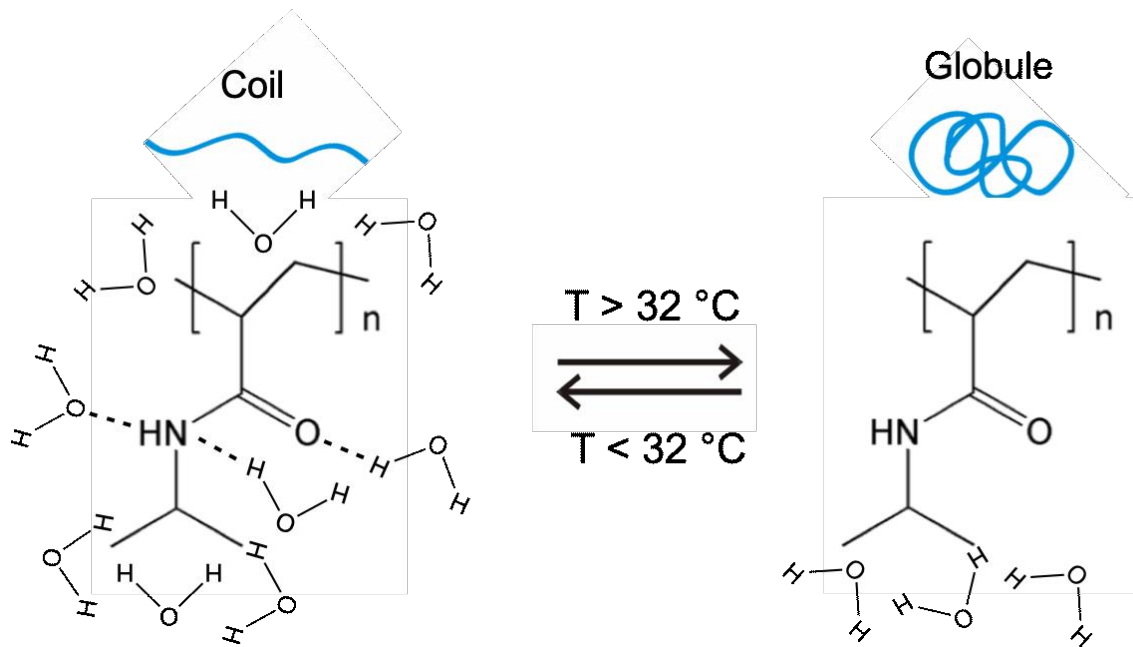
Figure 1-1. Schematic representation of pNIPAm's temperature-induced reversible phase transition.

Poly(N-vinylcaprolactam) (PNVCL) is another well-studied thermoresponsive polymer, second only to poly(N-isopropylacrylamide), the most popular temperature-responsive polymer. PNVCL is soluble in both polar and non-polar solvents, such as alcohols, tetrahydrofuran (THF), chloroform, and dichloromethane. PNVCL is very stable to hydrolysis; it was found that only 1.5% of its units could be hydrolyzed

when the polymer aqueous solution is heated up 100 °C with 1 M hydrochloric acid (HCl) for 60 h.[22] Also, the polymer shows similar LCST behavior as pNIPAm in water at about 31 °C, which means a swelling to collapsing transition in water at the temperature of 31 °C. Furthermore, both pNIPAm and PNVCL have been reported to be biocompatible, making them ideal candidates for biomedical applications.[23] However, by increasing the chain length of the polymer, the LCST is almost independent of the chain length of the pNIPAm. That is, in the limit of infinite chain length, the critical point is characterized by a limiting polymer concentration (ϕ_L=0) at the corresponding Θ-temperature.[24, 25] As a result, the PNVCL polymer networks exhibit a continuous temperature controlled swelling to shrinking transition, whereas there is a discontinuous temperature controlled swelling to shrinking transition by pNIPAm. However, polymerizing *N*-vinylcaprolactam in a controlled method is quite difficult, and there has been a lack in popularity among researchers to investigate PNVCL compared to pNIPAm to date.

Besides the poly (*N*-isopropylacrylamide) (pNIPAm) and poly(*N*-vinylcaprolactam) (PNVCL) covered in the previous sections, there is a plethora of examples of thermoresponsive polymers with a LCST, shown in Figure 1-2, such as poly(oligo ethylene glycol (meth)acrylate) (POEGMA), and poly(*N,N*-diethylacrylamide) (PDEA). Despite the favorable properties of pNIPAm and PNVCL, there has been an ongoing search for alternative LCST polymers with an easier synthesis by controlled radical polymerization. However, many other polymers can exhibit LCST behavior if the proper

hydrophilic-hydrophobic balance is present in the macromolecules. Poly(methyl vinyl ether) (PMVE), poly(phosphoester)s with ethyloxy side chains, and poly(2-ethyl-2-oxazoline)s, also present temperature-responsive behavior, with LCST behavior at about 34 °C, 38 °C and 60 °C respectively. Such thermoresponsive behavior can be altered by either variation of the ethylene glycol length or changing the formation of side chains.[26-28]
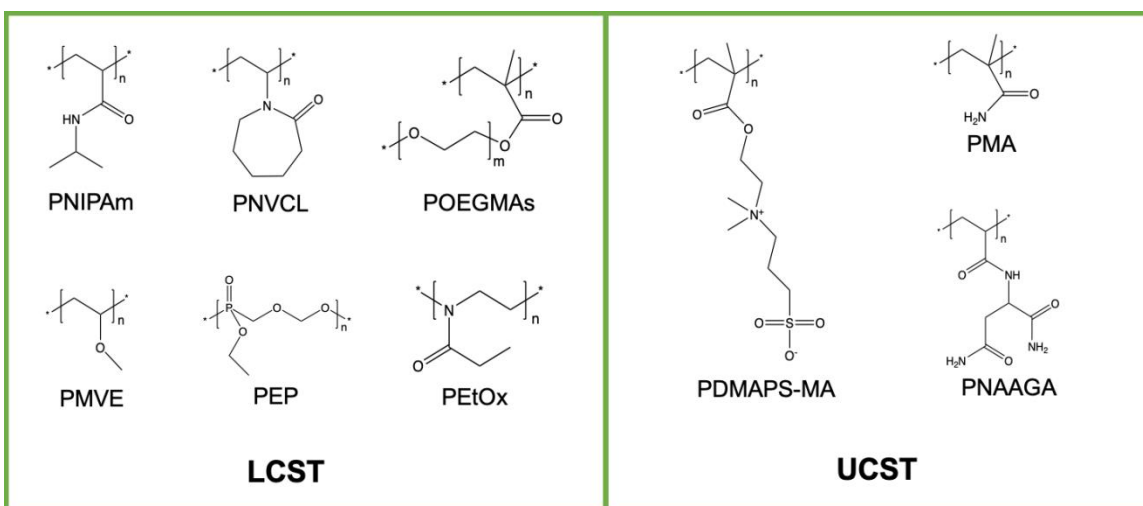
Figure 1-2. Chemical structures for typical polymers with LCST and UCST.

Compared to an LCST polymer, thermoresponsive polymers with UCST behavior in water are quite rare. In order to understand UCST behavior further, another ΔH term, the change in the enthalpy due to the supramolecular association of the polymer chains, needs to be mentioned in the Gibbs free energy equation. The strong supramolecular polymer-polymer interactions cause a UCST behavior in water under ambient pressure conditions. That is, the dependency of the transition temperature will be correlated directly to the strength of the supramolecular interactions because the UCST phase

transition in water is related to associative interactions. This may lead to counterintuitive effects, like increased transition temperatures upon incorporation of hydrophobic side chains. Also, if the solution is heated up, such a UCST transition of a polymer in superheated water is not related to a major change in polymer properties or polymer association but to a change in solvent properties, which means the polarity of water decreases, making it a better solvent for the polymer and resulting in dissolution of the precipitated polymer chains.[29, 30] Generally, the difference between LCST and UCST transitions is that the LCST transition is a cooperative entropy-driven process, whereas the UCST transition is an enthalpic process.

The most popular polymer with UCST behavior in water is the poly(2-dimethyl[methacryloxyethyl] ammonium propane sulfonate) (PDMAPS-MA), as it has both positive and negative charges in every repeat unit. As such, strong polymer-polymer interactions are present based on electrostatic interactions leading to collapsed structures that are more hydrophobic than the solubilized polymer chains at elevated temperatures due to a charge compensation and the release of counterions into solution. The phase behavior of PDMAPS-MA was reported to be highly dependent on the polymer chain length, whereby the UCST transition increases with increasing chain length, as would be expected from the enhanced number of electrostatic interactions that increase the polymer-polymer interactions. Besides electrostatic interactions in the polymer chain, hydrogen bonding in the polymer-polymer interactions is another way to

achieve UCST behavior such as in poly(methacrylamide) (PMAm) and poly(*N*-acryloylasparaginamide) (PNAAGA), and so on.[31, 32]

1.1.2 pH-responsive polymer

pH-responsive polymers are a group of stimuli-responsive polymers that can undergo structural and property changes, such as solubility, surface activity, chain conformation, and configuration, in response to the pH of solutions.[33] In general, a pH-responsive polymer commonly is used to define polymer protonation or deprotonation of functional groups in polymer chains where ionization depends on the pH of the solution. Due to such beneficial properties of pH responsive polymers, their use has increased dramatically in various applications, such as drug/gene delivery, sensors, water remediation etc.[34-37]

Ionizable polymers typically are composed of weak acids and/or bases that can be ionized by manipulating the pH of the solution to generate polyanions, polycations, and polyzwitterions. As a result, physical properties, such as chain conformation, solubility, and configuration, can be tailored by manipulating the charges along the polymer backbone or the electrolyte concentrations. There are two kinds of pH-responsive polymers, polymers with acidic groups and polymers with basic groups. Polyacid polymers will collapse at low pH due to the protonation of acidic groups, and hydrophobic interactions dominate, resulting in volume withdrawal of the polymer that

contains the acidic groups. With increasing pH, a negatively charged polymer will form

due to the dissociation of acidic groups into acidic ions, causing the polymer to swell.

The chain configuration of a weak polyacid is a function of the pK_a of the polymer.

However, polybasic polymers show the opposite behavior, as the ionization of the basic

groups will increase with decreasing pH, as shown in Figure 1-3. Some representative

pH-responsive acidic polymers are shown in Figure 1-4.
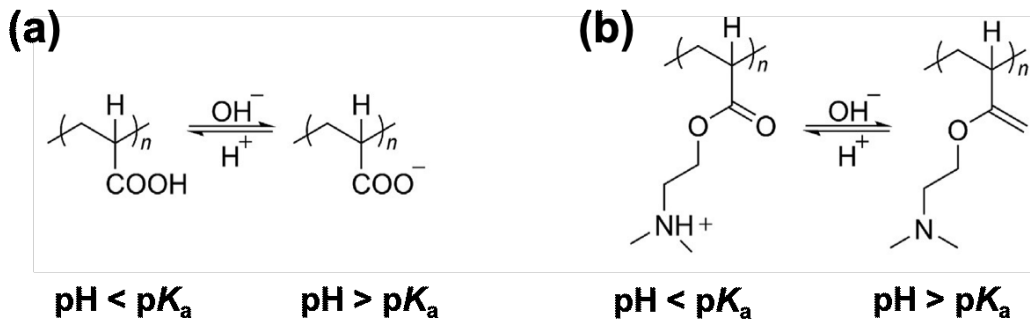
Figure 1-3. Structures depending on the ionization of the ionic chain groups of pH-responsive polyelectrolytes (a) poly(acrylic acid) and (b) poly(*N*,*N*-dimethylaminoethyl methacrylate) (PDMAEMA).
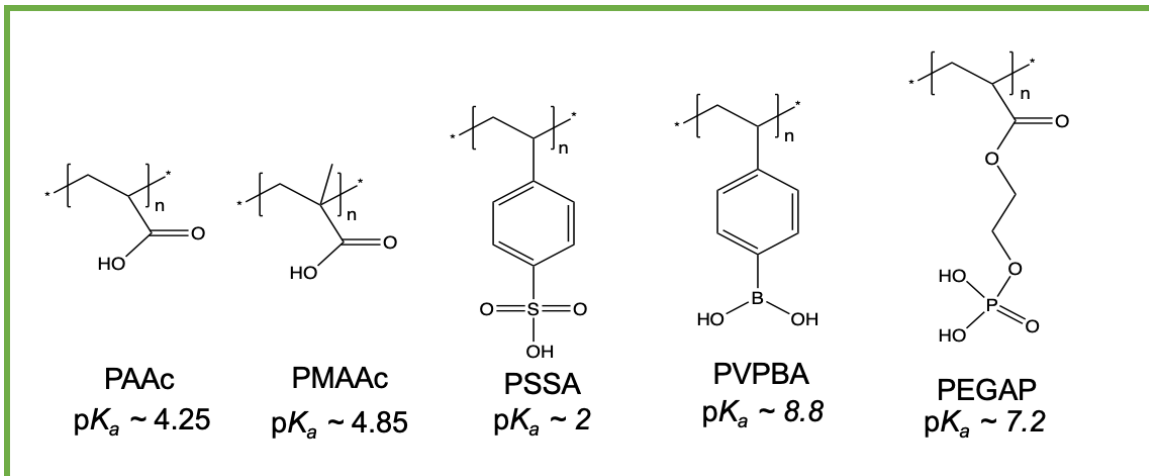
Figure 1-4. Chemical structures of some typical pH-responsive acidic polymers.

1.1.2.1 pH-responsive acidic polymers

pH-responsive acidic polymers consist of acidic functional groups in their structures. The total number of negatively charged groups of the polymer chain is dependent on external pH variations in aqueous solutions. The pH-responsive acidic polymers can be classified based on their functional groups on the polymer chain.

The weak acidic carboxylic groups (> 50%) lose acidic protons at pH > pK_a, forming anionic polyelectrolytes. At low pH, where the pH is below the pK_a, a neutral polymer (> 50%) is formed by the carboxylic groups accepting protons. Of all pH-responsive polymers containing carboxylic acids groups, poly(acrylic acid) (PAAc) and poly(methacrylic acid) (PMAAc) are the most commonly studied. The presence of carboxylic acids groups (-COOH) plays a crucial role in the configuration change of polymer. In terms of PAAc, the pK_a of AAc is reported to be ~4.25. When the pH of the environment is < 4.25, the COOH groups are protonated and the polymers are mostly neutral. When the pH is > 4.25, the polymers are deprotonated and mostly negatively charged. The pH of the environment at which the acid becomes (de)protonated is determined by the dissociation constant (K_a). Because of the variation in polymeric composition and molecular weight, the value of the dissociation constant can be tuned in the different polymer chains.[38]

Additionally, the most widely used sulfonic acid based polymers that have pendant sulfonate groups in their structure are poly(2-acrylamido-2-methylpropane sulfonic acid)

(PAMPS) and poly(4-styrenesulfonic acid) (PSSA). Such polymers usually are preferred in the preparation of strong polyelectrolyte hydrogels due to their high degree of ionization. Such sulfonic acid based hydrogels swell extensively, as the pH is above the pK_a of the related sulfonic acid groups. Such groups are well known to be more hydrophilic in their anionic form.[39] Moreover, phosphorus-based polymers with (meth)acrylate-based monomers have been studied widely, as they exhibit very unusual and unique properties. Among (meth)acrylate-based monomers, (monoacryloxy)ethyl phosphate and 2-(methacryloyloxy)ethyl phosphate are the most commonly used monomers that are employed for a wide range of technological applications.[40] Similar to the sulfonic acid based polymers, the phosphorus-based monomers usually are used in the synthesis of hydrogels, which are swollen under basic pH environments. Finally, boronic acid based polymers exhibit a lot of interesting properties, such as glucose-sensitivity, reversibility and self-healing. As reported in the literature, polymers with the phenylboronic acid-containing monomer (Ph-B(OH)$_2$) are very common and dominant among them.[41] These materials have found important applications in many areas, especially in biomedical areas, usually as phenylboronic acid (PBA)-containing hydrogels.

1.1.2.2 pH-responsive basic polymers

pH-responsive basic polymers, also called polybases, contain basic functional groups in the polymer chain, usually undergoing ionization/deionization transitions from pH 7 to pH 11. The amount of positively charged groups can be tuned in response to the external pH variation. The primary, secondary, or tertiary amine groups are located in their side chains. Particularly, vinyl, (meth)acrylamide and (meth)acrylates containing tertiary amine groups are some of the typical monomers used to synthesize pH-responsive basic polymers. For example, poly(N,N- diethyl aminoethyl methacrylate) (PDMA) is a widely used polymer, whose pK_a is about to 7.4. That is, a tertiary amine group could accept protons at low pH values, < 7.4 by forming polyelectrolytes and releasing them under basic conditions.[42] Another class of polybases is nitrogen-containing polymers that present a lone pair of electrons available for proton bonding; these include pyridine, imidazole, pyrrolidine, or morpholine. Among all, poly (vinyl pyridine) based polymers, which include poly(4-vinylpyridine) (P4VP) and poly(2-vinyl- pyridine) (P2VP), are used widely as polymers. These polymers are able to undergo a phase transition above pH 6 by deprotonation of pyridine groups. Some representative pH-responsive basic polymers are shown in Figure 1-5.
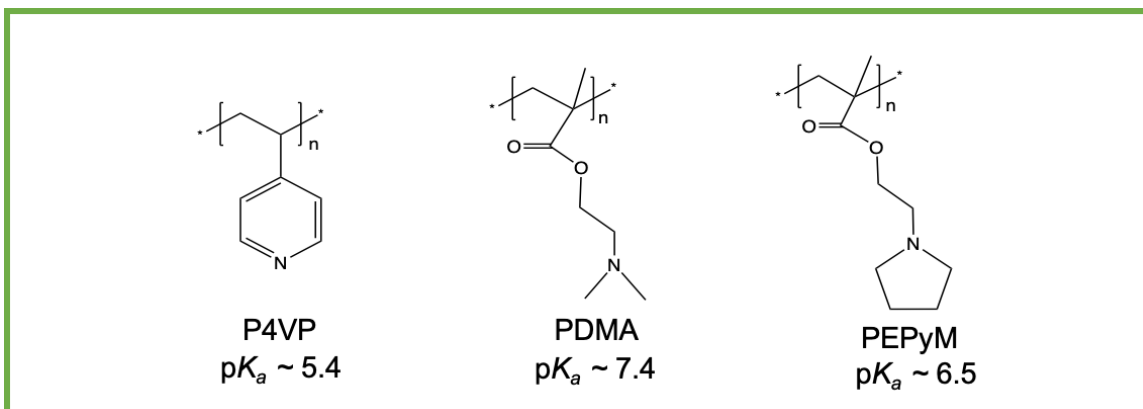
Figure 1-5. Chemical structures of some typical pH-responsive basic polymers.

1.1.2.3 pH-responsive natural polymers

Recently, natural polymers have emerged as promising materials due to their good biocompatibility and facile modification by simple chemistry. Some natural polymers also are used in pH-responsive self-healing gels and protein/drugs delivery systems.[43] Dextran, hyaluronic acid, alginic acid, and chitosan are among the most widely used natural polymers. The chemical structures of chitosan, alginate, and hyaluronic acid are shown in Figure 1-6. For example, chitosan is the only cationic natural polysaccharide that is obtained by partial deacetylation of chitin. The pH sensitivity is mainly dependent on the degree of deacetylation, which the pK_a value of chitosan is 6.5. That is, chitosan dissolves below pH 6.5 due to the protonation of amine groups, but it will precipitate above pH 6.5 since hydrogen bonds are formed by amine groups and hydroxyl groups in the polymer chain. On suitable chemical modification, these polymers can provide better properties for a variety of biomedical applications.
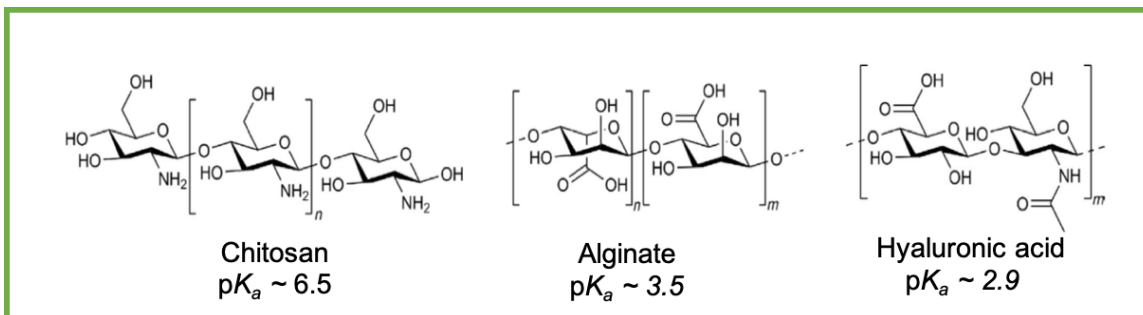
Figure 1-6. Chemical structures of representative pH-responsive natural polymers.

1.1.3 Light-responsive polymer

Besides the above-mentioned temperature and pH as physical and chemical stimuli, light also has attracted a tremendous amount of consideration when it comes to designing stimuli-responsive polymers. Light has the specific physical attributes that it can be applied remotely with a high degree of spatial control over the region of excitation. Moreover, such stimulation can be tuned simply by turning the excitation source on/off, by modulating the excitation source intensity/wavelength, and by changing exposure time.[44] The wavelength of the light is typically in the range of UV to near infrared (NIR), and even X-rays as well. Light-responsive polymers could be achieved by incorporating a light-responsive functional group (chromophores) into polymers, either in the backbone or side chain, which undergo a photo-induced structural and conformational change. Such light responsive behavior can be either reversible or irreversible, depending to the type of chromophore. Some commonly light-responsive compounds are displayed in Figure 1-7.
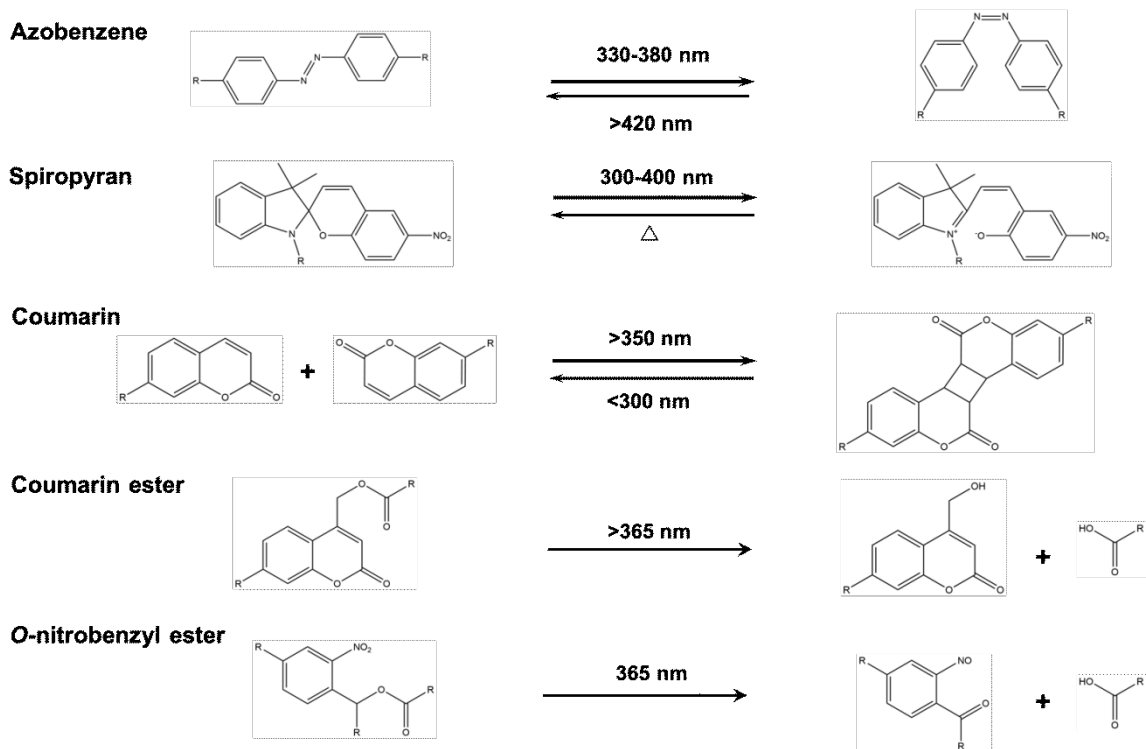
Figure 1-7. Structures and light-induced reactions of light-responsive compounds.

Reversible light-responsive groups respond to exposure to a particular wavelength with isomerisation, which causes changes in the polarity, optical chirality, and color of the chromophore units. For example, some of the most frequently used light-responsive small molecules are azobenzene photoswitches, which have two isomers, the thermally stable trans and the metastable cis, which can be interconverted with light irradiation (in both directions) or by thermal relaxation (cis to trans).[45] Moreover, spiropyran (SP) contains the (spiro) C-O bond that can change from a closed SP state to an open merocyanine (MC) state upon exposure to ultra-violet (UV) light. The SP-MC conversion process triggered by light exposure results in changes of the material properties, such as solubility, conductivity, and mechanical properties.[46]

15

Irreversible light responsive groups often are composed of photodegradable or photocleavable units, such as *o*-nitrobenzyl ester (*O*-NBE) group. Such *o*-nitrobenzyl ester derivatives could be cleaved to yield a carboxylic acid and a molecule of nitrosobenzaldehyde with UV irradiation. Such nitrobenzyl chemistry, specifically based on the UV light induced photolysis reaction of *o*-nitrobenzyl ester derivatives, was utilized extensively to control the release of small-molecule drugs and biomolecules such as proteins and oligonucleotides from various materials.[47] Compared to other light-responsive functional groups, *o*-nitrobenzyl ester derivatives have several benefits, such as long-term stability under ambient light, fast degradation kinetics, and non-toxicity of photodegradation products, which make them preferable.[48] Therefore, *O*-NBE derivatives become excellent candidates in terms of designing materials for light-stimulated drug delivery systems. In this dissertation, we exploited this ability of *o*-nitrobenzyl ester derivatives to achieve the goal of light-responsive controlled drug delivery.

1.2 Stimuli-responsive polymer microgels

The term microgel is defined as a "particle of gel of any shape with an equivalent diameter of approximately 0.1 to 1 μm". Baker's group was one of the first that studied microgels.[49] Microgels are cross-linked polymer chains and are similar to macrogels,

which consist of a soft domain that can change shape and size in response to mechanical stress, temperature, or chemical environment (like pH and ionic strength). Specifically, microgels respond to a changing environment much faster than macrogels because they have a high surface area-to-volume ratio. Tanaka and Fillmore (TF) also showed that the time required for the volumetric change of a gel (τ) is directly proportional to the gel's size (R) but inversely proportional to the diffusion coefficient (D).[50]

$$\tau = R^2/\pi^2 D \qquad (1\text{-}2)$$

Thus, due to a high surface to volume ratio, colloidal nature, high water content, porous structure of the internal network, fast response, biocompatibility, tunable sizes, and ideal mechanical features, microgels are attractive materials for many applications in the field of sensor and biosensing, controlled drug delivery, actuation, and water remediation systems.

1.2.1 Temperature-responsive pNIPAm microgels

Owing to those excellent aspects of microgels, researchers have designed various stimuli-responsive microgels with different functionalities to advance the field of biomedical applications, especially developing controlled drug delivery systems. Among them, temperature-responsive pNIPAm microgels are the most extensively studied and promising ones by far. In this dissertation, all the microgels and microgel based materials and devices are prepared by pNIPAm microgels.

Poly (N-isopropylacrylamide) (pNIPAm) based microgels belong to physical stimuli (thermal)-responsive materials, with pNIPAm microgels showing an excellent thermally-reversible shrinkage or swelling above or below their LCST of 32 °C. Such a transition temperature can also be called a volume phase transition temperature (VPTT). That is, the transition from the preferential polymer-polymer interactions to favorable polymer-water interactions at a temperature below VPTT forces the microgels to swell by absorbing water from the environment of solvent. The VPTT can be affected by crosslinking density, microgel conformation, functional groups in the copolymer, and solvent property as well. For example, the VPTT will rise by adding more hydrophilic groups into the backbone of the polymer microgel, while more hydrophobic groups will cause the VPTT to decrease.

1.2.1.1 pNIPAm microgels synthesis

Stimuli-responsive microgels can be synthesized by direct polymerization of monomers or post-polymerization modification of an already synthesized polymer.[51] Free-radical precipitation polymerizations have been used widely to synthesize pNIPAm microgels with properties that can be tuned by controlling the content of functional monomers in the final polymer.[52] NIPAm served as monomer, with N,N'-methylene(bisacrylamide) (BIS) or poly(ethylene glycol) diacrylate (PEGDA) as the crosslinkers, and ammonium persulfate (APS) or potassium persulfate (KPS) as

initiators, which are indispensable to synthesize pNIPAm microgels. In this dissertation, free-radical precipitation polymerizations have been utilized to synthesize all the microgels. The mechanism of synthesis of pNIPAm based microgels is illustrated in Figure 1-8.
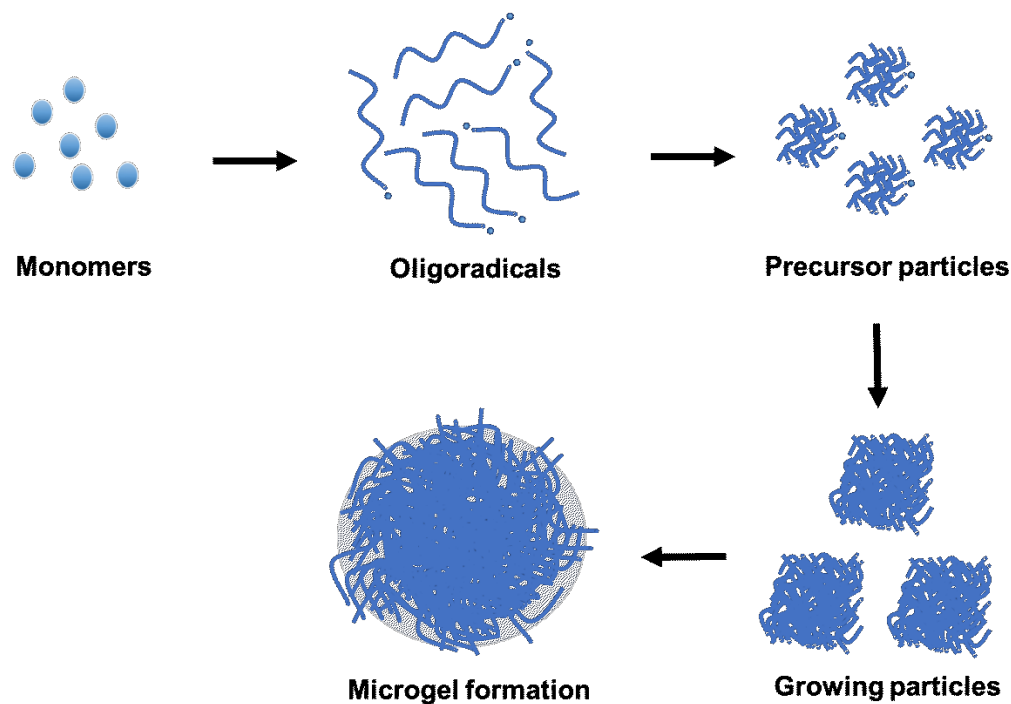
Figure 1-8. Mechanism of microgels formation in free radical polymerization.

Importantly, it is crucial that the polymerization temperature should be much higher than the VPTT of pNIPAm for the synthesis of uniform and stable pNIPAm microgels. One reason is that the free radicals can be quickly and efficiently formed to initiate the polymerization, resulting in a homogeneous nucleation. Moreover, it allows all the polymer chains to collapse when reaching a critical chain length, forming the precursor particles at high temperatures. Then, the precursor particles can attach by aggregation with other growing oligoradical chains upon reaching a critical size to form larger and

more stable growing particles until all the monomers are consumed. Such stabilization of microgels is due to the negative charges of the initiator fragments imparted into the polymer chains during the polymerization process. That is, colloidal stability could be achieved by the electrostatic repulsion with a highly electrophoretic mobility of the particles. Specifically, the hydrodynamic size of micorgels can be modulated by varying the concentration of initiator, surfactants, and temperature as well. For instance, a lower concentration of surfactant and a temperature reduction could lead to larger microgels and vice versa.[53, 54]

The mechanical behavior and properties of the pNIPAm microgel can be tuned easily during the synthesis by the addition of functional chemical groups. That is, the pNIPAm-based microgels also can be responsive to other stimuli besides temperature by copolymerization with other functional monomers, such as pH responsive monomer, or crosslinkers into the pNIPAm network.[55] Importantly, the charges of the selected initiator should be the same as the charges of comonomer in certain solutions since opposite charges between the initiator and comonomer would prompt the aggregation of particles. To date, the most commonly used pH responsive monomer is acrylic acid (AAc): a well-known pNIPAm-*co*-acrylic acid microgel (pNIPAm-*co*-AAc) can exhibit both thermal and pH responses. With these methods, mutli-functional properties, such as redox agents and light can be designed to temperature-responsive pNIPAm-based microgels.

1.2.2 pNIPAm microgel assemblies

Microgels can be assembled into useful larger objects such as one dimensional (1D) monolayer, two dimensional (2D) assemblies of air-water and oil-water interfaces, three dimensional (3D) hydrogels, colloidal crystals, environmentally sensitive optical properties, and layer-by-layer assemblies. For example, the Richtering group developed the ultra-low crosslinked poly(N-isopropylacrylamide) microgels which can behave as flexible polymers by covering the substrate with a uniform film, or as colloidal microgels leading to a monolayer of particles, depending on compression or other external stimuli.[56] In the Serpe group, a microgel based device that is called an "etalon", which could show excellent optical properties, was assembled first. In this dissertation, we applied this device into sensing and drug delivery systems.

Etalons are composed of a highly packed microgel layer confined between two thin gold (Au) layers (usually 15 nm) to generate the "mirror-dielectric-mirror" configuration of a classic Fabry-Pérot etalon system, which exhibits colors and has characteristic peaks in the reflectance spectra. An illustration of an etalon device is shown in Figure 1-9.
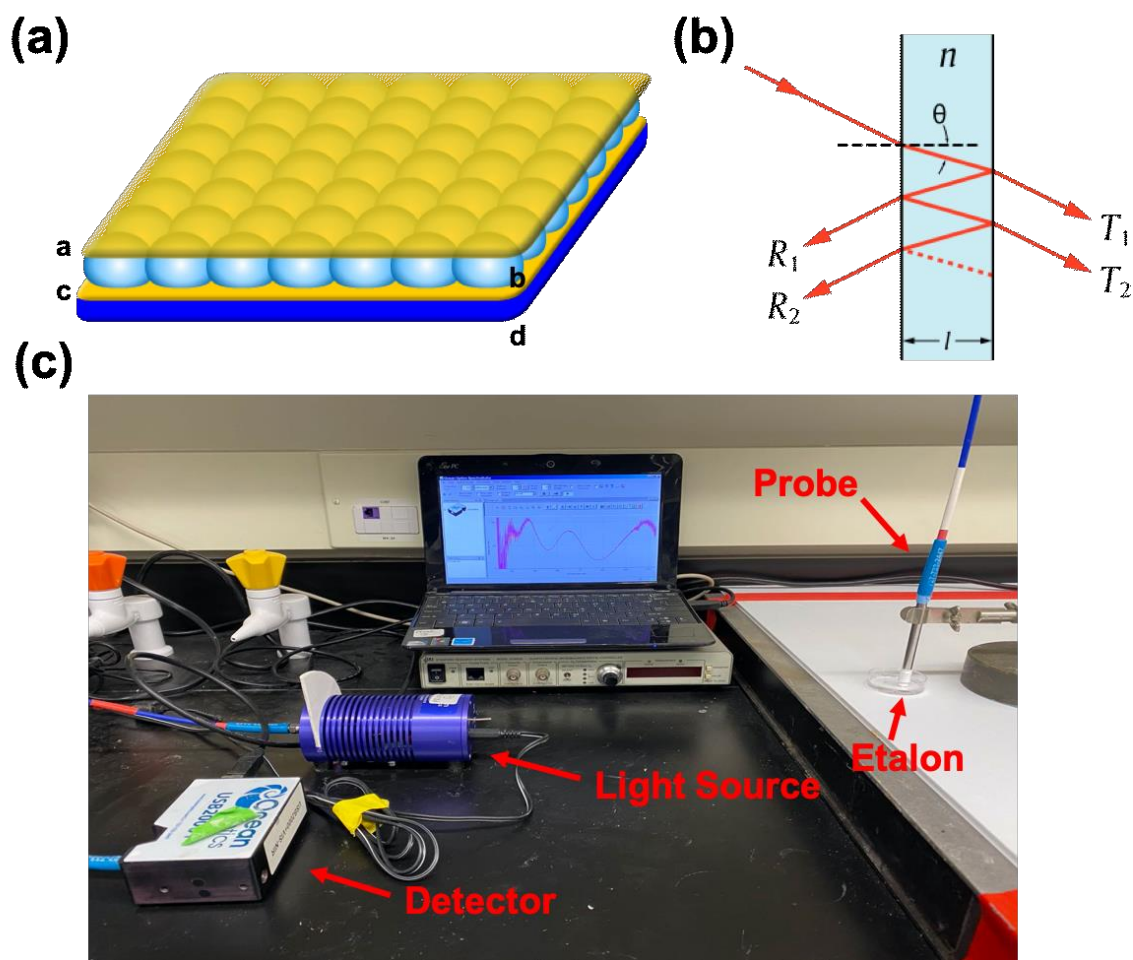
Figure 1-9. (a) Schematic of a pNIPAm microgel-based etalon; a: 15 nm Au overlayer; b: microgels layer; c: 15 nm Au bottom layer; d: glass substrate. (b) Schematic of the light resonance and interference in an etalon. (c) Illustration of set-up to collect the reflectance spectrum of an etalon.

The color of etalons is a result of light interference within its structure, similar to an etalon interferometer. That is, light striking the surface of the device enters the etalon's microgel layer and undergoes constructive and destructive interference, which leads to specific wavelengths of light being reflected that can be predicted from equation 1-3:

$$m\lambda = 2nd\cos\theta \tag{1-3}$$

where m is the order of the reflected peak (e.g., 1, 2, 3,...), λ is maximum wavelength being reflected, n is the refractive index of the dielectric layer, d is the distance between the two Au layers, and θ is the incidence angle. While the wavelength (λ) of light reflected from the etalon (and hence the etalon's color) depends n, θ, and d, we have shown in numerous studies that λ depends primarily on d at a fixed angle.[57] Therefore, any change in the size of the microgels in response to stimuli between the two Au layers leads to a change in d, and ultimately λ, and the $\Delta\lambda$ that can be related to the etalon's environment. Obviously, etalons can be utilized for the detection of pH, salt, vapor of organic compounds, and biomolecules.

1.3   Applications of stimuli-responsive microgels and their assemblies

As mentioned above, microgels exhibit high surface to volume ratios, high water content, porous structure of internal network, and biocompatibility. They have been utilized widely for many applications in the fields of sensor and biosensor, controlled drug delivery, and water remediation

1.3.1 Sensor and biosensor

A sensor/biosensor is a self-contained integrated device that is capable of quantifying the concentration of analytes by transferring signals into a form that is

readable by an observer or by another instrument to provide a result.[58] For sensing, analytes can be used to trigger the conformational change of the polymer resulting in changes in physicochemical properties, such as volume, color, solubility, and conductivity. In general, a sensor/biosensor should enable quick and accurate results in a time such that the patient can be treated if needed. To develop novel sensing/biosening systems, some are turning to thermal/pH responsive microgels. For example, Wen et al. successfully functionalized a 5-tetra(4-pyridyl) porphyrin (TPyP5)-into the thermoresponsive ionic microgels (TPyP5-MGs), and followed the detection of trace Pb^{2+} ions in aqueous solution with high sensitivity and selectivity among other 19 other species of the metal ions matrix.[59] Importantly, the sensitivity of TPyP5-MGs toward Pb^{2+} could be enhanced at the solution temperature of 50 °C. What is more, our group synthesized pyridine-containing microgels that are pH responsive MGs to fabricate CO_2 responsive microgel-based etalons.[60] That is, when the pyridine-containing microgels react with CO_2 in DI water, they will decrease the pH of the solution from 6.8 to 3.8, leading to the conformation change of pH responsive microgels; as a result, the etalon will change color.

1.3.2 Controlled drug delivery

Stimuli-responsive microgels also have been investigated comprehensively in the development of controlled drug delivery because of their porous structure and water

swellability. As a drug carrier, microgels have a sponge-like structure, with interstitial spaces filled with water. Drug molecules can be loaded by equilibrium partitioning between the drug solutions and microgel phases via electrostatic interaction, hydrophobic interaction, and/or hydrogen-bonding since the porosity of microgels permits the drug molecules to be incorporated onto the microgel interiors. The subsequent drug release occurs at a rate that is dependent on the diffusion coefficient of the drug molecules in the microgel network in response to internal or external stimuli. For instance, the Gu group generated a wearable, tensile strain-triggered drug delivery device consisting of a stretchable elastomer, which was integrated with the poly(lactic-co-glycolic acid) (PLGA) microgel.[61] The drugs could be stored temporarily in the microdepots, and the release system can be achieved by daily joint motions or intentional stretching of the elastomer film; this is an efficient and effective approach to promote the release of therapeutics from the materials. Our group developed a novel microgel-based reservoir device for the use of controlled drug delivery. The Au-overlayer of the device is used as a drug diffusive barrier to achieve the controlled drug release process.[38] Furthermore, a single microgel-based reservoir device also could be utilized for a sequential and controlled release of two different drugs in one system by simply functionalizing microgels with different chemistries. Thus, microgels can be ionized at different pH solutions, resulting in the controllable and tunable release of small molecules.[62] The delivery of various small molecules to a system, which can be triggered by tuning the solution of pH in a system,

has been achieved. In this dissertation, we will investigate a mechanical force triggered microgel-based etalon for controlled drug release and discuss the mechanism of such controlled drug release behavior.

1.3.3 Water remediation

Besides sensor/biosensor and controlled drug delivery, microgels also have been utilized in the field of water remediation systems due to porous structures that are able to absorb/desorb fine particles, colloids, heavy metals, and organic compounds.[63] Coagulation and flocculation play a critical role in removing the contaminants in waste water treatment systems. Microgels also are capable of flocculation under certain environmental conditions.[64] For instance, polyelectrolytes based microgels are able to absorb or bind heavy metal ions, which cause flocculation and result in decreasing the potential energy of repulsions. Such microgels can be regenerated easily by altering the pH of the solution.[65]

1.4 Stimuli-responsive polymer in controlled drug delivery

To date, scientists have shown great interests to the development of stimuli-responsive polymers (SRP) for the use of in vivo drug treatment since SRPs could be non-toxic, biocompatible, and biodegradable. Such a smart drug delivery polymeric system could

store and protect various drugs, deliver the cargo without any deactivations, and deliver a

controlled release of the drug into the target cells in response to any internal or external

stimuli. Thus, the efficacy of chemotherapy could be enhanced by the use of SRPs drug

delivery systems.[66]

1.4.1 Background of controlled drug delivery

Controlled drug delivery technologies exist to provide a more effective way to

release drugs due to sustained release versions of drug formulations.[67-69] Back in the

1950s, the sustained release formulation was first mentioned in the process of controlled

drug delivery. The controlled drug release systems can be classified into three generations

that were described by Kinam Park.[70] The 1st generation (1950s-1980) of drug delivery

came out, and oral and transdermal sustained release systems were established during that

period. The 2nd generation (1980-2010) of drug delivery focused on smart delivery

systems, including self-regulated drug delivery systems, long-term depot formulations,

and nanotechnology-based delivery systems, and also investigated the drug release

mechanism. The development of the 3rd generation (2010-2040) is already established

and includes on-off switching on-demand drug release, targeted delivery of an anticancer

drug, an extreme long-term delivery system, and in vitro and in vivo correlation. The

drug delivery field needs to take a bold approach to designing future drug delivery

formulations, primarily based on today's necessities, to produce the necessary

innovations.

Oral delivery is the most convenient approach of drug administration. However, some drugs exhibit quite poor water solubility, charge issues, or poor permeability across the cells, which it is quite challenging to promote oral formulations. Moreover, many biotech drugs, such as peptides and proteins, are much larger in size, less stable, and have a shorter half-life than the traditional small molecular drugs; thus, they usually are delivered by parenteral routes like injection or nanoneedle arrays.[71] Protein drugs delivered by injection usually can reach the intracellular or extracellular space (bloodstream or hypodermic tissues). Nevertheless, such injection methods have some drawbacks, such as invasiveness, chances of infection, and delivery protein drugs into cells (e.g., into the cytosol) is still challenging.[72]

Current efforts of drug delivery mainly focus on the development of targeted delivery, where the drug is only active in the target area of the body, and the drug can be released in a controlled manner over a period of time. The polymeric drug delivery systems, including mainly biodegradable polymeric injectable hydrogels, microneedles based patches, and implantable materials, are exploited widely in the area of disease/cancer treatments.[73-76] For example, biodegradable polymeric injectable hydrogels are responsive to particular physiological conditions in our body. When the drug (insulin or glucose oxidase) is trapped into polymeric precursor solutions, followed by the injection at the target site, it could form a long-term solid hydrogel in situ. With

the presence of analytes in the tissue, the drug could be released in a controlled fashion, achieving targeted delivery systems. Such biodegradable polymeric injectable hydrogels could reduce significant tissue irritation and damage.[77] Additionally, microneedle-based patches also have found their ways into controlled drug delivery. Compared to traditional syringe injections, microneedle-based patches offer a variety of merits by reducing the risks of needle reuse and accidental needle-associated injuries and by allowing for pain-free self-administration. Specifically, a series of drugs can be delivered efficiently with such a transdermal route. Various drugs can be loaded into biocompatible based microneedles, and as long as the microneedles puncture the skin, the drugs are released rapidly from the needles in response to physiological stimuli.[78, 79] Meanwhile, implantable polymeric devices, which can reduce the dosage significantly, minimize the potential side effects, and lighten the burdensome of treatment regimen, have been used in the field of drug delivery. Particularly, such implants are allowed for use in the treatment of brain tumors, prostate cancer and uterine fibroids.[80-83] In short, significant advances in the development of drug delivery technologies will have valuable contributions to our daily lives. We are convinced that polymeric drug delivery systems will play a significant role in future cancer therapy.

1.4.2 Polymeric material-based controlled drug delivery and mathematical models of release processes

In the past decades, polymeric materials have emerged as a most promising and viable technology platform for targeted and controlled drug delivery.[84] Polymeric material-based drug delivery systems confer various advantages, such as prolonged circulation time, enhanced accumulation in the tumor sites, reduced adverse effects, improved drug tolerance, lower toxicity, and increased patient comfort levels.[85-87] Although therapeutic macromolecular drugs have short half-lives in blood plasma, fast physical or chemical degradation, and cytotoxicity to both healthy cells and cancer cells, polymeric materials with typically micro/nanoscale sizes, such as PEGylated liposomes, and poly(lactide-*co*-glycolide) (PLGA) nanoparticles, block copolymer micelles and can be utilized to protect the drug, as a result of achieving the drug release in a controlled manner.[88-90]

The drug release from a polymeric material-based system is controllable with various methods, such as diffusion, dissolution, swelling, osmosis, and erosion.[91] Such drug release behaviors can be predicted with proper mathematical models, such as the zero-order model, first-order model, Higuchi model and Hixson-Crowell model.[92-95] With the mathematical models, researchers can understand the release mechanism easily and try to reduce the number of experiments. Herein, the mathematical models of

different drug release systems, including classical drug diffusion, polymer degradation, and erosion will be discussed.

1.4.2.1 Zero-order model

Zero-order release, in which a drug is released at a constant rate over a certain period of time, leads to the best control of plasma concentration. In principle, a polymer membrane that is permeable to both the drugs and water surrounds the drugs. The drug release occurs when it is dissolved up to its saturation concentration. The drug then permeates into the membrane and diffuses across the membrane into the plasma or tissues with a constant rate. Such zero-order or diffusion-based drug release can be explained by Fickian diffusion, in which the release rate is independent of the drug concentration in the tablets.[96] The zero-order release is given in Equation 1-4:

$$Q_t = Q_0 + k_0 t$$

(1-4)

where Q_t is the cumulative amount of drug released at time t, Q_0 is the initial amount of drug, k_0 is the release kinetic constant, and t is the time at which the drug release is calculated or measured. Such a zero-order model can also describe the dissolution of the drugs in the release systems, and it is ideal to describe the membrane controlled release formulations.[97]

1.4.2.2 First-order model

The first-order model could be simulated to illustrate absorption and/or elimination of a great diversity of therapeutic drugs. However, first-order kinetics cannot be described using a basic theory. In typical first-order release kinetics, the drug release rate depends on its concentration. The first order release equation can be explained as shown in Equation 1-5:

$$dC/dt = -kC \qquad (1\text{-}5)$$

where C is the concentration of drug in the reservoir and k is the first-order release rate constant. Since the active agents exhibit a higher solubility in aqueous solutions, the concentration of drug in the reservoir would decrease gradually as a function of time when the active agents begin to be released in the first order system, as a result of an equivalent concentration gradient across the membrane. However, if the volume of the medium is constant, equation 1-6 can be described as follows:

$$\log Q_t = \log Q_0 + kt/2.303 \qquad (1\text{-}6)$$

where Q_t is the amount of active agent released on time t, Q_0 is the initial amount of drug dissolved, and k is the first-order rate constant.[98]

1.4.2.3 Higuchi Model

Higuchi developed several theoretical models to study the release of water soluble and insoluble drugs incorporated into solid matrixes, and described the drug dissolution

from matrix systems.[99] Back in the 1960s, Higuchi developed a mathematical equation that was able to describe the release rate of drugs from matrix systems, such as ointment bases (planar systems).[100] The Higuchi model showed that particles of active agents were dispersed in homogeneous matrices, followed by diffusion into medium. In terms of the drug dissolution planar matrix, Equation 1-7 was proposed by Higuchi:

$$Q = \sqrt{D(2C - C_s)C_s t}$$

(1-7)

where Q is the amount of drug released on time t by area unit, C is the initial amount of drug contained in dosage form, C_s is the solubility of the active agent in the matrix medium, and D is the diffusion coefficient in the matrix medium. This relationship is valid over the time of dissolution in most cases. However, when the drug-released levels tend to saturate in the matrix system, it could not be proposed by that equation, and thus, Higuchi proposed Equation 1-8 for the case of a matrix saturated with a drug:

$$Q = \sqrt{2C_0 \varepsilon D t / \pi \tau} \qquad (1\text{-}8)$$

where C is the concentration of diffusing liquid contained in a porous matrix, ε is the porosity of matrix, and τ is the capillary tortuosity factor.[101] Obviously, it can be concluded that the amount of drug released is proportional to the square root of time, given in Equation 1-9:

$$Q = K_H \sqrt{t} \qquad (1\text{-}9)$$

where K_H is the Higuchi release constant. Such a simplified Higuchi model shows a

linear correlation between the amount of drug release and the square root of time.

Higuchi models were used to develop a number of mathematical models, such as the

Korsmeyer-□Peppas model and the Baker-Lonsdale model, which played a critical role

in classifying the possible release profile of active agents in formation of matrices.[102]

1.4.2.4 Hixson-Crowell model

Hixson and Crowell proposed a correlation between drug release from the particle

and the surface area and diameter area of the particle.[103] The proposed equation shows

that the drug release from the particle is proportional to the cube root of its volume, and is

given in Equation 1-10:

$$\sqrt[1/3]{W_0} = \sqrt[1/3]{W_i} + K_{HC}t \tag{1-10}$$

where W_0 is the initial amount of the drug in the system; W_i is the amount remaining in

the system on time t; and K_{HC} is the constant of incorporation, which relates surface and

volume.[93] In light of the concentration, drug density, and the number of spherical

particles, Equation 1-10 also can be described by:

$$\sqrt[1/3]{W_0} = \sqrt[1/3]{W_i} + k'\sqrt[3]{N}DC_st/\delta \tag{1-11}$$

where k' is a constant that relates surface, form, and particle density, N is the number of

particles, D is the diffusion coefficient, C_s is the solubility at the equilibrium at the

temperature of process, and δ is the thickness of the diffusion layer. Importantly, the

Hixson-Crowell model assumes that the drug release behavior is constrained by the

dissolution velocity of dosage forms through the polymeric matrix instead of by diffusion. Thus, the Hixson-Crowell equation is for the use of dosage forms such as tablets, where the surface of the dosage form decreases proportionally over time when the surface dissolution occurs; however, the geometrical characteristics of dosage forms remain constant.[104]

Besides the above, there are many different mathematical models for the understanding of controlled drug delivery with various dosage formations, such as the Hopefenberg model, and the Weibull model, etc. In this dissertation, zero-order and first-order models will be investigated to study the mechanism and controlled release behaviors of our systems.

1.4.3 Stimuli-responsive polymers for controlled drug delivery

As mentioned above, stimuli-responsive polymers have attracted great interest for the use of controlled drug delivery systems due to their porous, biocompatible, soft, and easy functionalization. Notably, the designs of smart drug-delivery polymeric systems and approaches have to meet the challenges associated with administration in the body. That, the system should undergo a complex chain of responses to survive in vivo, deliver the carriers, and release the drug into the target cells. Among them, the use of stimuli-responsive polymeric materials shows a very promising approach to enhance the efficacy of chemotherapy in response to stimuli such as changes in temperature, pH, light,

or the specific enzymes that are selectively encountered in relevant cell organelles.

1.4.3.1 Temperature-responsive drug release

Among all of the internal and external stimuli, temperature is one of the best signals in terms of easy and safe medical applications; thus temperature-responsive drug delivery has been sought widely in applications from hyperthermia therapy to solid tumors.[105] Temperature-responsive liposomes, polymer micelles, and nanoparticles have been investigated mostly. They all show a lower critical solution temperature behavior, meaning that a rise in temperature could enhance the drug release. For example, poly(*N*-isopropylacrylamide-co-*N*,*N*-dimethylacrylamide)-b-PLA micelles were developed by Nakayama for quick drug release with a lower critical solution temperature, around 40 °C. When the temperature exceeds the phase-transition temperature, the outer shell shrinks and becomes hydrophobic, forming intermicellar aggregates due to the strength of the shrunken outer shell layer's hydrophobic interactions, resulting in enhanced the drug release.[106] Sun prepared hybrid poly(2-(dimethylamino)ethyl methacrylate-*co*-3-dimethyl(methacryloyloxyethyl) ammonium propanesulfonate)-coated mesoporous silica nanoparticles that showed controlled release behaviors and low cytotoxicity. The preload rhodamine B could be released by adjusting the temperature in normal saline solution and could be released faster with a higher temperature.[107]

1.4.3.2 pH-responsive drug release

The pH responsive drug release systems also have attracted much interest by researchers. One reason is that the endosomes into which nanoparticles are incorporated via endocytosis generate markedly acidified lumens (pH_{en} 4.5-5.5) by the activity of V-type H^+ ATPase, thus such a mechanism offers a chance to release the drug from the endosomal compartment at low pH.[108] Moreover, acidosis in tumor tissue may be helpful for selective targeting of tumors relative to normal tissues, achieving the selectivity by the enhanced permeability and retention effect. Therefore, the developments of pH responsive drug release systems play an important role in the biomedical areas. To date, pH-responsive liposomes, polymeric nanoparticles, micelles, and polymersomes have been designed to exploit low extracellular or endosome pH (pH_{ex} or pH_{en}).[109-111] There are a variety of mechanisms of pH-responsive drug releases, based on these nanocarriers, such as functionalized protonatable groups and acid labile bonds in the polymers of the carriers.[112] For instance, Zhou developed pH-sensitive micelles, based on self-assembly of amphiphilic HPMA copolymers with hydrazone linkages. The hydrophobic drug doxorubicin can be conjugated into the *N*-(2-hydroxypropyl) methacrylamide (HPMA) polymer backbone via hydrophobic interactions.[113] The micelles remained stable at pH 7.4 with less than 20% of the drug released during circulation, whereas 80% of the drug was release by cleavage of the hydrazone bond at pH 5.0 within 8 h of incubation. Furthermore, the Serpe group developed a novel microgel-based assembly as

a novel platform for a sequential and controlled release of more than one drug, based on a pH triggered protonation mechanism.[62] Particularly, crystal violet (CV) loaded pNIPAm-co-AAc microgels and methylene blue (MB) loaded poly(N-isopropyl-acrylamide-3-(acrylamido)phenylboronic acid) (pNIPAm-co-APBA) microgels were used to construct reservoir devices. At pH 10.0, positively charged CV and MB exhibited strong electrostatic interactions with the negatively charged AAc and APBA-modified microgels, respectively. When the pH is 7.0, MB could be released only by the deprotonation of the APBA groups of the microgels. At an even lower pH of 3.0, the AAc groups of microgels are neutralized; as a result, the CV is released from the microgels. Such a system offered a versatile way of releasing small molecules sequentially in a pH-triggered fashion.

1.4.3.3 Light-responsive drug release

Besides the temperature and pH responsivity, light also has garnered significant interest as a polymer stimulus owing to its fast responsiveness, remote spatiotemporal control, non-invasiveness, in addition to an easy operation of wavelength, on/off frequency, intensity, illuminated area, and time.[114] Thus, light responsive polymers provide a promising approach in the application of drug delivery. Three different light responsive polymers can be used for a light triggered drug release system. In the first one, the use of reversible photo-switchable group functionalized polymers, such as

azobenzene functionalized polymers, can change their molecular structure reversibly at a different wavelength of light.[115] In the second one, irreversible photo-cleavable group functionalized polymers, in which the photo-cleavable bonds can be broken by light irradiation, are good candidate. For instance, Zhao and co-workers created a light-sensitive micelle based on the photolysis of a photolabile chromophore (*o*-nitro benzyl linkers) to achieve the stimulated delivery of Nile Red.[116] The last one is nanoparticles/polymers composites that can be responsive to light and control the drug release. For example, Kawano developed a novel near-infrared (NIR) sensitive gold nanorods/pNIPAm nanogels hybrid material.[117] Upon NIR-irradiation, the preload drug can be released rapidly by the shrinkage of gold nanorods/pNIPAm nanogels composites, thereby achieving light-controllable release behavior, which can indicate its promising therapeutic effect as a light-responsive drug delivery system. In this dissertation, light-responsive polymeric materials on the basis of *o*-nitro benzyl and its derivatives will be investigated in detail for the controlled drug delivery applications.

1.5 Research goals and thesis outline

The main goals of this thesis are using stimuli-responsive polymers and polymeric based devices to study drug delivery and sensing systems that are human health issues. To achieve these goals, the thesis was outlined as the following sections.

In Chapter 2, a description of microgel-based stretchable reservoir devices for

elongation enhanced small molecule release rate is given. Stretchable poly(N-isopropylacrylamide)-co-acrylic acid (pNIPAm-co-AAc) microgel-based reservoir devices were fabricated and used to control the release rate of the model drug tris(4-(dimethylamino)phenyl)methylium chloride (crystal violet, CV) into the solution. We demonstrated that the rate of release could be tuned by varying the Au layer thickness coating the microgels and by device elongation. The CV release kinetics was characterized by UV-vis spectra, which could transition from low ("off") to high ("on") when the devices are stretched. Such behavior could be exploited in future for autonomous release systems that release small molecules when stretched by natural processes, as in the movement of joints and muscles.

In Chapter 3, we developed a novel temperature/light-responsive poly(*N*-isopropylacrylamide-*co*-nitrobenzyl methacrylate) (pNIPAm-*co*-NBMA) microgel for the use of delivering the drug fluorescein. The prepared pNIPAm-*co*-NBMA microgels were characterized by dynamic light scattering (DLS), transmission electron microscopic (TEM), and fourier-transform infrared spectroscopy (FTIR). Moreover, we proved that either UV irradiation or heat can promote the on-demand release of a preloaded drug into the aqueous solution. It is well known that the stimuli-responsive polymers of pNIPAm and the photodegradation products of *o*-nitrobenzyl ester derivatives are non-cytotoxic, thus our novel pNIPAm-*co*-NBMA microgels could be employed extensively in the field of pharmaceutical sciences.

Chapter 4 followed the work in Chapter 3 and aimed at the controlled osteogenic differentiation of human mesenchymal stem cells (hMSCs) using dexamethasone-loaded pNIPAm-*co*-NBMA microgels. Dexamethasone (DEX) released by photo-responsive microgels was quantified further by liquid chromatography-mass spectrometry (LC-MS), and the controlled osteogenesis differentiation of hMSCs was performed by an alamarBlue assay and a normalized alkaline phosphatase (ALP) activity assay. Such DEX-loaded photo-responsive microgels were able to control hMSCs osteogenic differentiation upon light exposure, which has potential applications in bone tissue engineering.

Chapter 5 describes the study of chitosan-based supramolecular nanogels for pH and ATP competitive drug release. We demonstrated that chitosan-based supramolecular nanogels were prepared by crosslinking chitosan with glutaraldehyde via Schiff base reaction. The as-prepared supramolecular nanogels were characterized by DLS, TEM, nuclear magnetic resonance spectroscopy (NMR), and FTIR. The model drug, doxorubicin-hydrochloride (Dox-HCl), was loaded into supramolecular nanogels by hydrogen bonding interactions, and its release can be controlled via a conformational change when in an acid environment in the tumor cell (HepG2). The release profiles were conducted by fluorescence emission spectra. Finally, the cytotoxicity of supramolecular nanogels and the anticancer activity of the drug were performed by a Cell Counting Kit-8 assay (CCK-8). Such an pH and ATP-triggered drug release system provides a more

sophisticated drug delivery system as a result of the enhancing anticancer activity of drugs.

Chapter 6 describes the development of an optical sensor, based on poly(N-isopropylacrylamide) (pNIPAm)-microgels, for the analysis of volatile organic compounds, such as hexane, cyclohexane, chloroform, petroleum ether, and tetrahydrofuran (THF). pNIPAm-based microgels and etalon surfaces were characterized by DLS and SEM, respectively. The color change of the sensor was characterized and the cumulative peak shift of the wavelength was recorded using an optical reflectance probe. Among these vapors, the sensor showed high sensitivity and specificity towards THF, a short reaction time with limit of detection (LOD) of 1.27 mM, and was robust over at least three cycles.

The Chapter 7 concludes the results in the Chapter 2-6 and provides the future plan that should be carried out, and presents preliminary data of future work.

Chapter 2

Microgel-based Stretchable Reservoir Devices for Elongation Enhanced Small Molecule Release Rate

2.1 Introduction

Stimuli-responsive materials have found myriad applications, most important for the work here is their use for controlled/triggered drug delivery.[118, 119] Of the drug delivery systems that have been developed, triggered drug delivery systems have many advantages that allow them to be very effective for disease treatment, e.g., targeted delivery to tumors.[120-122] To trigger delivery, stimuli-responsive polymers/materials that respond to pH, temperature, light, ultrasound, magnetic field and electricity have been used.[10, 123-126] As such, many investigations have focused on generating biologically friendly hydrogels, microgels, and porous materials that can "encapsulate" small molecules (or drugs) and release them on demand in a controlled fashion.[127-130]

There are many known stimuli-responsive polymers that have found use for various

applications.[131-134] For example, the Moore group developed a spiropyran mechanophore-based polymeric material, in which the spiro C−O bond is cleaved selectively to generate merocyanine upon mechanical activation, resulting in the material developing a purple color.[135] Importantly, such mechanical force responsive materials can be good candidates for use in drug delivery systems, and ultimately coupled to muscle/joint movement for triggered release.[136-138] For instance, the Gu group generated a wearable, tensile strain-triggered drug delivery device consisting of a stretchable elastomer, which was integrated with poly(lactic-co-glycolic acid) (PLGA) microgels that can temporarily store drugs (e.g., doxorubicin). The release from the device could be associated with daily joint motions or intentional stretching of the elastomer film to promote the release of therapeutics from the materials.[61] What is more, the Grinstaff group utilized strain-induced crack propagation to result in triggered drug delivery.[139] Specifically, the anticancer drugs (e.g., cisplatin) were encapsulated between superhydrophobic electrosprayed microparticle coating polymers poly(glycerol monostearate carbonate-co-caprolactone) (PGC-C$_{18}$) as top layer, and poly(caprolactone) (PCL) as bottom layer, forming a "sandwich" structure. The entrapped drug was released in a manner that was controlled by the magnitude of applied strain due to the propagating patterned cracks in the coating. From the above discussion, we can conclude that there is a need for mechanoresponsive polymeric materials, which can have direct impacts in the fields of biology and medicine.

Poly (N-isopropylacrylamide) (pNIPAm) is the most extensively studied responsive polymer to date, which shows a temperature-induced volume phase transition at the lower critical solution temperature (LCST) of 32 °C.[51] That is, pNIPAm is fully soluble (swollen, extended state) in water <32 °C, while it transitions to a relatively insoluble (deswollen, collapsed state) when heated >32 °C; this transition is fully reversible over many cycles. pNIPAm-based nano and microparticles (called nanogels and microgels, respectively) can be easily synthesized via precipitation polymerization in the presence of a crosslinking agent. Like uncrosslinked pNIPAm, pNIPAm-based nanogels and microgels are responsive to temperature, collapsing (and decreasing in diameter) >32 °C. What is more, pNIPAm-based microgels can also be made responsive to additional stimuli via copolymerization with other functional monomers and/or crosslinkers, e.g., incorporation of acrylic acid (AAc) into the microgel structure can render their diameter responsive to solution pH.[140, 141] Specifically, AAc has a pK_a of 4.25, therefore when the solution pH > pK_a, the AAc groups are deprotonated (and negatively charged), which results in a swelling of the microgel due to Coulombic repulsion and osmotic swelling.[38] The negative charges of the pNIPAm-*co*-AAc microgels at high pH can also be used to bind positively charged small molecules (or drugs) that can be triggered to release by neutralizing the AAc group by decreasing the solution pH < pK_a.[38, 142, 143]

In previous work, we demonstrated that pNIPAm microgel-based devices (etalons) could be generated and used for sensing and biosensing, and triggered drug delivery.[58, 60,

[144] Etalons are composed of pNIPAm-based nanogels or microgels sandwiched between two thin gold (Au) layers (normally 15 nm), to yield the "mirror-dielectric-mirror" configuration of a classic etalon as shown in Figure. 2-1. Likewise, in previous work we demonstrated that the microgel layer of etalons can also serve as a "reservoir" to hold small molecules that can be triggered to release from the etalons in a pH-dependent fashion with the release rate being controlled by the porosity of the etalon's upper Au layer.[38, 145, 146] While these reservoir devices are unique in that they have a responsive microgel layer to allow modulation of the release and improved loading capacities, there are other examples of triggered release from Au-based devices. For example, the Wang group demonstrated that DNA modified ultramicroelectrodes could respond to various electrochemical parameters, inducing the release of DNA into a solution. Specifically, the Au microelectrodes were functionalized with thiolated DNA layers by exploiting the S-Au bond. When applying a potential of -1.3 V for only 2 min, the release of DNA was triggered by the electrochemically-induced cleavage of the S-Au bond at physiological pH. Thus, Au-based surfaces provide promising opportunities to control delivery of drugs and biomolecules to systems.[147, 148]
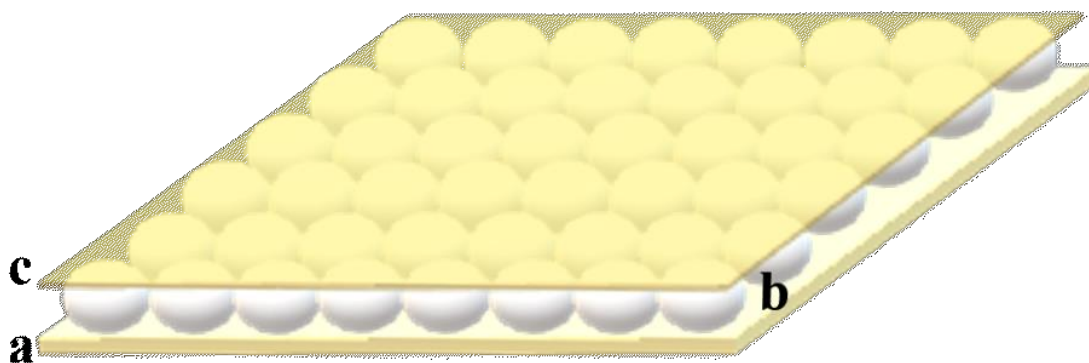
Figure 2-1. Etalon structure consisting of (a, c) Au layers sandwiching a (b) "jammed" layer of microgels, all on a support (typically glass).

While we have shown in numerous publications that triggered release from microgel-based etalons can be achieved by varying solution temperature, pH, and on application of an electric field,[149] here we show that mechanical stretching of etalons can be used to trigger small molecule release from etalons, and can control release rates. To achieve this, we generated etalon devices composed of pNIPAm-*co*-AAc microgels loaded with crystal violet (CV) on stretchable polydimethylsiloxane (PDMS) to allow for stretch-triggered release to a system. We were able to show that variations in etalon tensile elongation and Au overlayer thickness could be used to turn on and off release, as well as to control the CV release rate from the etalons. Specifically, the extent of etalon stretching, and the Au overlayer thickness, can both be used to control the release rate of small molecules from etalons. That is, stretched etalons can release faster than unstretched etalons due to stretch-induced crack formation that allows for facile exit of

CV out of the microgel layer after the acid solution enters the microgel layer to neutralize the AAc. Additionally, thicker Au overlayers lead to a reduction in the CV release rate from both stretched and unstretched etalons. Finally, we demonstrated that the release can be turned on by stretching and turned off by allowing the material to return to its initial state. Such stretchable etalon devices provide an alternative way to promote the small molecule release to systems that can aid in therapy.

2.2 Experimental Sections

2.2.1 Materials

N-isopropylacrylamide (NIPAm) was purchased from TCI (Portland, Oregon) and purified by recrystallization from hexane (ACS reagent grade, EMD, Gibbstown, NJ) prior to use. *N,N*'-methylenebisacrylamide (BIS) (~99%), acrylic acid (AAc) (~99%), and ammonium persulfate (APS) (~98%) were obtained from Sigma-Aldrich (Oakville, Ontario) and were used as received. Sylgard 184 silicone elastomer base and Sylgard 184 silicone elastomer curing agent were purchased from Dow Corning Corporation, Midland, MI, USA. Crystal violet was obtained from Sigma (St. Louis, MO). Deionized (DI) water, with 18.2 MΩ·cm resistivity, was obtained from a Millipore Milli-Q-Plus system (Billerica, MA). Sodium hydroxide (NaOH) and hydrochloric acid (HCl) were purchased from Caledon Chemicals (Georgetown, Ontario) and were used as received. Au was

99.99% and Cr was 99.999% that were obtained from ESPI Company (Ashland, OR) and MRCS Canada (Edmonton, AB), respectively. Glass slides were obtained from Fisher Scientific (Ottawa, Ontario) and cut into pieces (25×25 mm). Glass wool for filtration was obtained from Sigma-Aldrich (Oakville, Ontario).

2.2.2 Synthesis and Characterization of Poly (*N*-isopropylacrylamide)-*co*-acrylic acid Microgels

Poly (*N*-isopropylacrylamide)-*co*-acrylic acid (pNIPAm-*co*-AAc) microgels composed of 10% AAc were synthesized via free-radical precipitation polymerization as described in previous work.[150] Initially, the monomer NIPAm (11.9 mmol), and crosslinker BIS (0.703 mmol) were dissolved in deionized water (99 mL) with stirring in a clean beaker for 30 min. The mixture was then filtered through a 20-mL syringe affixed to 0.2 μm filter into a 250 mL 3-neck round-bottom flask. Subsequently, the 3-neck round-bottom flask was equipped with a thermometer, a reflux condenser and a N_2 gas inlet. The solution was stirred (500 rpm) while bubbling N_2 gas through the solution and heating to 70 °C for 1 h. Solutions of AAc (1.43 mmol) and APS (0.2 mmol) were then added to the solution in sequence via a pipet. Free radical precipitation polymerization was allowed to proceed for 4 h at 70 °C under nitrogen gas atmosphere. After polymerization, the solution was allowed to cool to room temperature overnight and

filtered through glass wool to remove any large aggregates. Finally, the resultant microgel

solution was centrifuged (~11000 rpm, 21 °C) and resuspended in fresh DI water 6 times

to remove unreacted monomer and linear polymer. The microgels were characterized via

dynamic light scattering (DLS) and showed a diameter of 1149 nm and 681 nm at pH 6.5

and pH 3, respectively which are displayed in Figure 2-2. The pH responsivity of the

microgels are a result of the microgel AAc groups deprotonated (pH 6.5) and protonated

(pH 3), causing the microgels to swell and collapse, respectively.
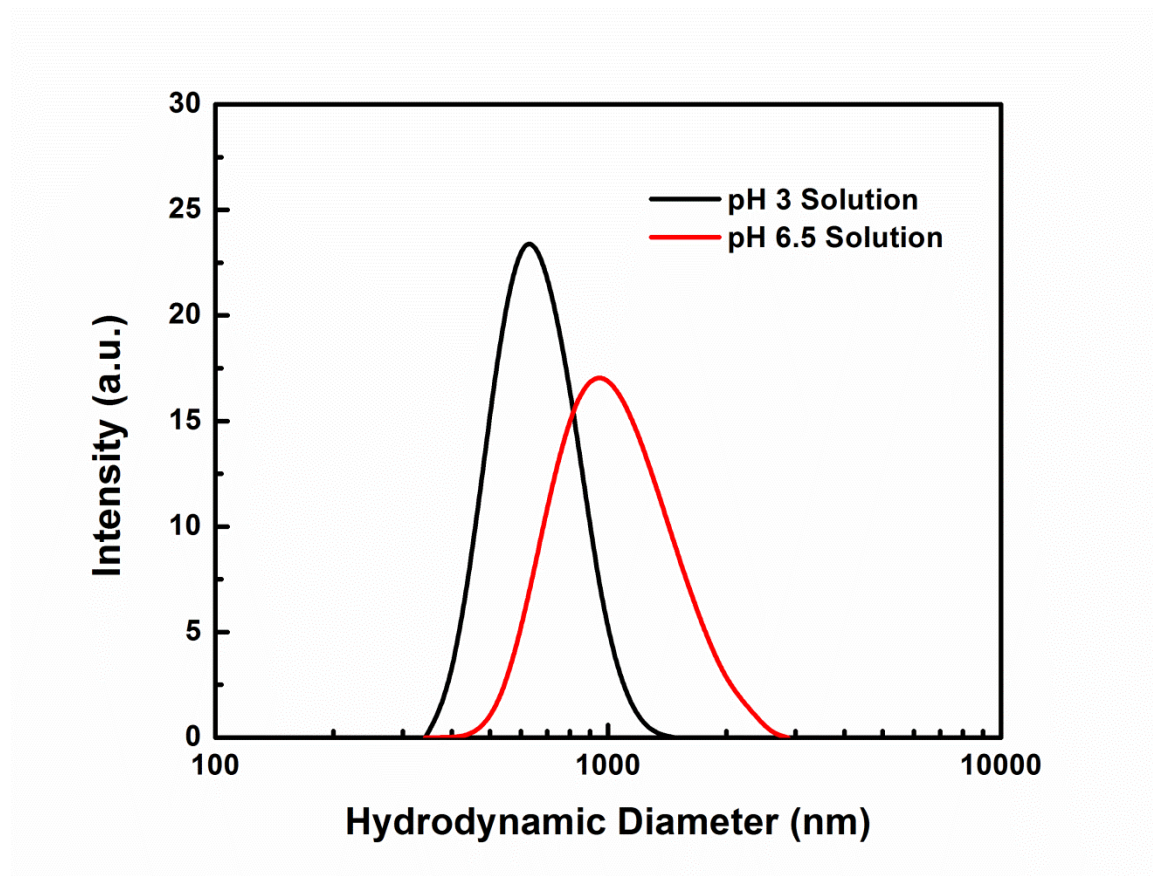
Figure 2-2. DLS measurements of prepared microgels at different pHs

2.2.3 CV-Loaded Stretchable Etalon Fabrication

Etalons immobilized on PDMS were prepared by following a previously reported procedure, with slight modification.[151] Initially, the PDMS substrate was generated by mixing silicone elastomer base and curing agent in a glass Petri dish with mass ratio of 10:1, respectively, and left overnight at 70 °C. Square pieces of PDMS were cut out of the mold with sizes of 20 mm x 10 mm with 0.5 mm thickness. The cut PDMS was rinsed with DI water, ethanol, and dried with N_2 gas, followed by deposition of 2 nm Cr then 15 nm of Au via thermal evaporation (Torr International Inc., Model THEUPG, New Windsor, NY). Subsequently, 40 μL of the concentrated microgel solution was transferred to the Au-coated PDMS substrate and spread over the whole surface using a micropipette tip. The microgel solution was allowed to dry completely at 35 °C for 2 h. After that, the dry films were rinsed with DI water to remove any excess microgels that were not bound directly to the Au film and dried with N_2 gas. To load the microgels with CV, the resultant microgel-coated surfaces were soaked in a CV solution (2 mg/mL, pH of 6.5) overnight. At this pH, the negative charges on the deprotonated AAc can bind the positively charged CV electrostatically. The substrates were then rinsed with pH 6.5 solution to remove excess CV not bound to the microgels, and incubated in pH 6.5 solution for 1 h followed by drying with N_2 gas. Finally, 2 nm Cr and either 50 or 120 nm of Au overlayer were deposited on the CV-loaded microgel layer. After the stretchable etalons were successfully fabricated with initial length (L_0), they were stretched to a certain length (L_1),

added to pH 3.0 solution, and the release of CV monitored. A schematic illustration of the process is shown in Scheme 2-1. Scanning electron microscopy (SEM) was used to image the etalons using a Zeiss Sigma Field Emission SEM, operated at 20 kV. UV-Vis spectra were collected using an Agilent 8453 UV-Vis spectrophotometer, equipped with an 89090A temperature controller and Peltier heating device.

2.2.4 CV Release Experiments

CV release experiments were conducted in pH 3 solution to trigger the release of CV from the microgels. Again, at this pH, the AAc groups were protonated (and neutralized) allowing for CV to be released from the microgels. An in house constructed device was used to stretch the PDMS-immobilized etalons to different (but well defined) lengths. The edges of stretchable etalon were sealed with nail polish, in order to hinder CV release from the edges, and promote release through the top Au layer. To characterize the release, 40 mL of pH 3.0 water (ionic strength of 2 mM) was stirred continuously at 300 rpm using a magnetic stir bar, with the solution temperature maintained at 25 °C. This solution was flowed through a UV-vis spectrometer using a peristaltic pump and a flow cell for 5 min for stabilization, then the dry etalons stretched to different lengths (tensile elongations of 1 mm, 3mm and 5mm) were added to the solution and UV-vis spectra collected every 30 sec. We point out that the solution was recirculated to maintain a

constant solution volume. The flow rate of the solution was set to a constant value, and measured to be 0.042 mL/s. Finally, the cumulative release ratio profiles, which is the ratio of the amount of CV released and total released CV at different times, were obtained.

2.3 Results and Discussion

As outlined above, stretchable pNIPAm-*co*-AAc microgel-based etalons were constructed, and the kinetics of CV release from the devices (stretched to varying degrees) investigated as the devices were triggered to release by exposing them to pH 3.0 solution. Again, at pH 6.5 the positively charged CV is electrostatically bound to the deprotonated AAc groups, while the AAc is neutralized and CV is released from the microgels at pH 3.0. When the CV exits the microgels, it diffuses through the pores of the etalon's upper Au layer, and here we hypothesize that stretching-induced cracks will allow CV to exit the etalons faster than if the etalon is unstretched. This is depicted schematically in Figure 2-3.

The morphology of the Au overlayer of etalons immobilized on PDMS was greatly impacted by stretching. Specifically, before stretching the "as-deposited" Au layers appeared relatively flat, with micron-scale "Au islands". When the etalon was imaged while stretched, the number of "islands" concomitantly increased as a result of crack formation.[152] Here, we confirmed that stretching of the etalon can indeed cause cracking

of the etalon's upper Au layer by collecting scanning electron microscopy (SEM) images of the etalon before and after stretching. As can be seen in Figure. 2-4(a), the surface of the etalon on PDMS was relatively smooth and flat, and exhibited the Au islands. While the Au layer exhibited many more islands after stretching to 5 mm and relaxation, as can be seen in Figure 2-4(b). In fact, previous investigations from Tricoli and coworkers have also shown that increasing elongation can indeed increase the crack number and dimensions.[153] Taken together, we hypothesize that a larger number of cracks will lead to faster release of CV from the etalons.
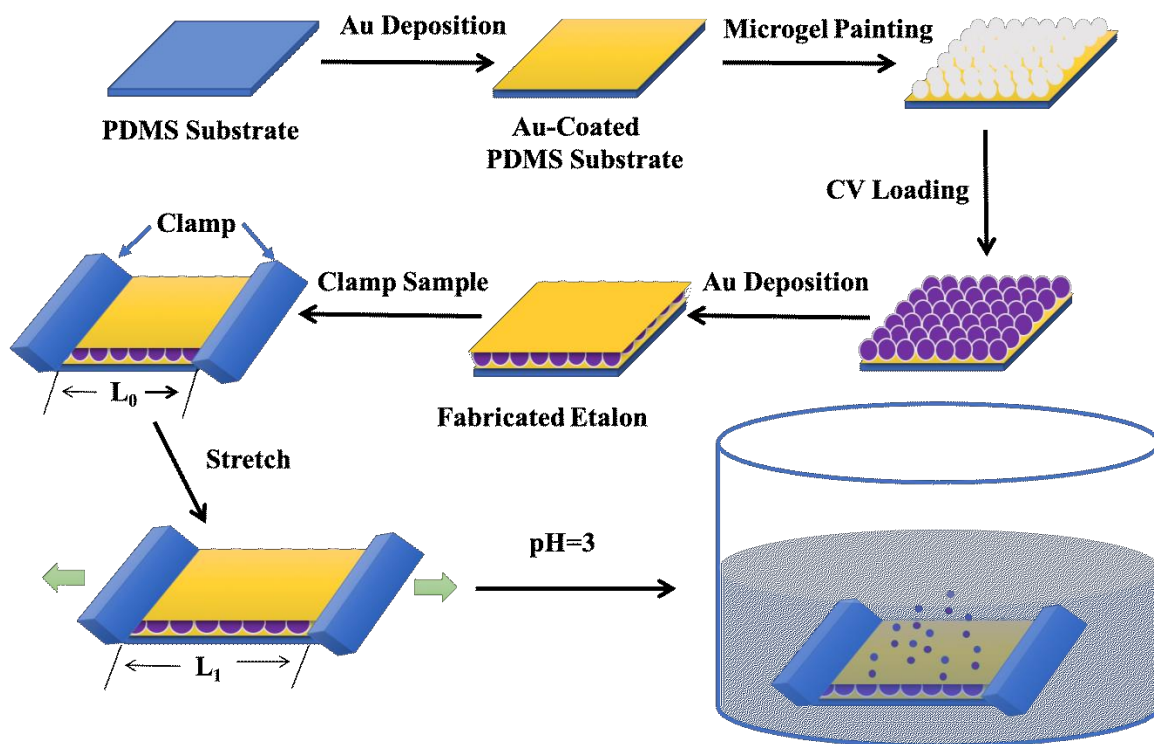
Scheme 2-1. Schematic of the fabrication of CV molecule (drug) loaded PDMS-based etalons and the release process. L_0 and L_1 are the initial and stretched length of etalon, respectively.

Stretch

Release

Release dominated by pores

Release dominated by cracks
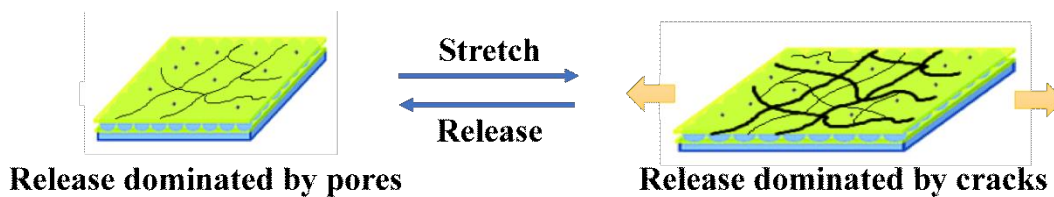
Figure 2-3. Proposed mechanism of stretch-induced release from etalons. When stretched, the crack number increases, allowing for faster CV release from the etalons.

(a) **(b)**
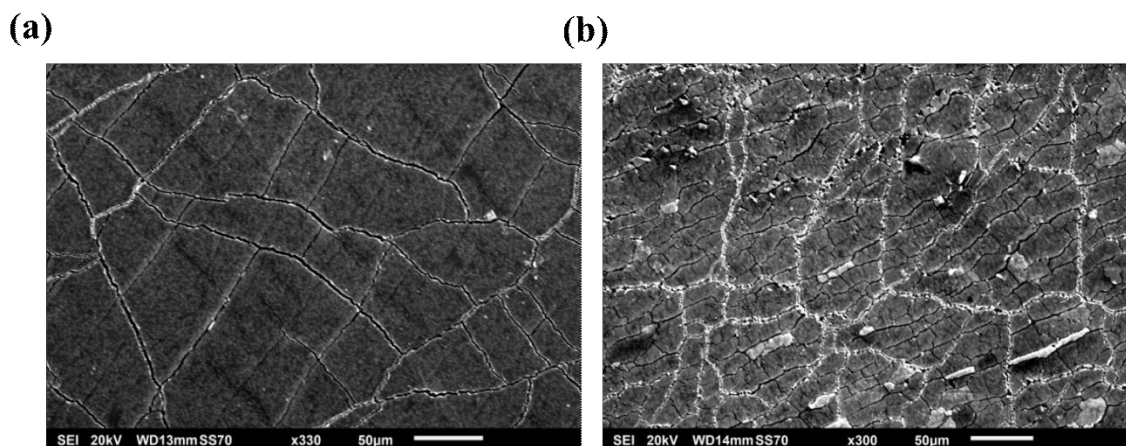
Figure 2-4. SEM image of the surface of the etalon immobilized on PDMS (a) before and (b) after stretching 5 mm and relaxation

To investigate the release kinetics, and how they depend on stretching, we immersed the elongated devices (1 mm, 3 mm, and 5 mm elongation) in pH 3.0 solution and tracked the CV release by collecting absorbance spectra using a UV-vis spectrometer as a function of time. We point out here, that we investigated the impact elongation had on the CV release kinetics for etalons with 50 or 120 nm of Au deposited on the CV-loaded microgel layer. This was done in order to tune the unstretched CV release kinetics (thinner Au releases faster than thicker Au), and understand how the Au thickness impacts

how stretching influences the release rate. As can be seen in Figure 2-5, for the 50 nm Au coated device, elongation had a significant impact on the release kinetics. When the dry CV-loaded etalons were directly added to pH 3 solutions, the first 3 min of release were similar for both the stretched and unstretched etalons, which is likely a result of the etalon hydration process, and perhaps non-specifically bound CV releasing to the solution. This phase of release is followed by release kinetics that are dependent on how much the etalon was stretched; CV release kinetics increased with stretching, and reached a maximum at the highest elongation we probed of 5 mm that took only ~15 min to release to its maximum capacity. Fitting an exponential equation (increasing form) to the release curves of stretched etalons, we were able to determine release rate constants (K), which can be seen in Table 2-1.
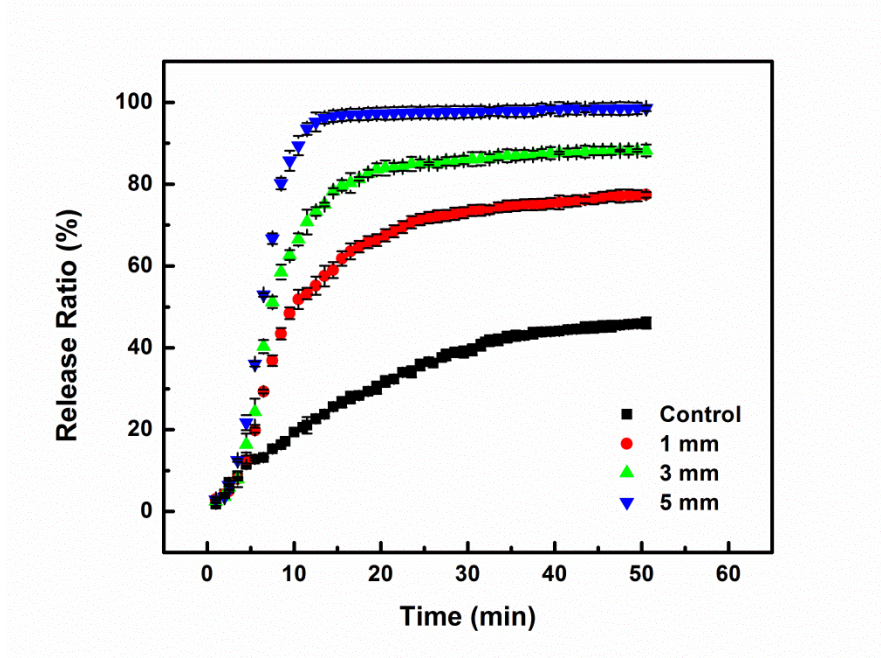
Figure 2-5. Release profiles for the PDMS-based etalon devices with different tensile

56

elongations with 50 nm Au overlayers

Table 2-1. Release rate constants (K) as a function of elongation for etalons with 50 and

120 nm Au overlayers

Elongation, (mm)	50 nm Au overlayer, K(Abs/min)	120 nm Au overlayer, K(Abs/min)
1	0.140	0.078
3	0.185	0.097
5	0.261	0.130

As can be seen in Table 2-1, for elongations investigated, the release rates (K) for

the devices with 50 nm Au overlayers were all higher than the devices with 120 nm Au

overlayers. These data are also plotted in Figure 2-6. Based on these results, we can

conclude that increased release kinetics can indeed be achieved by elongation, likely due

to crack formation that allows the pH 3.0 solution easier access to the microgels for their

neutralization and more efficient release of CV through the upper Au layer.
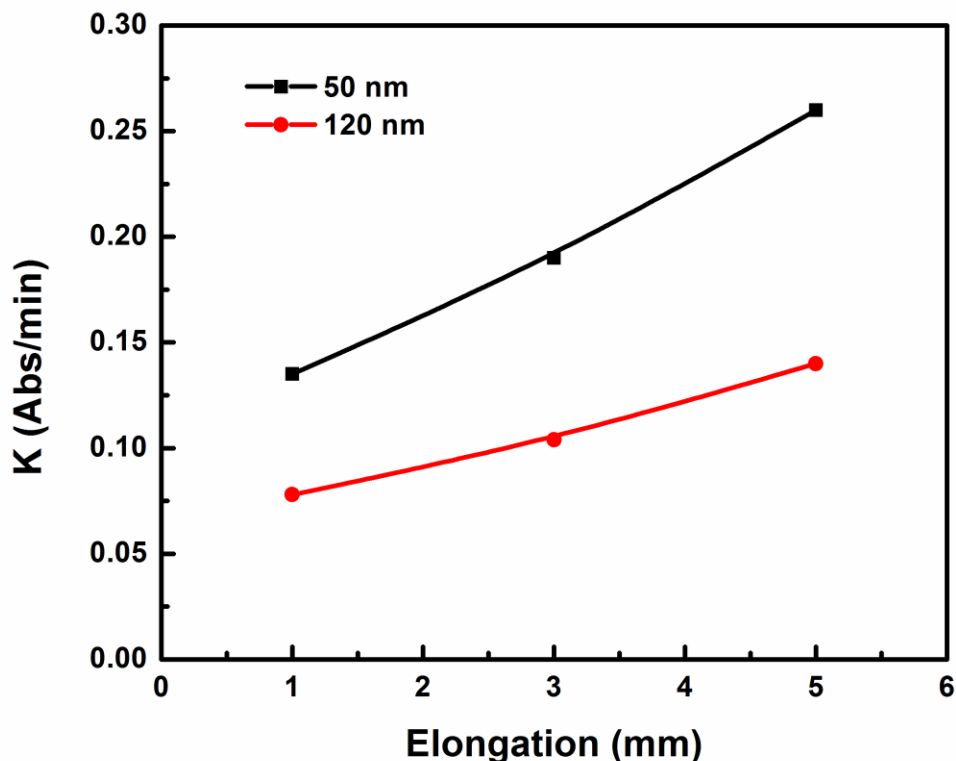
Figure 2-6. The release rate constant (K) as a function of elongation with different Au-overlayer thickness (■)50 nm and (●)120 nm

Interestingly, we found that etalons composed of 120 nm Au overlayer behaved in a slightly different manner on elongation compared to the etalons composed of 50 nm Au overlayer. As shown in previous studies, thick Au overlayers are less porous than thin layers that decreases the release kinetics. We believe that this is primarily a result of the pH 3.0 solution requiring more time to pass through the thicker (and less porous) Au and enter the microgel layer to neutralize the AAc. Likewise, the CV needs more time to travel through the thicker (and less porous Au) to enter the solution.[38, 154] Figure 2-7 shows the release ratios for the etalons composed of 2 different Au overlayer thicknesses,

as a function of elongation. As can be seen in Figure 2-7(a), when the etalons were unstretched, the release profiles were very similar, although the 120 nm devices release slightly slower than the 50 nm device. In this case, the release from the devices is dominated by the native pores and cracks of the Au layer of the etalon. Particularly, Figure 2-7(b) shows the release profiles for the devices at 1 mm elongation. In this case, the release kinetics are dramatically increased in both cases when the devices are stretched, although the 50 nm Au coated etalon appears to release faster than the 120 nm Au coated etalon. The results indicate that the cracks induced from elongation are allowing the CV to come out of the device faster, although the pores in the Au overlayer are still playing a role in the observed release kinetics as the etalon with the thicker Au layer releases slower than the 50 nm Au overlayer device. The data in Figure 2-7(c) at 3 mm elongation follows the same trend, although we noted that the release profiles for the different thicknesses were more similar than they were for the 1 mm elongation, while the release profiles in Figure 2-7(d) for the 5 mm elongation were even more similar. From these observations, we hypothesize that the release profiles for the different Au overlayer thicknesses are dominated by the pore size and number when the devices are unstretched (or stretched by small amounts), while the cracks are so extensive in number (and relatively large) at high elongation, that the pores do not play a large role on the release kinetics, hence the release profiles for the devices with different Au overlayer thicknesses become similar. Therefore, thicker Au overlayers yield slower release kinetics for all

59

elongations investigated here. Such different tensile elongations and the thickness of the Au overlayer of etalon are crucial to control the release kinetics rate of CV molecules. Here, the videos of CV molecules release by unstretched and stretched etalon in pH 3 solutions were shown in Video A-1 and Video A-2. We can clearly see that CV molecules can be released in pH 3 solutions via stretched etalon. However, we cannot apparently observe the release of CV molecules from unstretched etalon in the same condition by our naked eyes since CV molecules could come out through the pores of Au-overlayer instead of cracks.
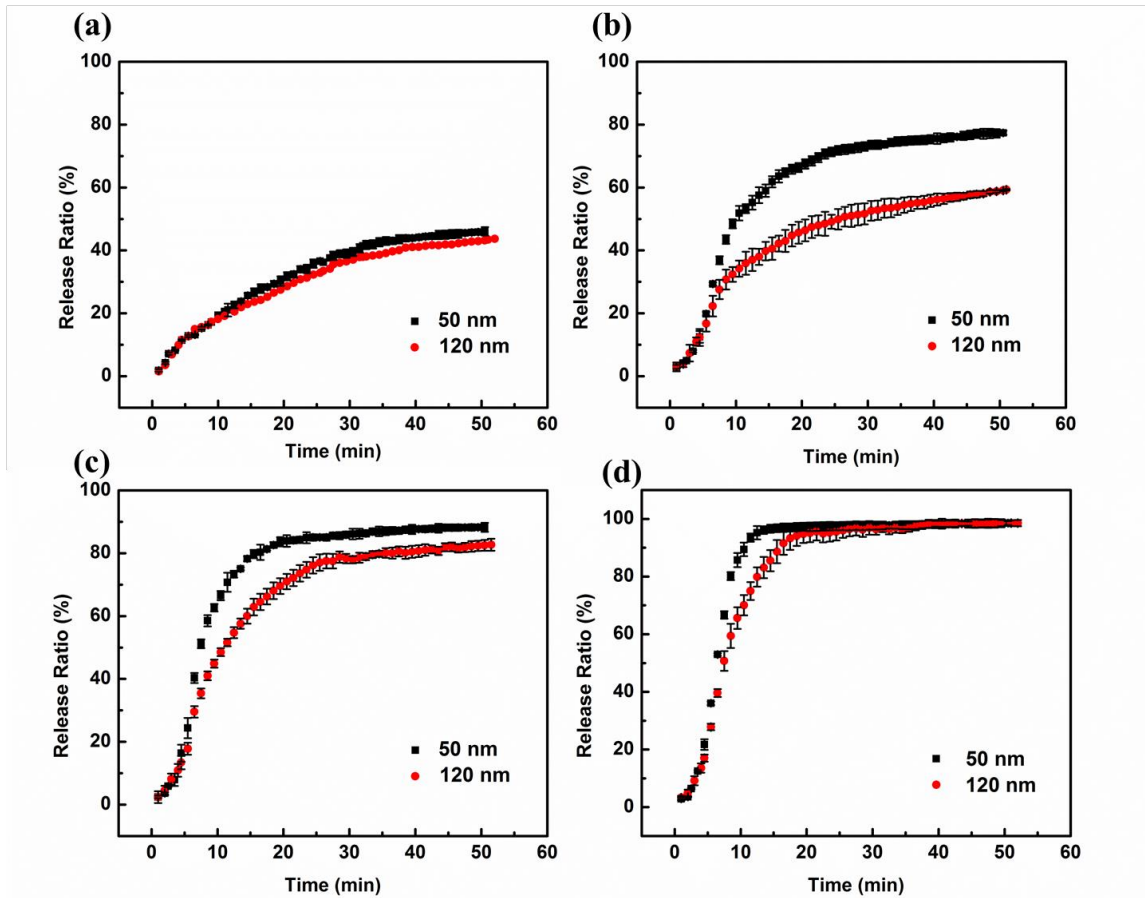
Figure 2-7. Release profiles for stretchable etalon devices with (■)50 nm and (●)120 nm

Au overlayers (a) unstretched, and (b) 1mm, (c) 3mm, (d) 5mm elongations.

Video A-1. CV molecules release video from the unstretched etalon in pH 3 solutions

Finally, we showed that the release of CV to our system could be turned "on" and "off" by stretching and relaxation of the etalon, respectively. Specifically, as can be seen in Figure 2-8, CV can be released to solution when the device was stretched, while the release was halted when the devices were released. We also showed that this on/off behavior can be induced over many cycles. Such stretchable etalons provide a promising new mechanism for achieving mechanical force-induced drug delivery.
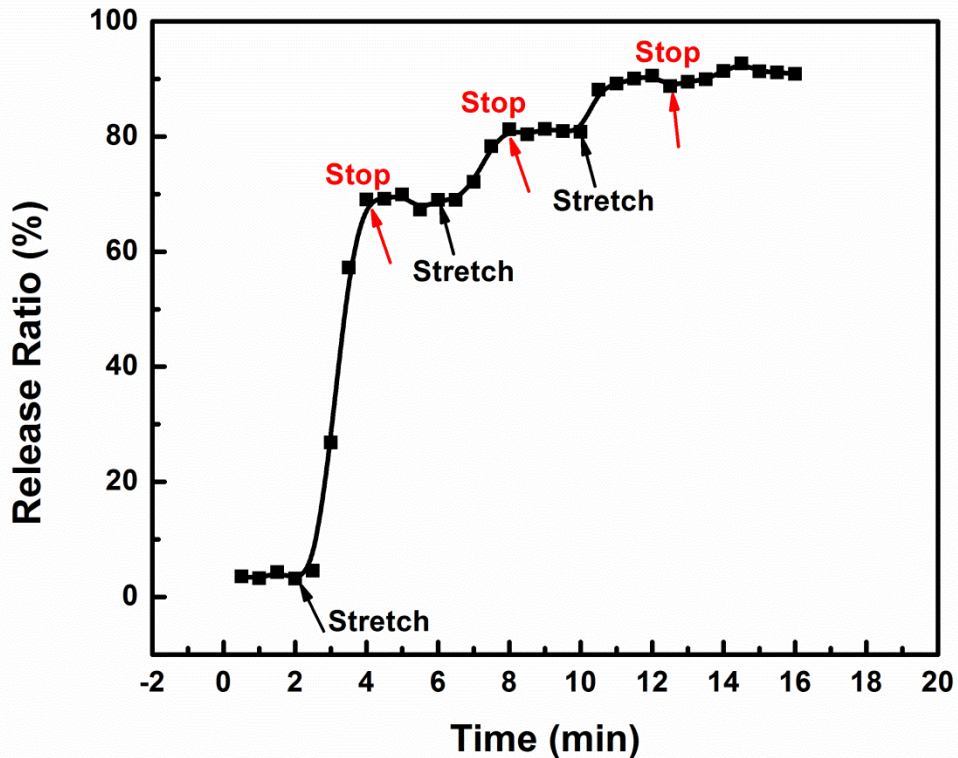
Figure 2-8. Mechanical force triggered controlled release profiles from stretchable etalon

devices. The etalon was stretched by 5 mm elongations for each time.

2.4 Conclusions

In summary, a stretchable pNIPAm-co-10%AAc microgel- based etalon immobilized on PDMS was fabricated, and elongation was used to control the CV release rate to aqueous solution. Specifically, CV was preloaded into the microgels by exploiting electrostatic interactions between the negatively charged microgels and the positively charged CV at pH 6.5. When the devices were exposed to a pH 3.0 solution, CV could be released from the device and release rates were determined at different device elongations of (1, 3, and 5 mm) and Au overlayer thickness (50 and 120 nm). We observed the release rate to be high for devices with thin Au overlayers and high elongation, while thick Au overlayers, and low elongation slowed the release rate. Based on our findings, we propose that the release is dominated by the Au pores at low elongations, while release through the stretching-induced cracks is dominant when elongations are high. We also showed that the release can be turned "on" and "off "by stretching and relaxation, respectively. Hence, this behavior can be used to achieve release via a ubiquitous daily motion that induces device stretching and small molecule release.

Chapter 3

Triggered Small Molecule Release from Dual-Stimuli Responsive Microgels

3.1 Introduction

Stimuli-responsive polymers have found their way into numerous technologies, and have numerous health care and biomedical applications.[122, 123, 155] For example, they can be used for tissue engineering, biological imaging and controlled drug delivery.[114, 156-159] The breadth of their applications is in part due to their ability to be rendered responsive to a myriad of stimuli, including: pH, temperature, light, ultrasound, magnetic field, electric field, and enzymes.[149, 160-166] While stimuli-responsive polymers can take on many different forms, e.g., hydrogels, micelles and nanocapsules, stimuli-responsive hydrogel particles (microgels) are used here for triggered small molecule delivery. Indeed, it is the case that microgels have been used for small molecule/drug delivery,[119] although here we show that light responsive microgels can be used to release small molecules in a light triggered fashion.

Microgels are crosslinked hydrogel particles with diameters on the micrometer scale, and have many properties that render them ideal for biomedical applications, e.g., they

are highly porous, highly water swellable, and have mechanical properties that approach living tissue.[44, 167] Additionally, they are relatively easy to modify chemically to achieve diverse applications, e.g., controlled drug delivery systems.[168] Among them, poly (*N*-isopropylacrylamide) (pNIPAm)-based microgels are the most extensively studied to date. pNIPAm-based microgels are well known to exhibit thermoresponsivity, i.e., pNIPAm microgels are fully soluble in (and swollen with) water at a temperature below 32 °C, and collapse (expel their water) when the water temperature exceeds 32 °C. The temperature of the transition is referred to as the lower critical solution temperature (LCST) of 32 °C, and the transition is fully reversible over many cycles. Since the LCST of pNIPAm is close to physiological temperature, pNIPAm-based microgels have been explored for *in vivo* controlled drug delivery applications.[58, 60, 169]

Besides the above-mentioned temperature responsivity, light has also garnered significant interest as a polymer stimulus. Light can be used to trigger polymer responses remotely, and by tailoring the light intensity, position, and on/off frequency, one can readily impact the polymer response. For instance,[170, 171] Zhao and co-workers created light-sensitive micelles based on the photolysis of a photolabile chromophore to achieve the stimulated delivery of Nile Red. Lu and coworkers developed a novel DNA aptamer-grafted photoresponsive hyperbranched polymer that can self-assemble into nanoparticles, followed by loading their loading of Nile Red or doxorubicin into the as-prepared nanoassembly. Upon UV-irradiation, the small molecule/drug can be rapidly

released by disassembly of the self-assembled nanoparticles, thereby achieving light-controllable release, which can be used as a smart drug delivery system. Recently, *o*-nitrobenzyl ester (*O*-NBE) derivatives are investigated to achieve light-triggered small molecule release. *O*-NBE derivatives are known to undergo ultraviolet (UV) light-induced photolysis, and have been used in the past to control the release of small-molecule drugs and biomolecules (e.g., proteins and oligonucleotides) from various materials.[47] Compared to other light-responsive functional groups with spiropyran and azo groups, *O*-NBE derivatives have several benefits which make them more preferable: long-term stability under ambient light, fast degradation kinetics, efficiently cleaved under UV irradiation. and good biocompatibility of photodegradation products.[48] Therefore, *O*-NBE derivatives become excellent candidates in terms of designing microgels for light-stimulated drug delivery systems.

Here, we explore the use of *o*-nitrobenzyl ester (*O*-NBE) derivatives to achieve light-triggered small molecule release. As mentioned above, *O*-NBE derivatives have several benefits that make them appealing to use, hence we generated *O*-NBE-modified pNIPAm-based microgels to achieve light triggered small molecule release. Poly(*N*-isopropylacrylamide- *co*-nitrobenzyl methacrylate) (pNIPAm-*co*-NBMA) microgels were synthesized via free radical precipitation polymerization and characterized by dynamic light scattering (DLS), transmission electron microscopy (TEM), UV-Vis spectroscopy (UV) and differential scanning calorimetry (DSC). The

pNIPAm-*co*-NBMA microgels were then loaded with fluorescein that was used as a model drug, via its interaction with the relatively hydrophobic NBMA group. We then showed that the microgels could release fluorescein in a light (or heat) triggered fashion, as depicted in Scheme 3-1. We concluded that the light-triggered release was a result of the photolysis of the NBMA group, which facilitated the fluorescein release, while the temperature triggered release was due to the collapse of the microgels pushing out the fluorescein. Importantly, this novel dual-stimuli responsive pNIPAm-*co*-NBMA microgels provide a new approach to controlling the release of small-molecule drug by exploiting external stimuli trigger.
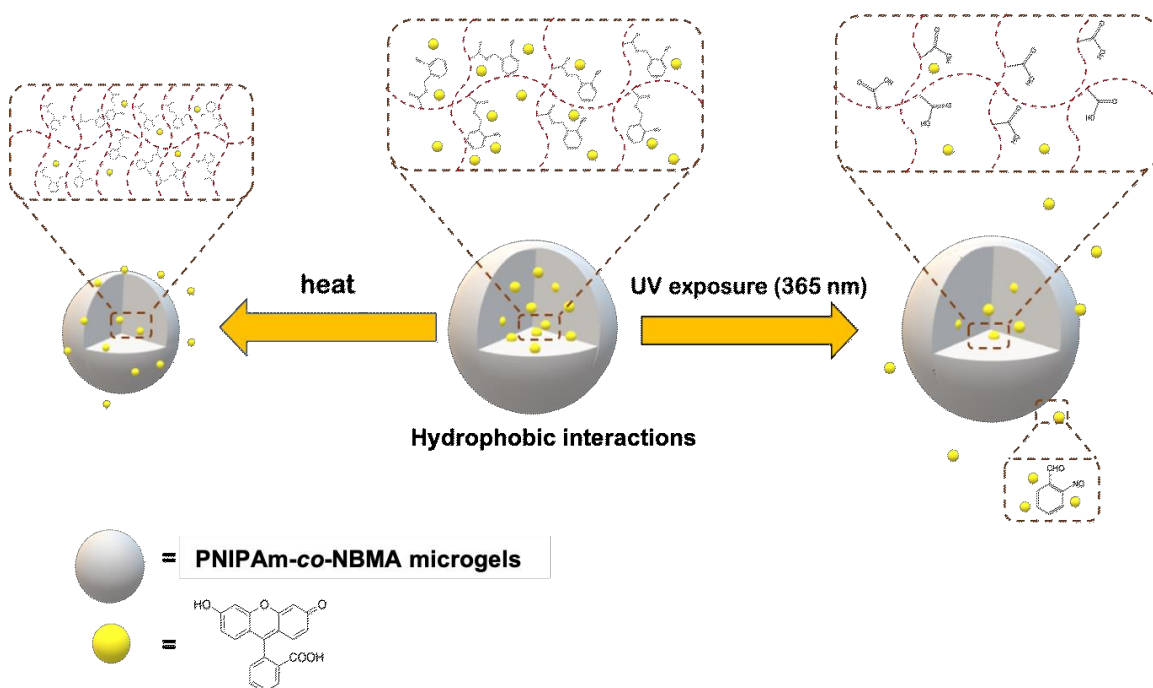
Scheme 3-1. Schematic of the dual stimuli (UV-light and temperature) triggered release of fluorescein molecules (drug) loaded pNIPAm-*co*-NBMA microgels.

3.2 Experimental Section

3.2.1 Materials

N-isopropylacrylamide (NIPAm) was purchased from TCI (Portland, Oregon) and purified by recrystallization from hexane (ACS reagent grade, EMD, Gibbstown, NJ) prior to use. *N,N'*-methylenebisacrylamide (BIS) (~99%) and ammonium persulfate (APS) (~98%) were obtained from Sigma-Aldrich (Oakville, Ontario) and were used as received. *o*-nitrobenzyl methacrylate (NBMA) (~95%) was purchased from Polysciences, Inc (Warrington, PA). The hydrophobic model drug fluorescein was obtained from Fisher Scientific. Deionized (DI) water with 18.2 MΩ·cm resistivity was from a Millipore Milli-Q-Plus system (Billerica, MA).

3.2.2 Synthesis of pNIPAm-*co*-NBMA Microgels

Microgels composed of poly(*N*-isopropylacrylamide-*co*-nitrobenzyl methacrylate) (pNIPAm-*co*-NBMA) were synthesized via free radical precipitation polymerization similarly to our previously published protocols with minor modifications.[38, 150] The reaction scheme can be found in Figure 3-1. The pNIPAm-*co*-NBMA microgels consisted of 85% *N*-isopropylacrylamide (NIPAm), 10% *o*-nitrobenzyl methacrylate (NBMA) and 5% *N,N'*-methylenebis(acrylamide) (BIS) as the cross-linker. First, the monomers NIPAm (3.2992 mmol) and NBMA (0.3965 mmol), as well as the cross-linker BIS (0.1949

mmol), were dissolved in deionized water (29 mL) with stirring in a beaker. After stirring for 30 minutes, the monomer mixture solution was transferred into a 3-neck round-bottom-flask equipped with a nitrogen gas inlet, a reflux condenser, and a thermometer. Then, the solution was degassed with nitrogen gas for 1 h with vigorous stirring, and the temperature was slowly increased to 70 °C during this period. Afterwards a 1-mL aqueous solution containing APS (0.0456 g) was introduced into the reaction mixture to initiate the polymerization. The reaction was allowed to proceed for 4 hours at 70 °C under nitrogen gas atmosphere. After polymerization, the reaction mixture was allowed to cool to room temperature and filtered through Whatman #1 filter paper to remove any large aggregates. The filtered microgels solution was purified via centrifugation at 10, 000 rpm for six times and concentrated in aluminum foil-wrapped centrifuge tubes to avoid any potential light-induced degradation of microgels.
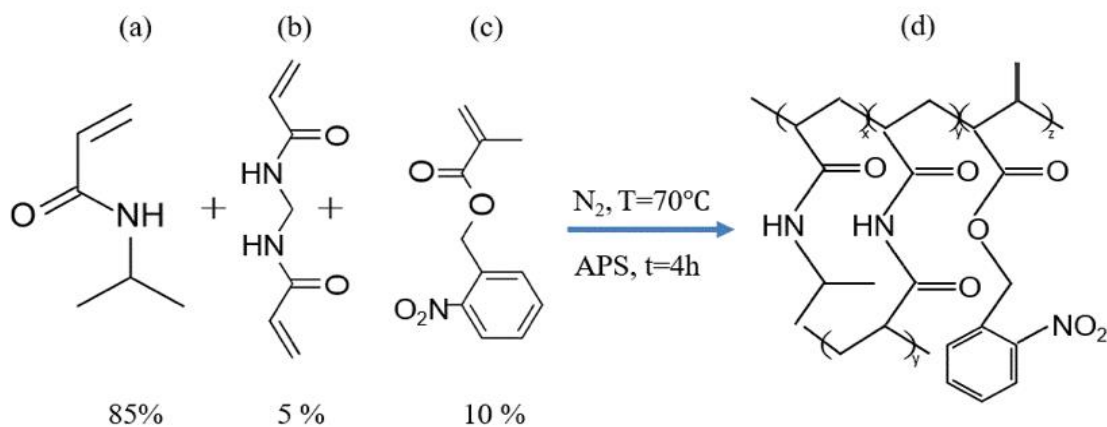
Figure 3-1. Synthesis of pNIPAm-*co*-NBMA microgels. (**a**) NIPAm, (**b**) the crosslinker BIS, and (**c**) NBMA were copolymerized via free radical precipitation polymerization to

yield (**d**) pNIPAm-*co*-NBMA microgels

3.2.3 Instrumentation

Morphologies of pNIPAm-*co*-NBMA microgels were characterized using a JEM-2010 EX/S transmission electron microscopic (TEM). The hydrodynamic diameter of the microgels was obtained by dynamic light scattering (DLS) measurements using a commercial Zetasizer Nano ZS - Malvern Instrument (Westborough, MA, USA) equipped with a light source with wavelength of 633 nm. UV-Vis spectra were obtained by a Hewlett Packard 8453 UV-VIS Spectrophotometer. Fourier-transform infrared spectroscopy (FTIR) of lyophilized microgels was performed by a Thermo Nicolet 8700 FTIR Spectrometer. Differential Scanning Calorimetry profile was characterized by a Perkin Elmer Pyris 1 DSC Differential Scanning Calorimeter. The fluorescence emission spectra of fluorescein were obtained using a Photon Technology International (PTI) MP1 Fluorescence System with an excitation wavelength of 437 nm. Fluorescence emission spectra were collected within the range of 450-600 nm. The fluorescence images of fluorescein-loaded microgels were captured by the fluorescence microscopy using an Olympus IX71 Inverted Research Microscope.

3.2.4 Loading of Fluorescein into pNIPAm-*co*-NBMA Microgels

The single emulsion method was used to load the hydrophobic model drug fluorescein into pNIPAm-*co*-NBMA microgels.[172, 173] Firstly, lyophilized pNIPAm-*co*-NBMA microgels (25 mg) and fluorescein (1 mg) were dissolved in 2.5 mL of a 3:2 mixture of dichloromethane and acetone. The solution was then added to 25 mL of DI H_2O. The mixture was stirred at 500 rpm for 10 minutes and then sonicated for 30 seconds to generate an oil-in-water (o/w) emulsion. The stable emulsion was stirred at room temperature overnight to evaporate the organic solvents. After removing the organic solvents, the fluorescein-loaded microgels were collected and purified by multiple rounds of centrifugation and washing with DI H_2O. The loading efficiency was determined by measuring the absorbance spectra of the suspension of fluorescein-loaded microgels in water and the supernatant of centrifuged fluorescein-loaded microgels (19.1%), which was shown in Figure 3-2.
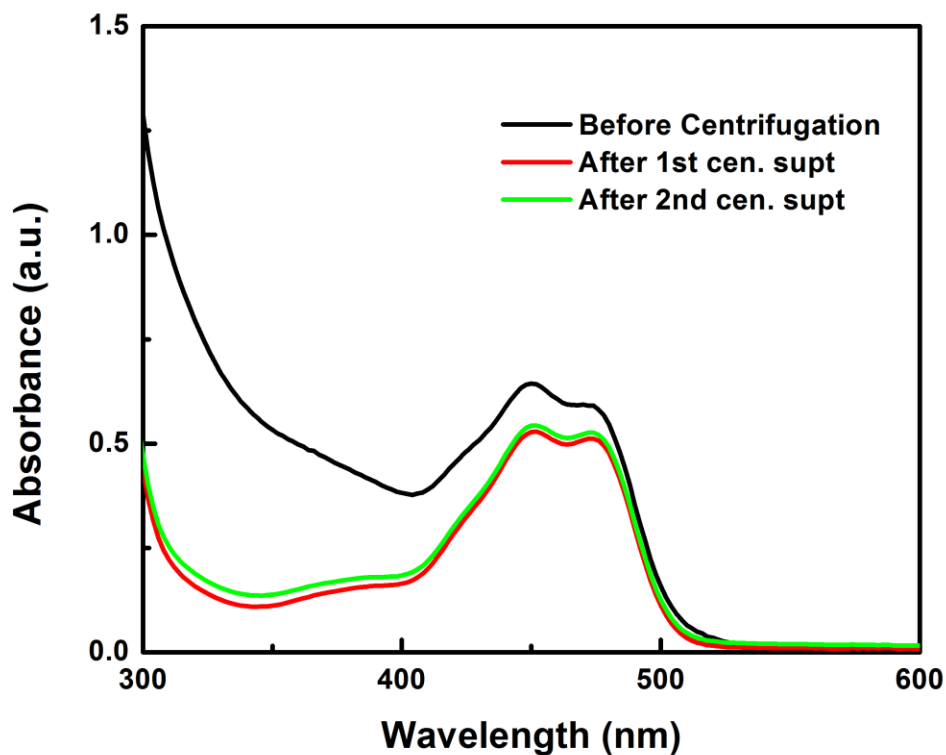
Figure 3-2. Determination of loading efficiency of fluorescein into pNIPAm-*co*-NBMA microgels by UV-Vis spectroscopy

3.2.5 Release of Fluorescein from pNIPAm-*co*-NBMA Microgels

The release mechanism of fluorescein-loaded pNIPAm-*co*-NBMA microgels is depicted in Scheme 3-1. The fluorescein can be released from pNIPAm-*co*-NBMA microgels by exposure UV-light or the heat. In detail, the concentrated fluorescein-loaded

pNIPAm-*co*-NBMA microgels were diluted to 20 mL with DI H$_2$O and suspended well. 1 mL aliquot of the mixture was diluted 25-fold and used for the experiment of photo/thermal triggered release of fluorescein. For the photo-triggered release, a cuvette containing 1 mL diluted aliquot was placed in the sample holder setting at 25 °C, and the sample was exposed to external UV light (365 nm) for 5 minutes. After that the fluorescence spectra were recorded after every 10 minutes. For the thermal-triggered release, the same setup was used except that the temperature was varied from 20 to 50 °C. The fluorescence spectra were recorded after each temperature being stabilized for at least 5 minutes.

3.3 Results and Discussion

3.3.1 Size Measurements and Morphology of pNIPAm-*co*-NBMA Microgels

The morphology and hydrodynamic size of pNIPAm-*co*-NBMA microgels were characterized by TEM and DLS, respectively. From TEM image of our microgels (Figure 3-3(a)), it could be found that those microgels were monodisperse and had round-shape structure with the size of around 200 nm, as expected. The DLS data (Figure 3-3(b)) also indicated that the microgels were monodisperse, and they had an average hydrodynamic diameter of 321.0 ± 41 nm, which was consistent with the image obtained by TEM.
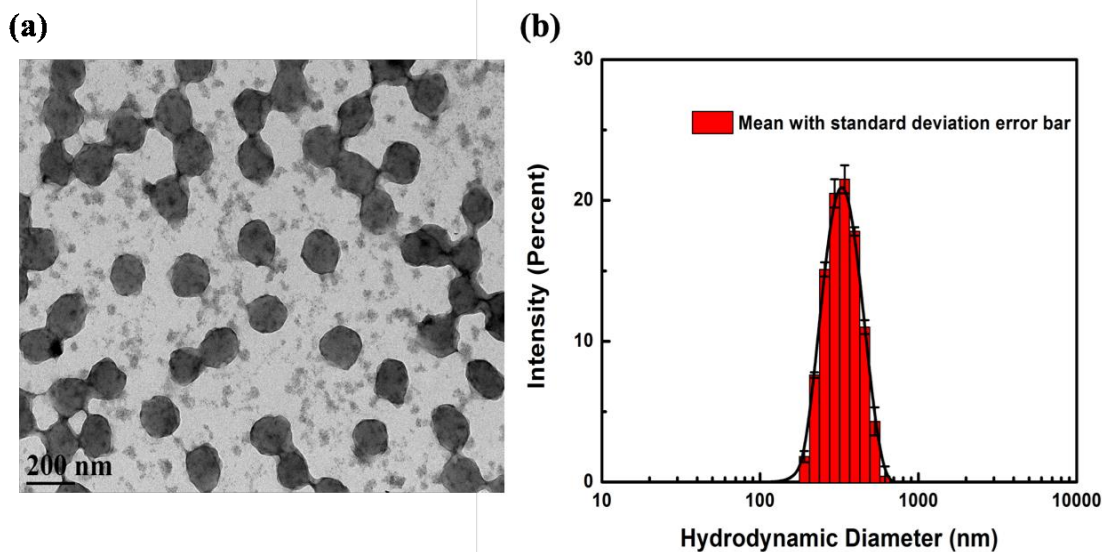
Figure 3-3. (a) TEM image and (b) DLS measurement of pNIPAm-*co*-NBMA microgels. The data in (b) were obtained by averaging 3 measurements of the solution, while the error bars indicate the standard deviation

3.3.2 Photo-responsive Properties of pNIPAm-*co*-NBMA Microgels

To evaluate the successful incorporation of NBMA into the microgel, we utilized the photo-responsive behavior of *o*-nitrobenzyl ester (*O*-NBE) upon ultraviolet (UV) irradiation. Briefly, upon UV irradiation at 365 nm, the ester group within NBMA would be cleaved to yield a carboxylic acid and a molecule of nitrosobenzaldehyde as a result. In the case of our pNIPAm-*co*-NBMA microgels, when the microgels were exposed to UV light, the molecules containing nitrosobenzaldehyde would be released from the

microgel network into the aqueous environment and carboxylic acid groups would remain attached to the microgel's polymer chain (Figure 3-4(a)). Upon UV irradiation for a short period of time (5 minutes), the microgels exhibited a significant color change from white to yellow brown (Figure 3-4(c)). This color change could be attributed to the generation of nitrosobenzaldehyde molecules. We measured the absorbance of the whole microgel solution before and after UV (Figure 3-5), and we found that the peak at 260 nm disappeared, which could be due to the releasing of the phenyl moieties from the microgel structure into aqueous environment. To further determine the existence of the released molecules, we centrifuged the aqueous solutions of microgels both before and after UV exposure and measured the UV-Vis spectra of the supernatant. As can be seen in Figure 3-4(d), the photographic images showed that the supernatant of microgels exposed to UV had an obvious yellow-brown color compared to microgels without exposure to UV. From Figure 3-4(b), the supernatant of the microgels before UV didn't display any obvious peak absorbance in its UV-Vis spectra whereas there was strong absorbance in the region of 200 to 350 nm for the supernatant of the microgels after UV. This distinct absorbance could be due to the absorbance of phenyl group in nitrosobenzaldehyde moieties. Noticeable, after UV irradiation, it could generate carboxylic acid group so that it made the microgels pH-responsivity.
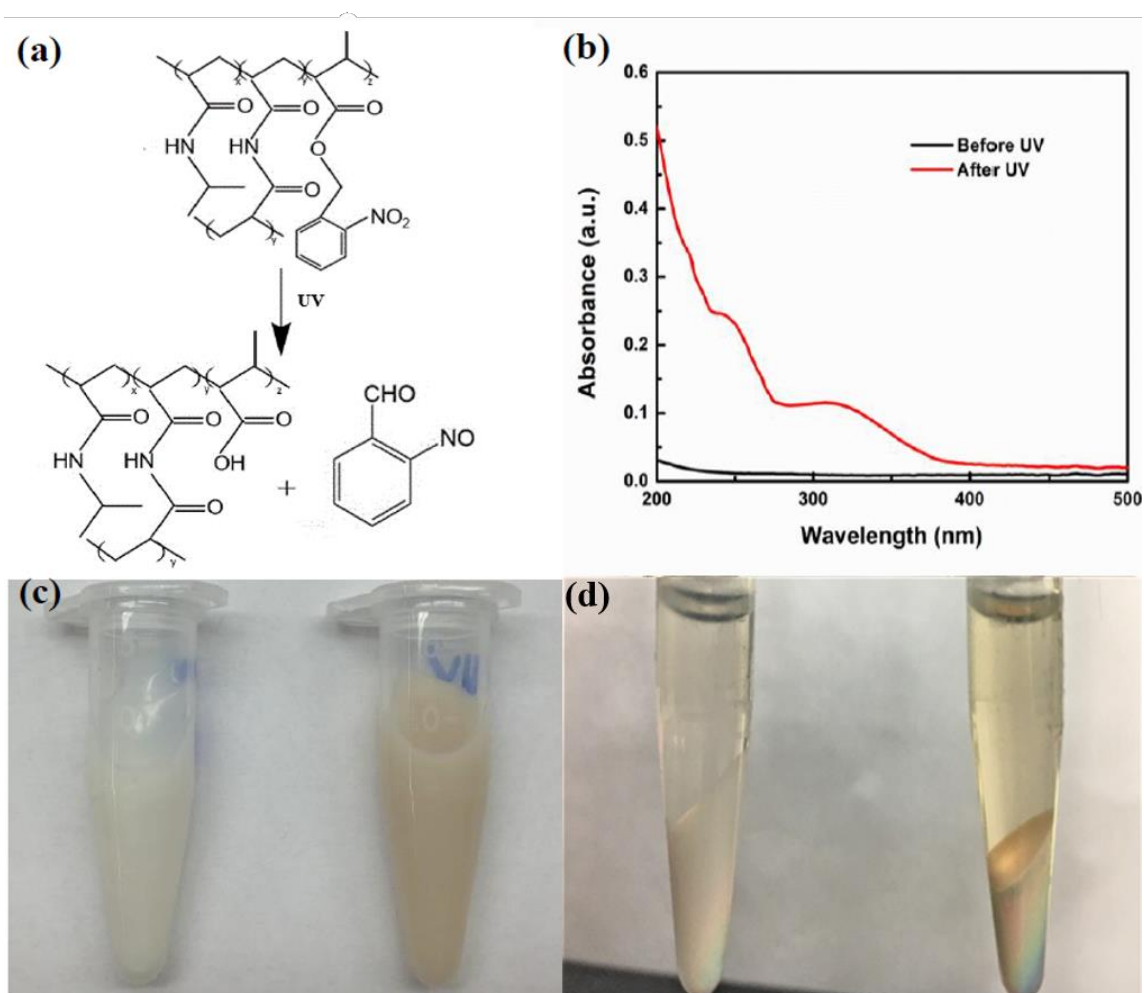
Figure 3-4. Photo-responsive properties of pNIPAm-*co*-NBMA microgels. (a) The photolysis reaction; (b) UV-Vis spectra of supernatant solution after centrifugation before and after UV exposure; (c) photographs of microgel solutions show distinct differences in appearance (left) before, and (right) after exposure to UV irradiation; (d) Photographs of the same microgel solutions in (c) after centrifugation at 18000 rpm for 30 min.
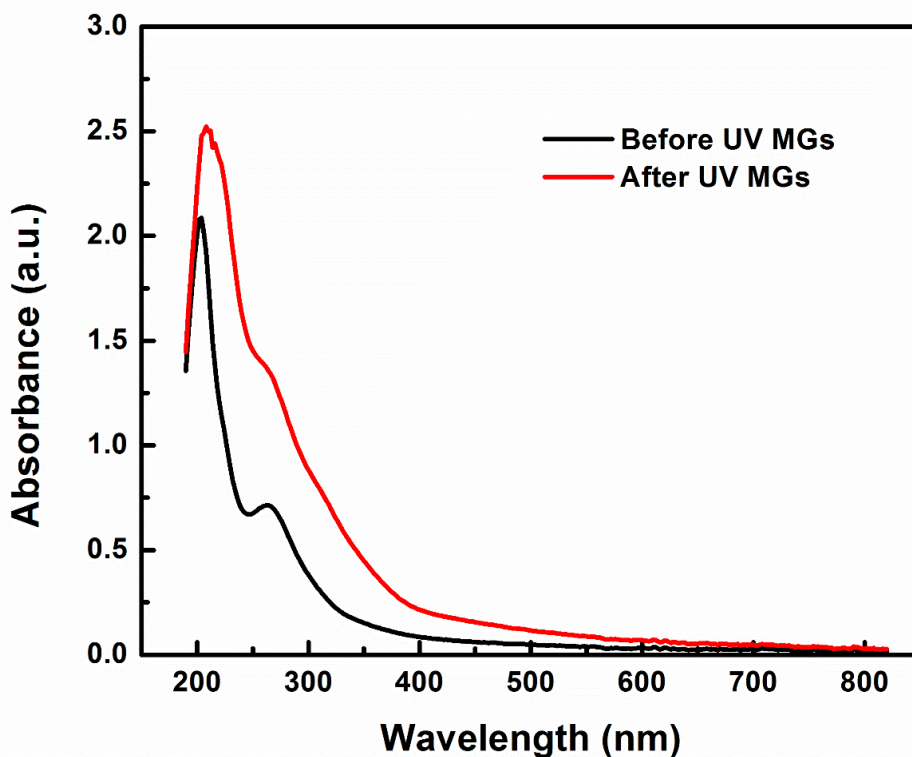
Figure 3-5. UV-Vis spectra of the whole microgel solution before and after UV exposure

Additionally, we utilized FTIR to evaluate the microgels before and after NBMA incorporation as well as after exposure to UV irradiation. As can be seen in Figure 3-6, bands around 3310 cm^{-1} and 1710 cm^{-1}, were indicative of the presence of NIPAm's N-H and C=O groups, which was expected as the microgels are primarily composed of NIPAm. As can also be seen, the FTIR spectrum of pNIPAm-*co*-NBMA microgels exhibited an additional peak at 1731 cm^{-1}, which was attributed to the ester C=O stretch in *O*-NBE moiety.[174] After 5 min of UV-irradiation, it was observed that the intensity of ester C=O peak (relative to the intensity of amide C=O peak of pNIPAm) decreased,

compared to pNIPAm-*co*-NBMA microgels before exposure, indicating that there were less *O*-NBE moieties in the UV-irradiated microgels and the *O*-NBE groups were dissociated from our light-responsive microgels upon UV exposure as a result.
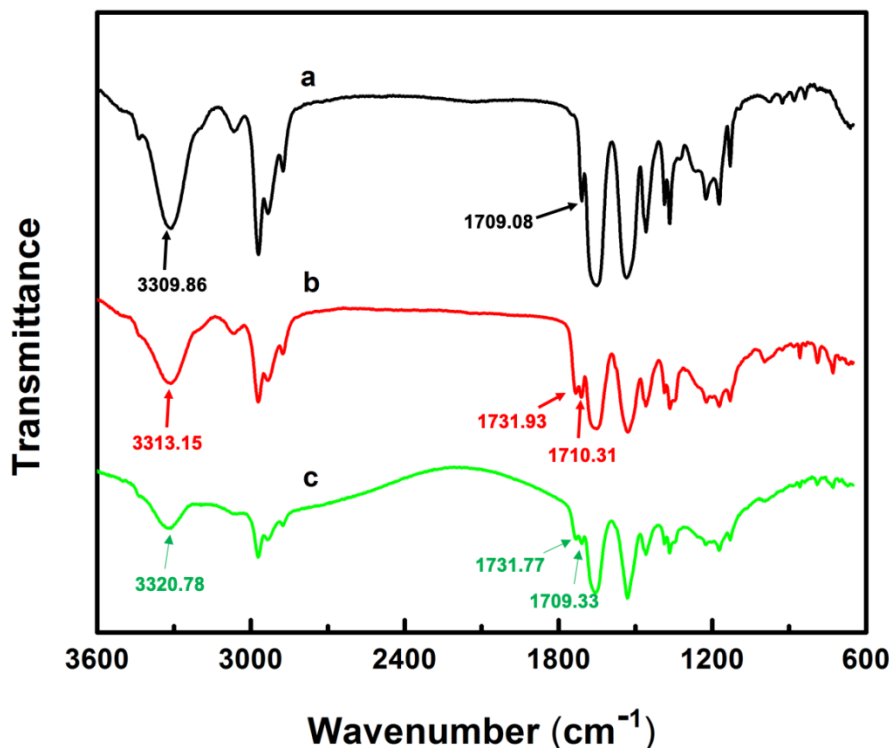
Figure 3-6. FTIR spectra of (a) pNIPAm MGs, (b) pNIPAm-*co*-NBMA MGs, and (c) UV-irradiation of pNIPAm-*co*-NBMA

Moreover, in order to confirm the generation of the carboxylic acid inside the microgel after the UV-induced photolysis reaction, we decided to utilize the charged properties of the newly formed methacrylic acid group. It is well known that the methacrylic acid has a pK_a of 4.65,[175] which indicates that when pH is above that value

the carboxyl group is negatively charged while below that value the carboxyl group contains no charge. When the carboxyl groups are negatively charged, our microgels will become swelled i.e. have a large size, due to Coulombic repulsion between the carboxylate groups inside the microgel network. Therefore, we measured the hydrodynamic size of UV-exposed microgels at different pH (pH=3, 5.5 and 7) and the result was shown in Figure 3-7. It was found that the microgel had a larger hydrodynamic diameter at a higher pH (pH>4.65) compared to the microgel at a lower pH, which was as expected.
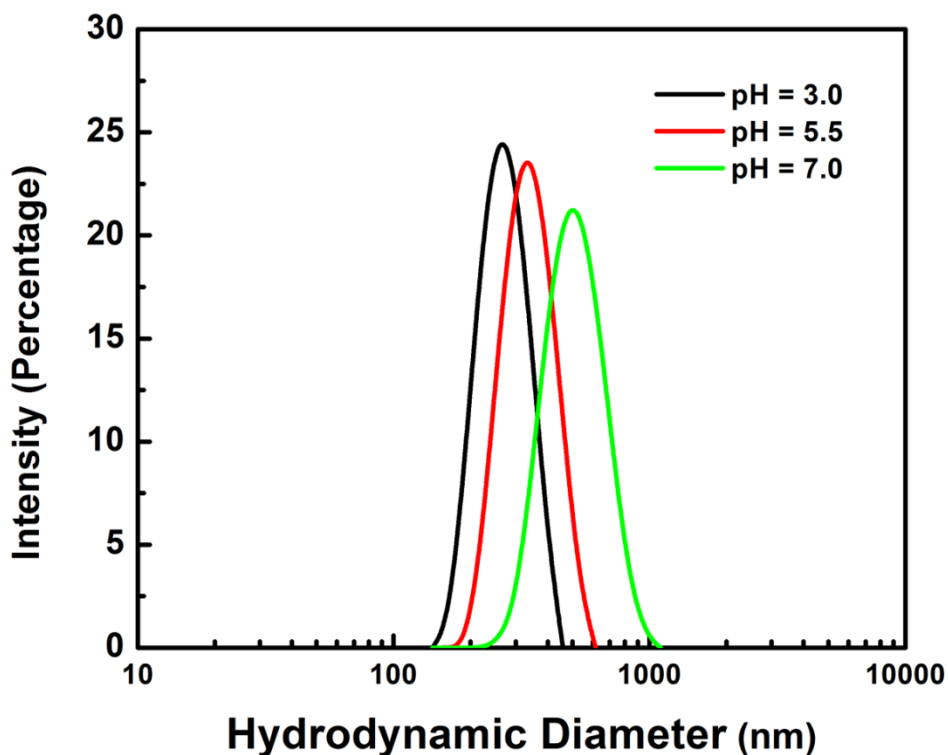
Figure 3-7. DLS measurements of UV-exposed microgels at different solution pH.

3.3.3 Thermo-responsive Properties of pNIPAm-*co*-NBMA Microgels

Since our microgels were based on pNIPAm by using NIPAm as the primary monomer, and pNIPAm is characterized by its famous thermo-responsive behavior i.e. having a volume phase transition temperature (VPTT) of 32 °C.[60] We then investigated the thermo-responsive behavior of our pNIPAm-*co*-NBMA microgels. We used UV-Vis spectroscopy to measure the absorbance (at 320 nm) variances associated with temperature changes of the microgels and the result can be found in Figure 3-8. It can be seen that the volume phase transition range of our microgels is very broad, which is different from the behaviors of microgels only containing pure pNIPAm. That can be explained by the incorporation of hydrophobic moiety into the microgel and this phenomenon is consistent with the findings by Ma et al.[176] We also investigated our microgel's thermo-responsive behavior by using DSC, and the result can be seen in Figure 3-9. DSC result also showed that pNIPAm-*co*-NBMA microgels had a broad transition range, which is consistent with our findings obtained by UV-Vis
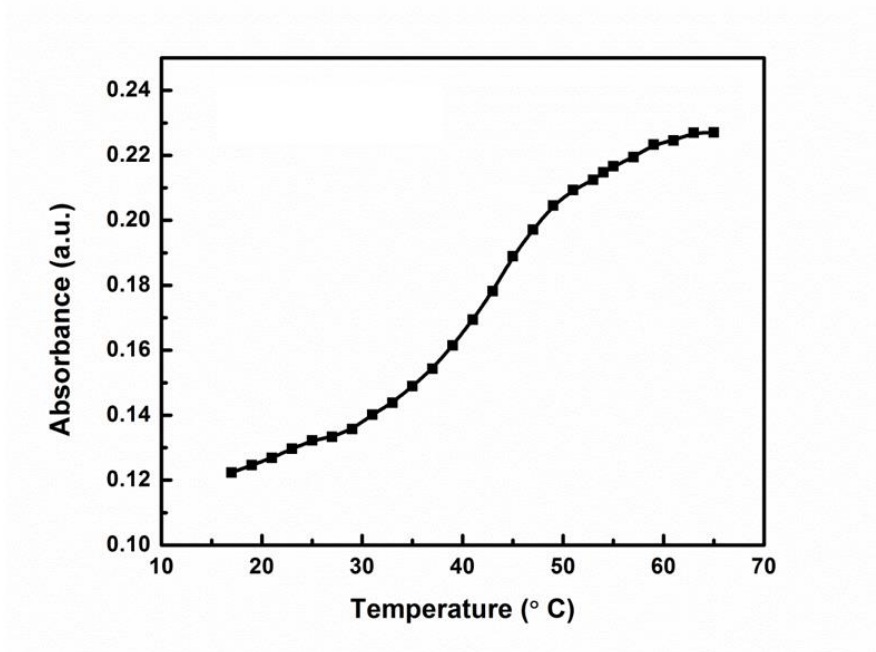
Figure 3-8. Absorbance at 320 nm (A_{320}) as a function of temperature for pNIPAm-*co*-NBMA microgels. In this case, absorbance is directly related to scattering from the microgels.
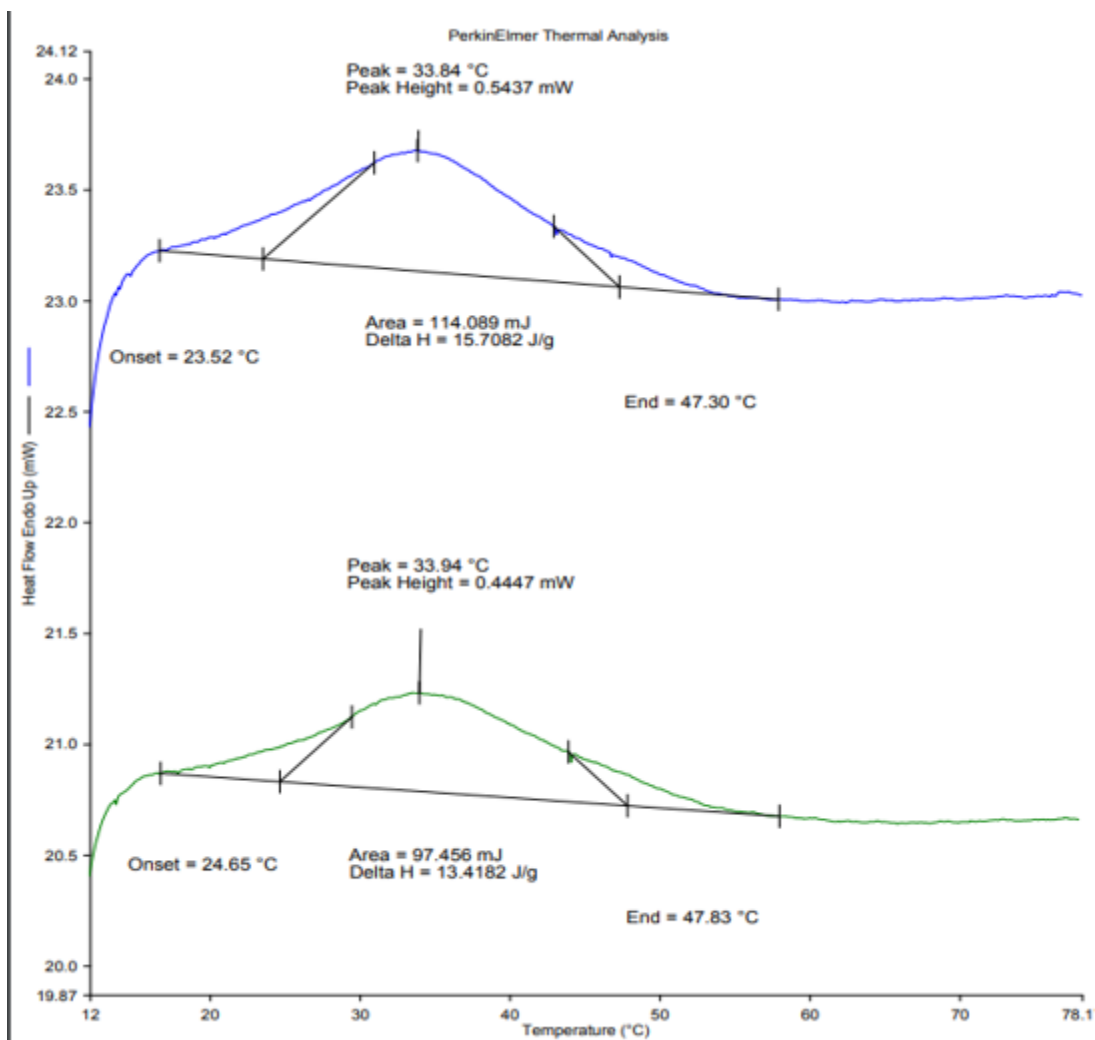
Figure 3-9. DSC result of pNIPAm-*co*-NBMA microgel's thermo-responsive behavior

lower critical solution temperature (LCST): 34 °C

3.3.4 Dual-Stimuli Triggered Release of Fluorescein from pNIPAm-*co*-NBMA Microgels

The encapsulation and release of hydrophobic molecules from hydrogels, microgels,

micelles and porous materials, which can be triggered only by pH, temperature or light etc., are less investigated. However, dual-stimuli triggered drug release from those materials are even less investigated. Herein, the *o*-nitrobenzyl esters (*O*-NBE) group that are incorporated into the pNIPAm microgels are hydrophobic; thus, it is expected that the pNIPAm-*co*-NBMA microgels will provide an opportunity to encapsulate not only hydrophobic small molecules, but also dual-stimuli triggered by light and temperature. Fluorescein, a fluorescent dye, was used as a hydrophobic model molecule to be loaded into the prepared pNIPAm-*co*-NBMA microgels. The fluorescein loaded pNIPAm-*co*-NBMA microgels were characterized by TEM and confocal microscope, which are shown in Figure 3-10. From TEM images, it was found that the microgels' morphology didn't experience significant changes after loaded with fluorescein i.e. the size and morphology were approximately the same as unloaded microgels shown in Figure 3-3(a). As shown in Figure 3-10(b), it is obvious that fluorescein-loaded microgels are visible as bright dots.
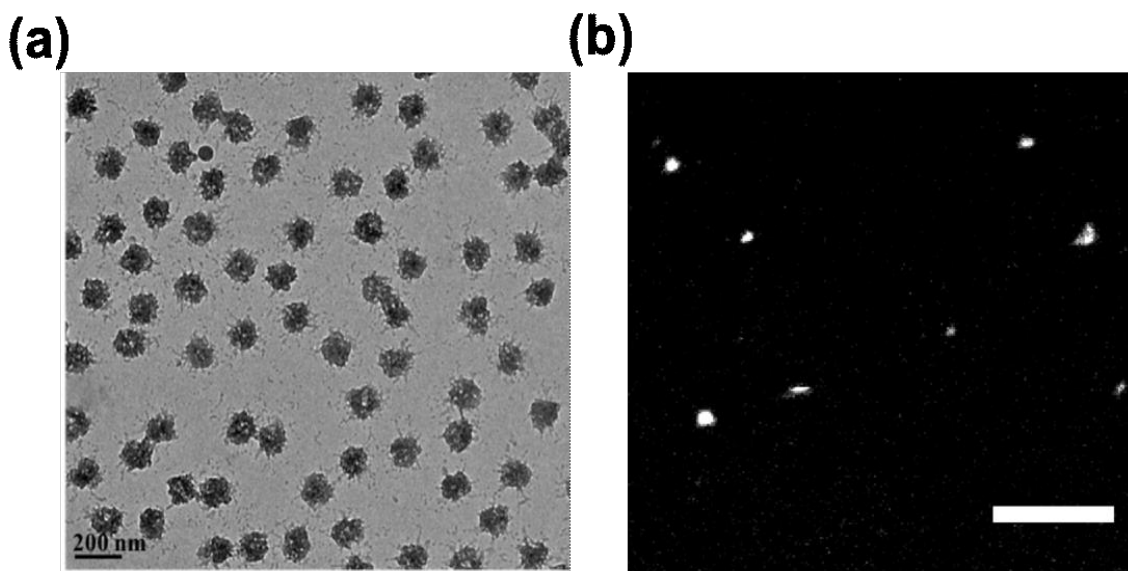
Figure 3-10. TEM (a) and confocal (b) images of fluorescein-loaded pNIPAm-*co*-NBMA

microgels; (488 nm Excitation, 492nm LP emission, Scale bar = 5 micron)

To confirm the dual-stimuli responsive effect of light and temperature on the release

process, the fluorescence emission spectra of fluorescein-loaded pNIPAm-*co*-NBMA

microgels were characterized. Firstly, fluorescein-loaded pNIPAm-*co*-NBMA microgels

without and with UV light irradiation were recorded at various times. As shown in Figure

3-11(a), in comparison with no UV light irradiation, the fluorescence emission intensity

of fluorescein-loaded pNIPAm-*co*-NBMA microgels increased obviously within 30

minutes when the sample was irradiated with UV light for 5 minutes. These results

suggested that the ester bonds of NBMA were broken by exposure to UV irradiation,

which transformed *o*-nitrobenzyl methacrylate into the nitrosobenzaldehyde group. Then,

the nitrosobenzaldehyde unit was disconnected from our resultant microgels and it could

diffuse out of from microgels, promoting the release and delivery of loaded fluorescein molecules into the aqueous solution surrounding. Since the microgels are able to scatter the light, which results in less encapsulated fluorescein molecules being excited, the fluorescence intensity of fluorescein is expected to be inhibited when fluorescein molecules are inside the microgels; Also, water can promote the ring-opening reaction of fluorescein, which can enhance the fluorescence intensity.[177] Hence, it is expected that the observed fluorescence intensity will increase when fluorescein molecules are released into aqueous environment. In order to confirm that the drug release of light responsive microgels is majorly due to the incorporation of NBMA, fluorescein-loaded pNIPAm-only microgels were investigated as controlled experiments. The fluorescence emission spectra (λ_{ex} = 510 nm) of fluorescein loaded in the pNIPAm-only microgels without and with UV irradiation (365 nm) were displayed in Figure 3-12. It is found that the amount of fluorescein released from pNIPAm-only microgels is negligible. One reason is due to the lack of light-responsive *O*-NBE moieties; the other explanation for this phenomenon is that the incorporation of hydrophobic NBMA unit increases the loading efficiency of fluorescein molecules by the hydrophobic interactions; whereas in the case of pNIPAm-only microgels, such strong hydrophobic interactions do not exist and fluorescein molecules can only be attached to the microgels surface by weaker non-specific adsorption.

Overall, it is demonstrated that the light-responsive *O*-NBE groups incorporated in

the microgels play an indispensable role in the UV-light triggered release process. We also found that the release rate and amount of the loaded fluorescein from the pNIPAm-*co*-NBMA microgels increased significantly with the time increasing within 2 hours, as shown in Figure 3-11(b). When the sample was irradiated with UV light, 69% of the loaded hydrophobic molecules was released in the first 15 minutes, compared with the pNIPAm-only microgels, which were shining UV-visible light on pNIPAm microgel loaded with fluorescein without NBMA, to 16% within the same period. Finally, the loaded fluorescein molecules could be released almost completely within 1 hour.
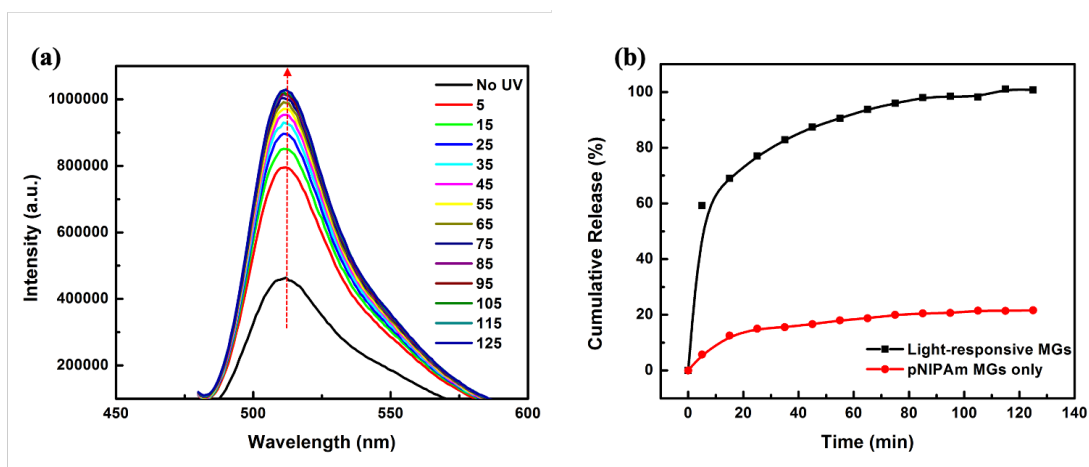
Figure 3-11. (a) Fluorescence emission spectra (λ_{ex} = 510 nm) of fluorescein loaded pNIPAm-*co*-NBMA microgels before and after UV irradiation (365 nm) for the indicated times. (b) Cumulative release profiles of fluorescein from the prepared pNIPAm-*co*-NBMA microgels at UV exposure times. The solid lines are simply to guide the eye, and are not intended to represent a model fit to the data. The concentration of the prepared fluorescein loaded pNIPAm-*co*-NBMA microgel solution was 0.05 mg/mL.
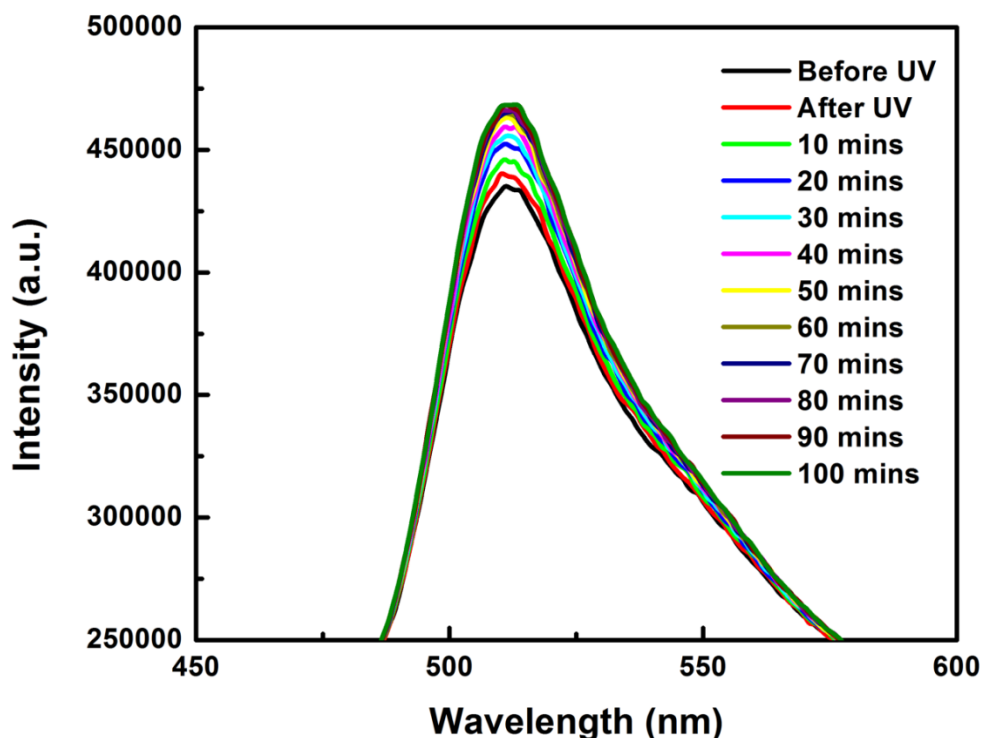
Figure 3-12. Fluorescence emission spectra (λ_{ex} = 510 nm) of fluorescein loaded in the pNIPAm-only microgels without and with UV irradiation (365 nm)

Moreover, we carried out the thermally controlled release by varying different temperatures. As shown in Figure 3-13(a), it is obvious that the fluorescence intensity did not change too much when the temperatures were around room temperature i.e. 20 and 25 °C. However, when the temperature went across the VPTT of our microgels, the fluorescence extremely increased, indicating the significant amount of release of fluorescein from microgels into aqueous solution. Due to the thermally induced shrinkage of our microgels, water molecules were expelled from our microgels, along with the

model drug fluorescein; as the reason mentioned before, an increase in fluorescence intensity was observed as a result. In addition, we conducted the same drug release test with pNIPAm-only microgels. The fluorescein release profile is displayed as Figure 3-14, which did not show a similar behavior as pNIPAm-*co*-NBMA microgels i.e. there is no significant release of fluorescein associated with increasing temperature. As mentioned above, fluorescein molecules were only attached to the surface of pNIPAm microgels by non-specific adsorption, instead of hydrophobic interactions in the case of pNIPAm-*co*-NBMA microgels. Therefore, when pNIPAm microgels shrink due to heat, the fluorescein molecules remain adsorbed on the surface of pNIPAm-only microgels and cannot be released into aqueous solution. As a result, there is no dramatic increase in fluorescence intensity. We also investigated the release profile of the loaded fluorescein from the pNIPAm-*co*-NBMA microgels as a function of temperature, shown as Figure 3-13(b). It indicates that 60% of fluorescein was released from pNIPAm-*co*-NBMA microgels at 30 °C and a maximum release of 80% of fluorescein was achieved at 50 °C. As a comparison, pNIPAm-only microgels did not display such release behavior. Such dual-stimuli responsive pNIPAm-*co*-NBMA microgels exhibit excellent properties for controlled drug delivery systems.
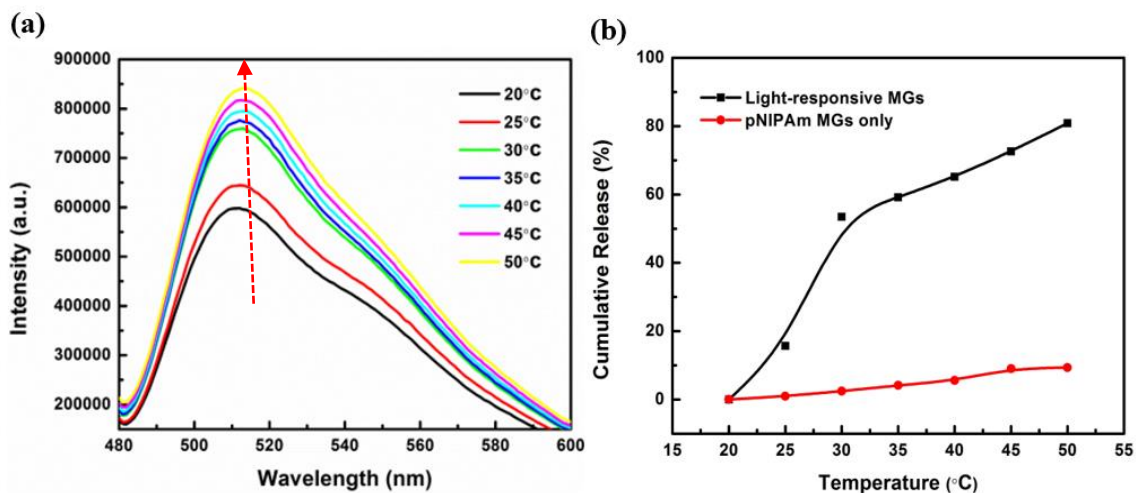
Figure 3-13. (a) Fluorescence emission spectra (λ_{ex} = 510 nm) of fluorescein loaded pNIPAm-*co*-NBMA microgels at the indicated temperatures. (b) Cumulative fluorescein release profiles from the prepared pNIPAm-*co*-NBMA microgels at different temperatures. The solid lines are simply to guide the eye, and are not intended to represent a model fit to the data. The concentration of the prepared fluorescein loaded pNIPAm-*co*-NBMA microgels was 0.05 mg/mL.
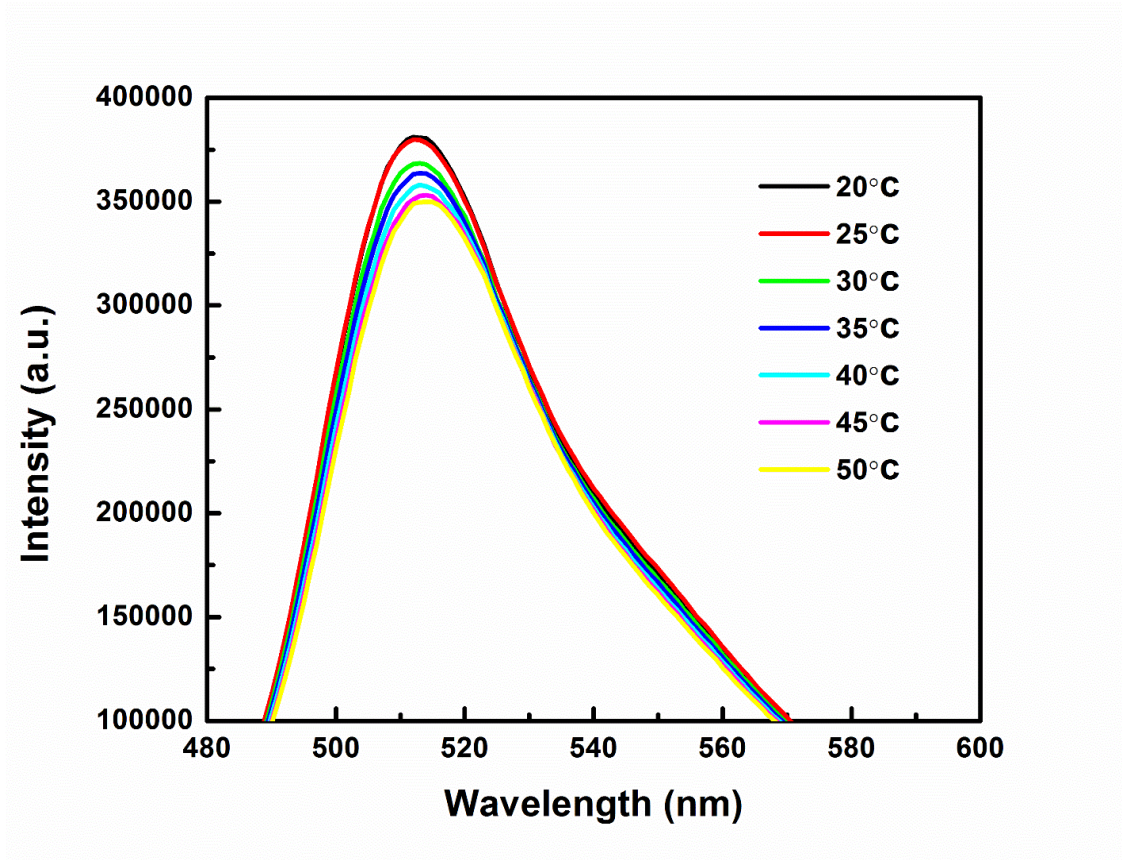
Figure 3-14. Fluorescence emission spectra (λ_{ex} = 510 nm) of fluorescein loaded in the pNIPAm-only microgels with different temperatures.

3.4 Conclusions

In summary, novel dual-stimuli responsive pNIPAm-*co*-NBMA microgels were designed and synthesized by a facile free radical precipitation polymerization method. We observed that pNIPAm-*co*-NBMA microgels are monodisperse and possess a uniform morphology with a size of 321.0 ± 41 nm. After confirming the light- and heat-dual-stimuli responsive properties of our microgels, the model drug, fluorescein, was

loaded with a high loading efficiency due to the physical interactions between hydrophobic moiety (*o*-nitrobenzyl methacrylate) of microgels and fluorescein. Upon exposure to either UV irradiation or heat, the fluorescein can be explosively released from pNIPAm-*co*-NBMA microgels into the aqueous solution; 69% of the drug was released within the first 15 minutes of UV exposure and 60% of the drug was released at 30 °C. We concluded that the light-triggered release was due to the presence of light-responsive *O*-NBE moiety in NBMA groups, and the heat-triggered release was due to heat-induced deswelling behavior of pNIPAm-based microgels. Taken together, the prepared dual-stimuli responsive pNIPAm-*co*-NBMA microgels possess great potential for applications in controlled drug delivery.

Chapter 4

Controlled Osteogenic Differentiation of Human Mesenchymal Stem Cells Using Dexamethasone-Loaded Light-responsive Microgels

4.1 Introduction

Human mesenchymal stem cells (hMSCs), which are isolated from the bone marrow, have the potential to differentiate into different cell lineages, including osteoblasts, chondrocytes, and adipocytes.[178] Owing to their multilineage differentiation potency, hMSCs are considered to be a promising therapeutic source of regeneration of damaged injured tissues, and such tissue regeneration therapies, including treating bone defects, based on hMSCs have been heavily explored over the past few decades.[179] Interestingly, these stem cells have the ability to differentiate into osteoblasts, and have been explored to repair bone defects as opposed to using autografts and allografts, which have many drawbacks, e.g., limited supply, risk of donor site morbidity, and disease transmission.[179, 180] Therefore, to overcome the limitations mentioned above, the use of stem cells which

have the possibility of differentiating into osteoblasts serves as an alternative and promising therapeutic candidate for treating bone defects.

Using hMSCs to treat bone defects depends on the osteogenic differentiation of stem cells, which depends on the cellular microenvironment. For example, neighboring cells, extracellular matrix (ECM), biochemical cues (e.g., presence of soluble growth factors), and biophysical cues (e.g., stiffness, stress, and forces) can direct hMSC differentiation.[181] Osteogenesis is a particularly complex process that is regulated by various hormones, cytokines, and growth factors. Several studies have shown that bone morphogenetic proteins (BMPs), transforming growth factor-beta (TGF-β) and vascular endothelial growth factor (VEGF) are potent soluble protein growth factors that can induce osteogenesis of hMSCs *in vitro* and *in vivo*.[182] Hence, simple injection of these growth factors have been used to promote osteogenesis for regeneration and therapy. However, such protein growth factors can lose their bioactivity easily over a short period of time, rendering them inefficacious, and limits their use for local delivery. Additionally, due to other potential shortcomings, such as: limited resources, high cost, and their clearance by multiple proteases, the clinical use of protein growth factors as a stem cell therapy reagent for promoting bone regeneration and repair has been limited.[183-186] Importantly, the use of protein growth factors can result in undesired side effects, such as ectopic bone formation, inflammation response as well as tumorigenesis.[187-189] Therefore, stable and inexpensive low molecular weight molecules have been explored to replace

protein growth factors. One such low molecular weight molecule used for bone regeneration and repair is dexamethasone (DEX).

DEX is a potent synthetic member of the glucocorticoid class of steroid drugs that have found widespread use to promote cellular proliferation and is a well-known regulator of mesenchymal progenitor cell commitment to lineages of osteoblasts, chondrocytes, and adipocytes.[190] In addition, DEX, as one of the earliest and more readily osteogenic inducers that can control the expression of the osteogenic marker genes, has been routinely applied to direct the differentiation of multipotent mesenchymal stem cells and accelerate tissue remodeling.[191] Currently, several methods have been developed to achieve the delivery of DEX, such as such as systemic injection and the use of DEX-loaded biomaterials.[192-195] However, the side effects of DEX after long-term systemic injections are also undesirable due to increased risks of osteoporosis and nontraumatic osteonecrosis.[196] As such, more studies have been focused on incorporating DEX into degradable biomaterials for osteogenic differentiation and bone formation.[197, 198] Even though these materials are a promising solution for osteogenesis, they can still cause undesired side effects.[199] As a result, a biocompatible delivery system, which can locally deliver DEX safely and efficiently in a controlled/triggered manner, is highly desired.

Stimuli-responsive polymers have been utilized in the past for controlled/triggered drug delivery. Of particular interest to this publication are poly (*N*-isopropylacrylamide)

94

(pNIPAm)-based microgels that have the ability to encapsulate therapeutics and release them in a controlled/triggered manner.[168, 200] To trigger the release of small molecules from microgels, a variety of stimuli have been utilized, e.g., light, pH, and temperature.[38, 201] Among those, light is of particular interest as it can be applied remotely with highly controlled positioning, intensity, and exposure time.[201] A variety of light-responsive systems, which mainly utilize *o*-nitrobenzyl ester (*O*-NBE) derivatives, have been developed to trigger the release of small-molecule drugs and biomolecules such as proteins and oligonucleotides.[47] Thus, a system that can trigger hMSC osteogenic differentiation in a controlled manner could be translated to the clinic.

Herein, we synthesized light-responsive microgels for light triggered DEX release to allow for controlled hMSC osteogenic differentiation. The process is detailed schematically in Scheme 4-1. That is, light-responsive microgels were synthesized for loading and triggered of DEX release, which can dynamically change the cellular microenvironment and directly induce the osteogenic differentiation of hMSCs in a light-controlled manner. Particularly, pNIPAm-*co*-nitrobenzyl methacrylate) (pNIPAm-*co*-NBMA) microgels were synthesized by copolymerizing *N*-isopropylacrylamide (NIPAm) and *o*-nitrobenzyl methacrylate (NBMA) via free radical precipitation polymerization. The size, morphology, and light-responsivity of the as-prepared microgels was characterized by UV-visible spectroscopy, dynamic light scattering (DLS) and transmission electron microscopy (TEM). DEX was then loaded

into the pNIPAm-*co*-NBMA microgels likely via its hydrophobic interaction with the hydrophobic NBMA, and then the light-triggered release of DEX from the microgels was investigated via liquid chromatography-mass spectrometry (LC-MS). Subsequently, we evaluated the ability of DEX released from the microgels to trigger hMSC osteogenic differentiation using the alamarBlue assay and normalized alkaline phosphatase (ALP) activity assay, respectively. Ultimately, the progress of osteogenic differentiation of hMSCs in our system could be tuned by intermittent DEX released from light reponsive microgels. As such, DEX loaded light-responsive microgels were capable of inducing hMSCs osteogenic differentiation upon light exposure, which offers an efficient system for local delivery of osteogenesis-inducing small molecules for bone tissue engineering.
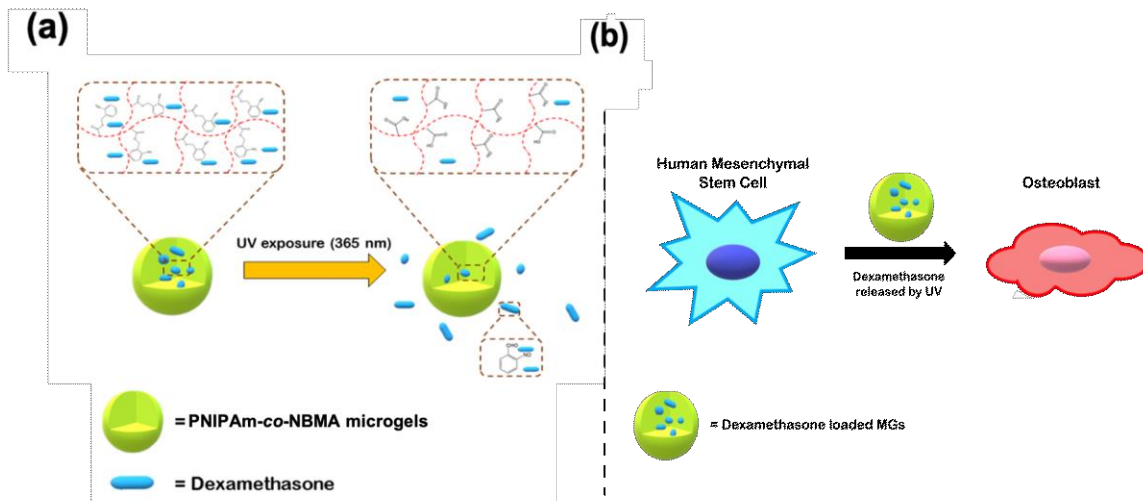
Scheme 4-1. Schematic illustration of dexamethasone delivery from pNIPAm-*co*-NBMA MGs (a) and *in vitro* dexamethasone delivery to induce stem cell osteogenesis (b)

96

4.2 Materials and Methods

4.2.1 Materials

N-isopropylacrylamide (NIPAm) was purchased from TCI (Portland, Oregon) and purified by recrystallization from hexane (ACS reagent grade, EMD, Gibbstown, NJ) before use. *N, N'*-methylenebisacrylamide (BIS) (~99%) and ammonium persulfate (APS) (~98%) were obtained from Sigma-Aldrich (Oakville, Ontario) and were used as received. *o*-nitrobenzyl methacrylate (NBMA) (~95%) was purchased from Polysciences, Inc (Warrington, PA). Dexamethasone (DEX) was obtained from Fisher Scientific (Toronto, Ontario). Deionized (DI) water with 18.2 MΩ·cm resistivities was from a Millipore Milli-Q-Plus system (Billerica, MA). Adult human mesenchymal stem cells (hMSCs) isolated from bone marrow aspirate were purchased from Lonza (Basel, Switzerland. Alamar blue reagent was obtained from Bio-Rad Laboratories, Inc (Mississauga, Ontario). Alkaline phosphatase yellow (pNPP) liquid substrate was purchased from Sigma-Aldrich (Oakville, Ontario). Bradford reagent was gained from Sigma-Aldrich (Oakville, Ontario). All other reagents and solvents were obtained from commercial suppliers and used without further purification unless specified.

4.2.2 Synthesis of Light-Responsive pNIPAm-*co*-NBMA Microgels

Microgels composed of poly(*N*-isopropylacrylamide-*co*-nitrobenzyl methacrylate) (pNIPAm-*co*-NBMA) were synthesized via free radical precipitation polymerization similarly to our previously published protocols with minor modifications.[150] The reaction scheme can be found in Figure 4-1. The pNIPAm-*co*-NBMA microgels consisted of 85% *N*-isopropylacrylamide (NIPAm), 10% *o*-nitrobenzyl methacrylate (NBMA) and 5% N,N′-methylenebis(acrylamide) (BIS) as the cross-linker. First, the monomers NIPAm (3.2992 mmol) and NBMA (0.3965 mmol), as well as the cross-linker BIS (0.1949 mmol), were dissolved in deionized water (29 mL) with stirring in a beaker. After stirring for 30 minutes, the monomer mixture solution was transferred into a 3-neck round-bottom-flask equipped with a nitrogen gas inlet, a reflux condenser, and a thermometer. Then, the solution was degassed with nitrogen gas for 1 h with vigorous stirring, and the temperature was slowly increased to 70 °C during this period. Afterward, a 1-mL aqueous solution containing APS (0.0456 g) was introduced into the reaction mixture to initiate the polymerization. The reaction was allowed to proceed at 70 °C under N_2 atmosphere for 4 hours. After polymerization, the reaction mixture was allowed to cool to room temperature and filtered through Whatman #1 filter paper to remove any large aggregates. The filtered microgels solution was purified via centrifugation at 12000 rpm for six times

and concentrated in aluminum foil-wrapped centrifuge tubes to avoid any potential light-induced degradation of microgels.
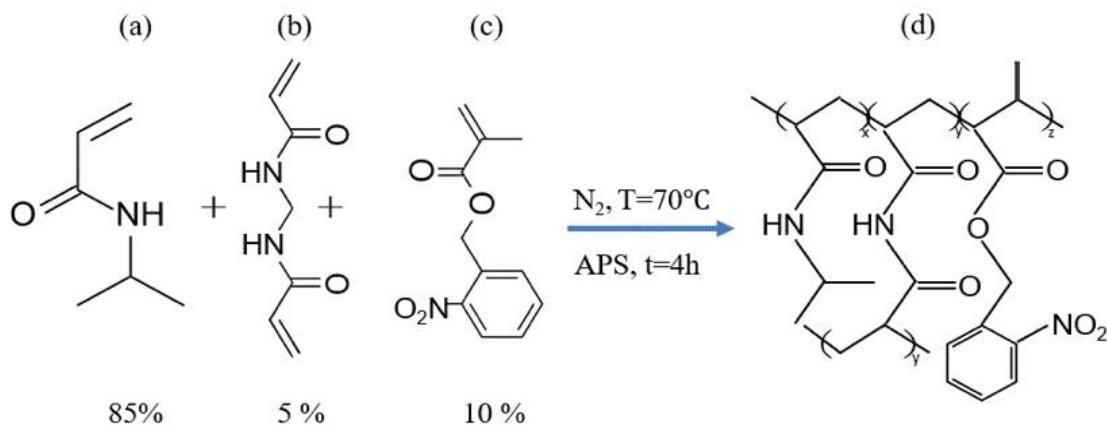
Figure 4-1. Synthesis of pNIPAm-*co*-NBMA microgels. NIPAm (a) and comonomer NBMA (b), along with crosslinker BIS (b) were copolymerized to yield pNIPAm-*co*-NBMA microgels (d)

4.2.3 Characterization

Morphologies of pNIPAm-*co*-NBMA microgels were characterized using a JEM-2010 EX/S transmission electron microscopic (TEM). The hydrodynamic diameter of the microgels was obtained by dynamic light scattering (DLS) measurements using a commercial Zetasizer Nano ZS - Malvern Instrument (Westborough, MA, USA) equipped with a light source with a wavelength of 633 nm. UV-Vis spectra were obtained by a Hewlett Packard 8453 UV-VIS Spectrophotometer. Liquid chromatography-mass

spectrometry (LC-MS) spectra were measured on an Agilent Technologies 1260 HPLC with G6130B MSD (Santa Clara, CA, USA).

4.2.4 Loading of DEX into pNIPAm-*co*-NBMA Microgels and Subsequent Light-Triggered in Vitro Release

DEX was loaded into the microgels by dissolving lyophilized pNIPAm-*co*-NBMA microgels (4 mg) in 2 mL of ethanol in a glass vial and the mixture was stirred at 600 rpm for 2 h, followed by slow addition of 2 mL of 0.2 mg/mL DEX ethanol solutions so that the final concentration of microgels and DEX were 1 mg/mL and 0.1 mg/mL, respectively. Next, the mixed solution was continuously stirred at 600 rpm at room temperature for 24 h. The resulting solution was subsequently lyophilized. After that, the DEX-loaded microgels were redissolved in ethanol and purified by multiple rounds of centrifugation and washing with ethanol. The loading efficiency of DEX in the microgels was calculated by centrifuging the microgel solution and collecting the supernatant solution. The UV-vis spectrum of the supernatant solution was collected, and the maximum absorbance value used to determine the concentration (and moles) of DEX in the supernatant solution (utilizing a calibration curve, see Figure 4-2). Subtracting this value from the number of moles of DEX initially added allowed the amount of DEX loaded in the microgels to be calculated. We determined the DEX loading efficiency for our system to be approximately 55 %. The resultant concentrated microgel solutions were stored at 4 ℃ until use

Equation	y = a + b*x	
Weight	Instrumental	
Residual Sum of Squares	39459.62884	
Pearson's r	0.9895	
Adj. R-Square	0.97215	
	Value	Standard Error
E Intercept	-0.05491	0.04938
Slope	20.17634	1.70135
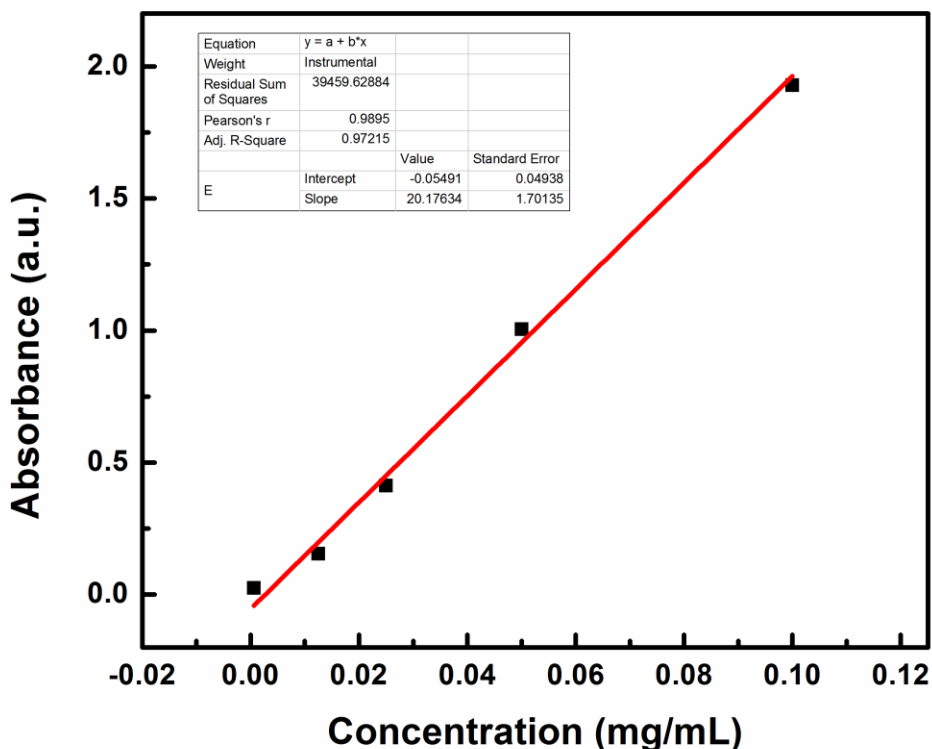
Figure 4-2. Calculation curve for DEX standard solution by UV-vis spectra.

The light-triggered release mechanism of DEX-loaded microgels is depicted in Figure 4-1(a). In detail, solutions of DEX-loaded microgels were made by dissolving a pellet (~4.2 mg) of concentrated microgels in 1 mL of ethanol and individual 0.8 mL suspensions were irradiated with UV light (365 nm) for 5 min, 10 min and 30 min. Afterward, the sample was centrifuged to reform the microgel pellet, and the supernatant solution was collected to determine the concentration of released DEX (using a calibration curve). We investigated the amount of DEX release as a function of UV exposure time. The LC-MS spectra of the supernatant and the DEX standard solutions were recorded using a Waters Xevo triple quadrupole mass spectrometer with Waters Acquity Ultra Performance Liquid

Chromatography (UPLC) system. The column used was an Agilent 2.7 µm Poroshell 120 SB-C18 with dimensions 2.1 x 50 mm. The mobile phases were water with 0.1% formic acid and acetonitrile with 0.1% formic acid.

4.2.5 hMSCs Culture

Adult human mesenchymal stem cells (hMSCs) isolated from bone marrow aspirate were expanded in a growth medium (GM) consisting of phenol-red free, low-glucose dulbecco's modified eagle medium (DMEM) containing 10% fetal bovine serum and 1% penicillin/streptomycin at 37 ℃ in a humidified atmosphere with 5% CO_2 concentration. The cells in passage 4 were used in the following experiments.

hMSCs in 0.5 mL of GM were seeded into each well of a 24-well cell culture plate at a density of 30,000 hMSCs/well and incubated in 5% CO_2 at 37 °C. The hMSCs were allowed to attach for 24 h followed by introduction of fresh GM to each well. The hMSCs were then allowed to expand until 80% confluency was reached. For control experiments, the hMSCs cultured in a basal medium (BM), which was GM supplemented with β-glycerophosphate (βGP) and ascorbic acid (AA), served as the negative control; and hMSCs cultured in a osteogenic medium (OM), which was BM with 100 nM DEX added, served as the positive control. For the UV-treated microgel experimental groups, microgel solutions (0.8 mL) were exposed UV-light (365 nm) for 5 min (this was determined as the ideal exposure time, from experiment), centrifuged, and the supernatant

solutions added to hMSCs in BM; this was done for both the initial culture and for all BM replacements. BM was replaced every 2 to 3 days, along with the supernatant from freshly UV-exposed-microgels, and a total of 21 days of culture was used to induce the osteogenic differentiation of hMSCs. For the experimental microgel group without UV treatment, the same procedure as for the UV-exposed microgels was used.

4.2.6 Morphological Analysis and Imaging

hMSCs cultures were routinely examined under an inverted phase-contrast fluorescence microscope (Nikon Eclipse Ti2). Images were captured with an electron-multiplying CCD (EM-CCD) camera coupled to an inverted microscope, using the NIS-Elements software (Nikon).

4.2.7 Cell Viability Assay

AlamarBlue assay was used to determine the cytotoxicity of the pNIPAm-*co*-NBMA microgels toward hMSCs. Specifically, hMSCs were seeded in 24-well plates with 0.5 mL of the medium at a density of 30,000 hMSCs/well and cultured in 5% CO_2 at 37 °C and different concentrations of microgels were added to the growth medium and incubated. After incubation for 24 h, the alamarBlue reagent was added into each well to a concentration of 10% v/v, and the hMSCs were incubated for another 4 h at 37 °C. 100 μL of the alamarBlue reagent from each well was transferred into a 96-well plate and the

fluorescence (560 nm excitation, 590 nm emission) was determined with a SpectraMax i3x plate reader (Molecular Devices LLC, USA). hMSCs cultured in growth medium without any microgels treatment were used as the control/normalized groups. The cytotoxicity was expressed as a percentage of the cell viability for the experiment compared to the control.

4.2.8 Evaluation of hMSC Osteogenic Differentiation: Alkaline Phosphatase (ALP) Activity Assay, and Bradford Assay

Alkaline phosphatase (ALP) activity of hMSCs was evaluated using the ALP assay, which can quantify the conversion of p-nitrophenol phosphate (pNPP) to yellow p-nitrophenol (pNP) by ALP from the differentiated hMSCs. Briefly, on day 3, 7, 10, 14 and 21, the hMSCs were rinsed with PBS twice and then lysed with CelLytic M cell lysis buffer. Next, 50 μL of the cell lysate was treated with 50 μL of pNPP and incubated at 37 °C for 30 min and quenched with 25 μL of 3M NaOH. The absorbance was read at 405 nm with a plate reader.

Another 50 μL of the cell lysates were treated with 50 μL of Bradford Reagent. The reaction was incubated for 20 min and the absorbance was read at 595 nm with a plate reader. Normalized ALP activity was reported as the ALP assay absorbance divided by the Bradford assay absorbance (A_{405}/A_{595}).

4.2.9 Alizarin Red S (ARS) Staining Assay

After microgel UV exposure (or their incubation without UV exposure) for the indicated times, hMSCs were washed with 500 µL PBS, followed by incubation in 400µL of 4% formaldehyde solution (in PBS buffer) and incubated at room temperature for 15 min, followed by washing with 3×500µL DI water. Subsequently, 200 µL 2% (wt/v) ARS staining solution with a pH adjustment to pH 4.2 was added to the cells. After incubation at room temperature with gently stirring for 20 min, hMSCs were washed with 500 µL PBS several times until excess ARS was removed. The ARS staining was imaged by a digital single-lens reflection camera (Canon EOS T5i).

4.3 Results and Discussion

4.3.1 Size Measurements and Morphology of pNIPAm-*co*-NBMA Microgels

The morphology and hydrodynamic diameter of pNIPAm-*co*-NBMA microgels were characterized by TEM and DLS, respectively. From the TEM image (Figure 4-3(a)) of as-prepared microgels, it could be found that those microgels were monodisperse and had a round-shape structure with a size of around 190 nm, as expected. The DLS data (Figure 4-3(b)) also indicated also indicated the average hydrodynamic diameter of pNIPAm-*co*-NBMA microgels was 295.0 ± 37.1 nm. Note that the diameter for the

microgels determined by TEM is smaller than DLS due to microgel desolvation when imaged. Importantly, since the hydrodynamic diameter of our microgels at 37 °C is larger than 200 nm, which is the maximum acceptable diameter for a nanoparticle to be uptaken by cells via receptor-mediated endocytosis,[202, 203] we expect that the microgels are not entering the cells, thereby exhibiting reduced cytotoxicity compared to other types of biomaterials such as micelles, nanogels, and nanoparticles.
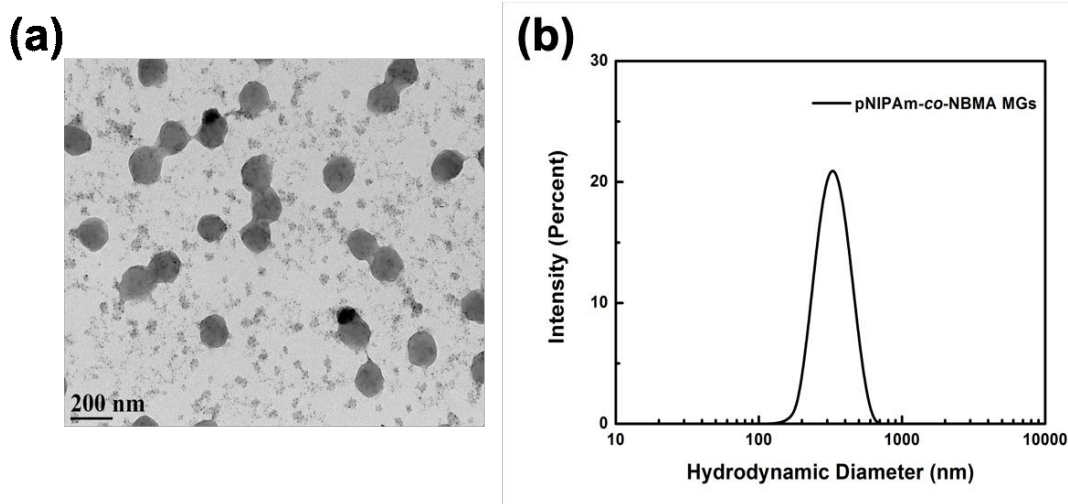
Figure 4-3. TEM image (a) and DLS measurement (b) of pNIPAm-*co*-NBMA microgels.

4.3.2 Light-responsive Properties of pNIPAm-*co*-NBMA Microgels

To evaluate the light-triggered cleavage of NBMA from the synthesized pNIPAm-*co*-NBMA microgels, we exposed them to 365 nm UV light, which cleaves the

NBMA ester group to yield a carboxylic acid and a nitrosobenzaldehyde-containing molecule that can be detected via UV-Vis spectroscopy. To determine the existence of the released nitrosobenzaldehyde-containing molecule in the supernatant solution, we centrifuged the aqueous solutions of microgels both before and after UV exposure and measured the UV-Vis spectra of the respective supernatant solutions. The spectra were shown in Figure 4-4(a). The supernatant of the microgels before UV exposure didn't display any obvious absorbance peak in the UV-Vis spectrum, whereas there was strong absorbance in the region of 200 to 350 nm for the supernatant solution of the microgels after UV exposure. This distinct absorbance is likely a result of light-induced release nitrosobenzaldehyde from the microgels upon cleavage, indicating that light exposure can be used to cleave the NBMA from the microgels. The findings here are consistent with previous reports.[204]

In addition, to further support the incorporation of NBMA moiety into our microgels and evaluate its associated UV-responsive behavior, we recorded the FTIR spectra of three different microgel samples (pNIPAm microgels, pNIPAm-*co*-NBMA microgels and UV-irradiation of pNIPAm-*co*-NBMA), as shown in Figure 4-4(b). Since all of the microgels were synthesized using NIPAm as the primary monomer, it was clear that all three spectra showed characteristic bands around 3310 cm^{-1} and 1710 cm^{-1}, which were assigned to the symmetric stretching of N-H bond as well as stretching amide C=O in NIPAm, respectively. In addition, compared to pNIPAm microgels, the FTIR spectrum of

pNIPAm-*co*-NBMA microgels exhibited a distinct peak at 1731 cm^{-1}, which was attributed to the ester C=O stretch in *O*-NBE moiety.[174] After exposing the pNIPAm-*co*-NBMA microgels to UV for 5 min, we observed that the intensity of ester C=O peak relative to the intensity of amide C=O peak decreased, compared to pNIPAm-*co*-NBMA microgels before exposure to UV-light. This was indicative of *O*-NBE groups being cleaved from the pNIPAm-*co*-NBMA microgels and diffusing out of the microgels upon UV exposure.
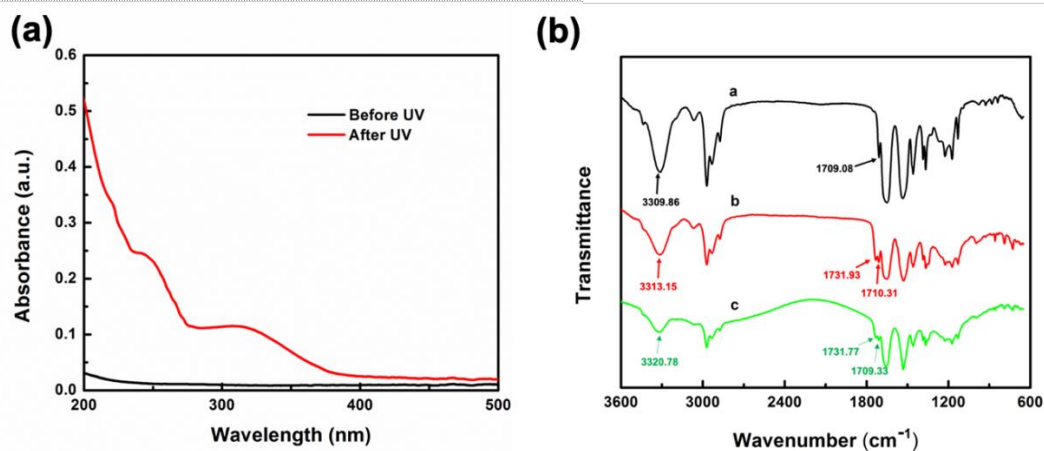
Figure 4-4. (a) UV-Vis spectra of supernatant before and after UV exposure and centrifugation of microgels and (b) FTIR spectra of a: pNIPAm MGs, b: pNIPAm-*co*-NBMA MGs and c: pNIPAm-*co*-NBMA after UV exposure.

4.3.3 Light-triggered *In Vitro* Release from DEX-loaded pNIPAm-*co*-NBMA microgels

As mentioned above, DEX is loaded into pNIPAm-*co*-NBMA microgels via what we think are hydrophobic interactions with the *o*-nitrobenzyl ester group of NBMA. If this is the case, DEX should be released upon cleavage of the NBMA from the microgels after UV exposure. To further investigate the release of DEX upon UV irradiation, we determined the amount of DEX released from the microgels as a function of UV exposure time, i.e., after 5, 10 and 30 min UV irradiation, followed by centrifugation and collection of the supernatant solution. To measure the amount of DEX released from the microgels into the supernatant solution, we utilized LC-MS. As shown in Figure 4-5, the amount of DEX found in the supernatant solution was highest at 5 min exposure, and exposure to the UV light for 10 min did not increase the amount of DEX found in the supernatant solution. However, 30 min UV exposure led to an observed decrease in the amount of DEX detected in the supernatant solution. This could be due to partial DEX decomposition as a result of the extensive UV-irradiation. It is worth mentioning that the release efficiency could reach the highest point after 5 min UV exposure. Importantly, previous studies have shown that extended (1h) exposure to low-dose, long-wave UV light does not affect gene expression of hMSC.[205, 206] Therefore, 5 min UV-irradiation was used for all further hMSCs experiments.
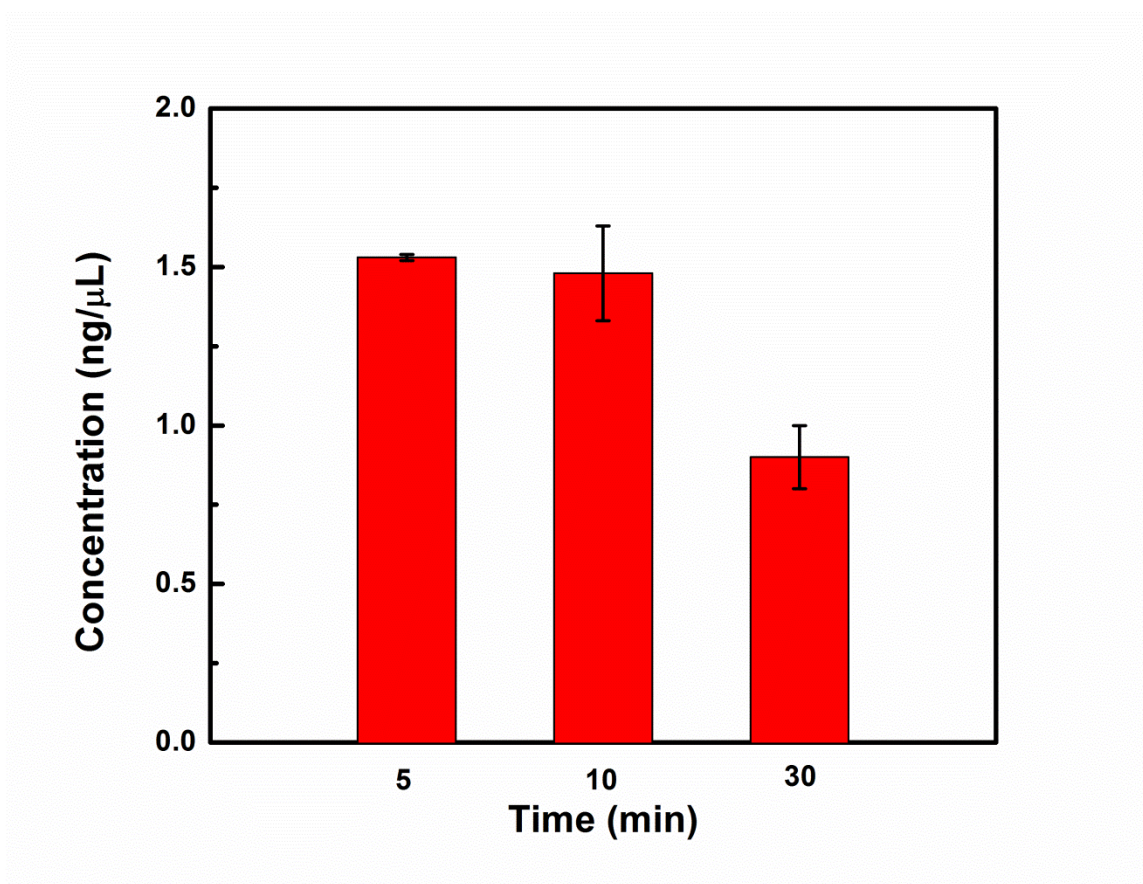
Figure 4-5. LC-MS results from photo-triggered in vitro release of DEX as a function of time of UV exposure

4.3.4 Cytotoxicity of pNIPAm-*co*-NBMA Microgels

Before considering adding microgels directly to the hMSCs, or any potential clinical applications, we investigated the cytotoxicity of the microgels. To do this, we exposed hMSCs to the prepared microgels at various concentrations (10, 25, 50, 100, and 200 μg/mL) and conducted an alamarBlue assay, which is a cell metabolic assay that we used to determine the impact of the microgels on hMSCs viability. As can be seen in Figure 4-6, after 24 h exposure to the microgels (with or without prior UV exposure), there is no

significant reduction in the viability of hMSCs at the microgel concentrations investigated. Interestingly, hMSCs exposed to microgels that were exposed to UV for 5 min exhibited higher cell viability compared to hMSCs exposed to microgels with no UV exposure at the concentrations of 100 and 200 μg/mL. For clinical applications these results are important as DEX-loaded microgels could be added to a site and stimulated locally, over many days using short UV-exposure cycles, to release small amounts of DEX upon each exposure, which has been shown to be beneficial for inducing osteogenic differentiation. Therefore, the results here suggest that the as-prepared microgels are non-cytotoxicity and can be examined for future osteogenic differentiation experiments in real world applications.
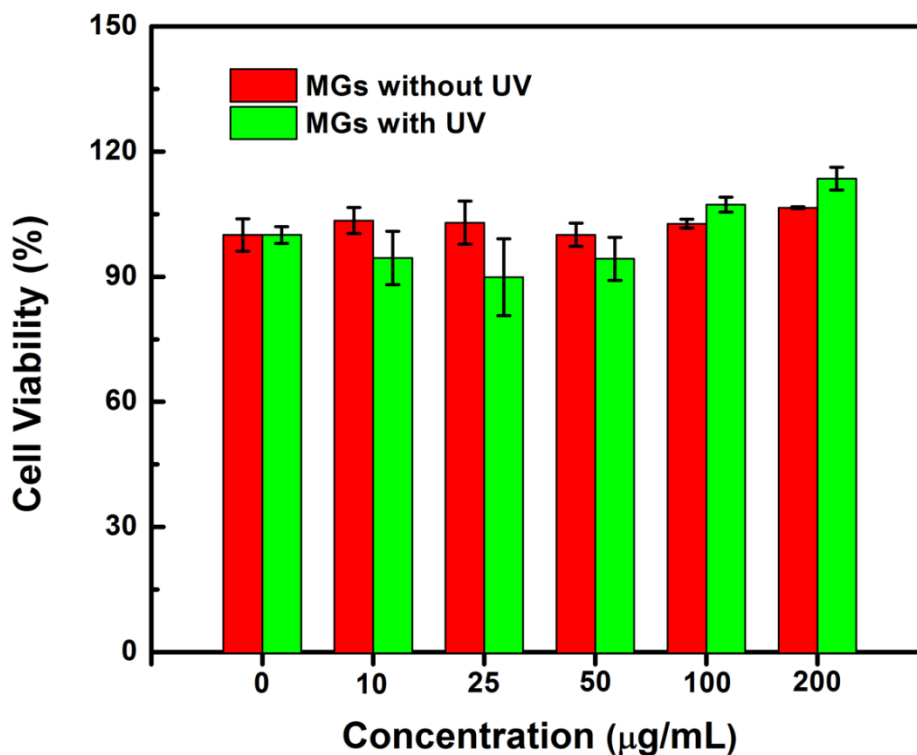
Figure 4-6. hMSCs viability after exposure to pNIPAm-*co*-NBMA microgels with and without UV exposure. All the data bars were obtained by averaging measurements obtained from ten different hMSC cultures, while the error bars indicate the standard deviation.

4.3.5 Evaluation of hMSC osteogenic differentiation

Utilizing DEX-loaded pNIPAm-*co*-NBMA microgels, we went on to show that light-triggered release from the microgels can support osteogenic lineage differentiation. To avoid the potential side effects from frequent UV light exposure to hMSCs (even though this is likely not an issue, as mentioned above), we decided to supplement BM with

supernatant solutions from centrifuged microgels after UV exposure. To evaluate the ability of DEX-loaded pNIPAm-*co*-NBMA microgels to induce hMSCs osteogenic differentiation in a light-triggered manner, we assessed the normalized ALP activity of cultured hMSCs on day 7, 10 14 and 21. ALP activity was chosen as the marker of osteogenic differentiation since the upregulation of ALP activity is a characteristic event during the early stages of osteogenesis.[207, 208] Specifically (and importantly), if the released DEX from UV-exposed microgels is added to BM, and can stimulate the proliferation and osteogenic lineage differentiation of hMSCs *in vitro*, then an increase in ALP activity should be observed.[209] To account for the background variations of cell numbers in different treatment groups, we also used the Bradford assay as a normalization method because protein content correlates with cell number. The experimental group was hMSCs exposed to the supernatant solution of DEX-loaded pNIPAm-*co*-NBMA microgels that were exposed to UV. Two negative controls were performed by exposing hMSCs to BM only and BM supplemented with supernatant solution from DEX-loaded pNIPAm-*co*-NBMA microgels that were not exposed to UV. A positive control was performed by culturing hMSCs in OM. The results for normalized ALP activity were shown in Figure 4-7. The osteogenic differentiation of hMSCs already occurred at day 7 in terms of the level of ALP activity, and the increase of normalized ALP activity was observed with increasing culture time for both experimental and positive control groups, however, both negative control groups (BM and BM + Non-UV

Sample) do not induce osteogenic differentiation. On day 21, the normalized ALP activity could reach the maximum value for experimental groups, which demonstrated that the introduction of supernatant of DEX-loaded light-responsive microgels upon UV-exposure can trigger the upregulation of ALP. Moreover, the hMSCs exposed to the DEX in the supernatant solution samples showed a similar ALP activity compared with the OM (positive control) group for all time periods.
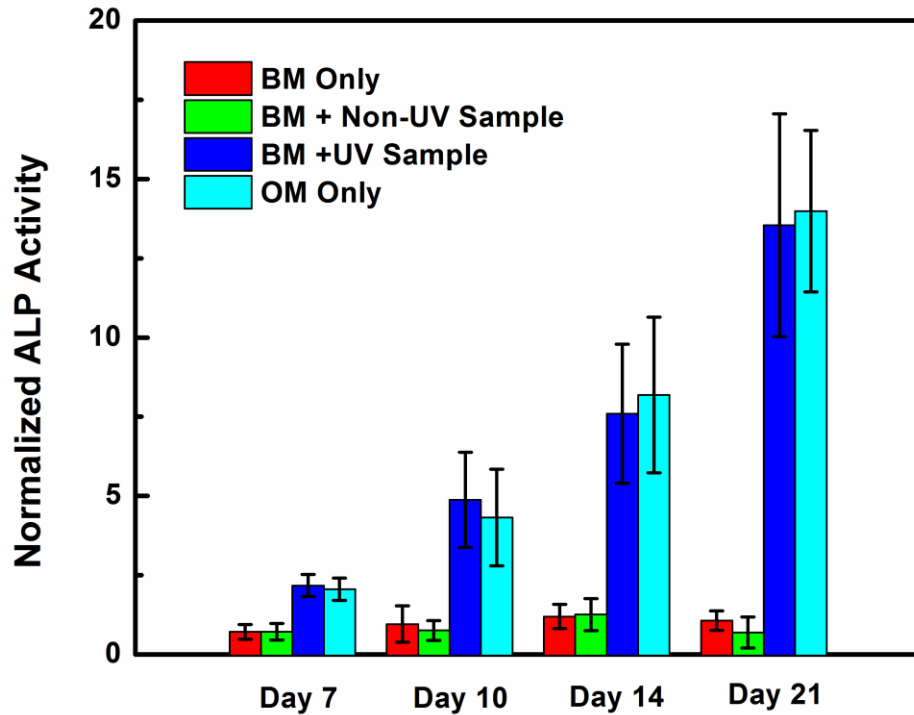
Figure 4-7. *In vitro* normalized alkaline phosphatase (ALP) activity of hMSCs after treated with various conditions for the different time period. The data was obtained by averaging measurements obtained from six different hMSC cultures, while the error bars indicate the standard deviation.

Morphological changes due to osteogenic differentiation of hMSCs was investigated using phase-contrast microscopy. Figure 4-8 shows that the control groups exhibit a spindle-shaped morphology, which indicates that the hMSCs did not undergo osteogenic differentiation, even after 21 days. However, we observed that hMSCs exposed to DEX released from the UV-exposed DEX-loaded microgels exhibited morphological changes at day 7, when the spindle-shaped morphology transitioned to a rounder shape. On day 14 and day 21, additional cuboidal/spherical shaped hMSCs could be observed (Figure 4-9(b)), which indicated additional osteogenic differentiation upon further DEX exposure. Since matrix mineralization is another marker for osteogenic differentiation, a ARS staining assay was used to identify calcium deposits. As depicted in Figure 4-9, compared with hMSCs cultured in basal medium only, hMSCs exposed to the DEX in the experimental group showed a significant increase in the amount of calcium deposits. The amount of calcium deposits also appears to increase with DEX exposure time. On the other hand, hMSCs exposed to the supernatant solution from DEX-loaded microgels not exposed to UV did not show obvious calcium deposits, even after 21 days of supernatant treatment.

What is more, we investigated how hMSCs differentiate when exposed to DEX for various time sequences. Specifically, we wanted to understand how hMSCs differentiate when exposed to DEX continuously, compared to intermittent DEX exposure. As shown

in Figure 4-10, hMSCs cultured in OM exhibited continuous osteogenic differentiation over 21 days, while hMSCs not exposed to DEX exhibited no osteogenic differentiation. Interestingly, hMSCs exposed to DEX in the supernatant solution from UV-exposed DEX-loaded microgels for the first 7 days exhibited osteogenic differentiation over the first 7 days. Once DEX exposure was stopped, the osteogenic differentiation was halted, and after 21 days, it is perhaps decreased. In another experiment, we exposed the hMSCs to DEX in the supernatant solution from UV-exposed DEX-loaded microgels for the first 7 days, stopped exposure for days 7-14, then resumed the exposure up to 21 days. As can be seen, differentiation was halted over days 7-14, while osteogenic differentiation resumed upon further exposure to DEX in the supernatant solution from UV-exposed DEX-loaded microgels. These results demonstrate the importance of continuous DEX exposure in order to achieve maximal osteogenic differentiation.
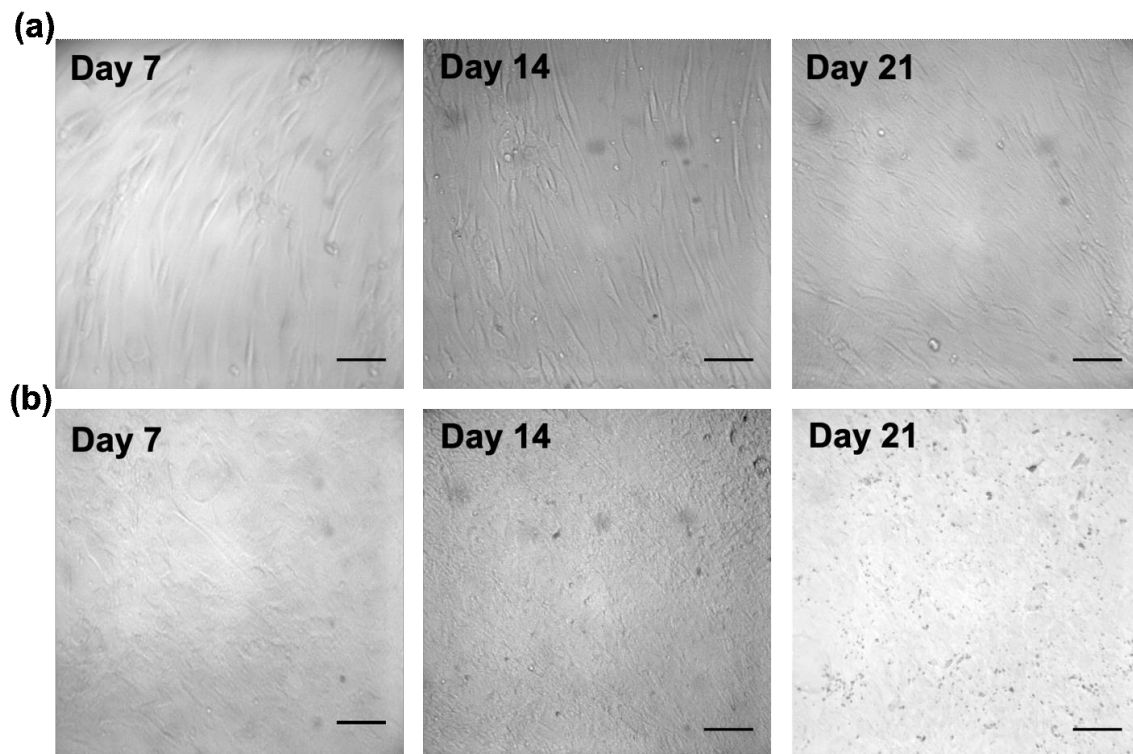
Figure 4-8. All cell groups were cultured with supernatant from DEX-loaded light-responsive microgels in basal medium (a) without UV-irradiation (b) with UV-irradiation. All of the images were observed through an inverted phase-contrast microscope. (Scale bar = 50 micron)
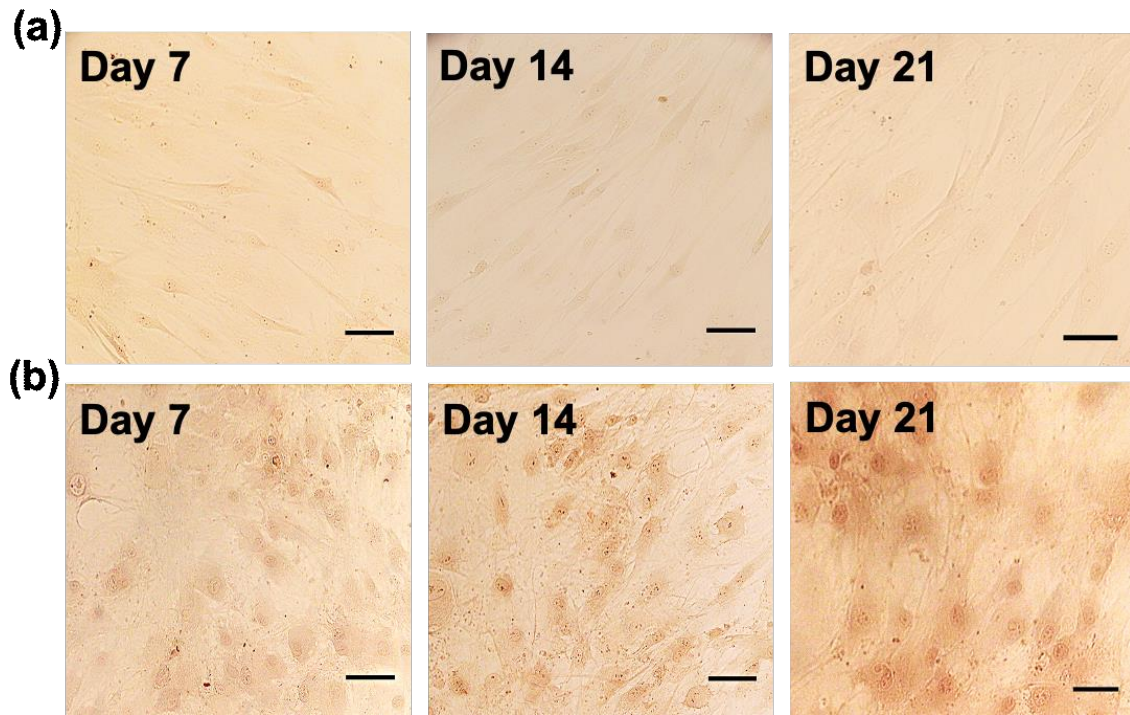
Figure 4-9. Evaluations of the mineralized extracellular matrix produced by Alizarin Red

S staining (a) basal medium without DEX in the supernatant solution; (b) basal medium

with DEX in the supernatant solution. (Scale bar = 50 micron)
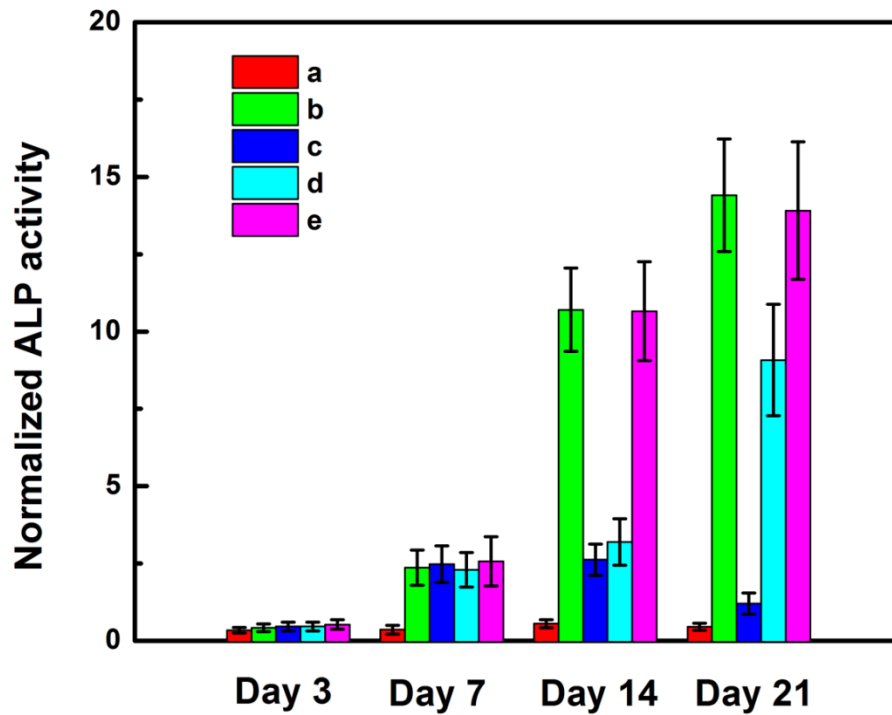
Figure 4-10. *In vitro* alkaline phosphatase (ALP) activity of hMSCs on day 3, 7, 14 and 21 after various DEX treatment sequences. (a) Basal medium only as the negative control; (b) osteogenic medium only as the positive control; (c) hMSCs exposed to DEX in the supernatant solution from UV-exposed DEX-loaded microgel for the first 7 days only; (d) hMSCs exposed to DEX in the supernatant solution from UV-exposed DEX-loaded microgels for the first 7 days, exposure stopped for days 7-14, then resumed DEX exposure up to 21 days; (e) hMSCs exposed to DEX in the supernatant solution from UV-exposed DEX-loaded microgels for the whole 21 days. All data bars were obtained by averaging measurements obtained from six different hMSC cultures, while the error bars indicate the standard deviation.

4.4 Conclusions

In summary, light-responsive pNIPAm-*co*-NBMA microgels were synthesized by free radical precipitation polymerization, followed by incorporation of DEX into the microgels via its putative hydrophobic interaction with the NBMA group. The light-triggered release of DEX was evaluated by LC-MS, and we assessed the ability of the released DEX to trigger osteogenic differentiation of hMSCs. The *in vitro* results showed that DEX released from the light responsive microgels could induce osteogenic differentiation, as observed by increased normalized alkaline phosphatase activity, as well as increased calcium deposits from the Alizarin Red S staining. Indirectly, we showed that the progress of osteogenic differentiation of hMSCs in our system could be controlled by turning on/off the UV light source. Overall, our results demonstrated that such DEX loaded light-responsive microgels were able to control the induction of hMSCs osteogenic differentiation upon light exposure. Lastly, with alamarBlue assays showing that our microgels were not toxic to hMSCs, we expect such DEX-loaded light-responsive pNIPAm-*co*-NBMA microgels have potential clinical applications including bone tissue engineering.

Chapter 5

Chitosan-Based Supramolecular Nanogels for pH and ATP Competitive Drug Release

5.1 Introduction

Stimuli-responsive polymers are capable of responding to numerous external chemical, physical or biochemical stimuli including pH, temperature, light, enzymes or a combination of them.[123, 125, 126, 135, 210-212] Considering the potential benefits brought by stimuli-responsive polymers, they are believed to be able to take advantage of broad opportunities for *in vitro/vivo* applications such as tissue engineering, biological imaging and controlled drug delivery systems.[119, 122, 213, 214] Among them, interests in stimuli-responsive polymers have seen an upsurge in the development of health care applications and disease therapy to date.[128, 200, 215, 216]

Chitosan is an attractive non-toxic, biocompatible and biodegradable polymer which is composed of copolymerization of D-glucosamine and N-acetyl-D-glucosamine derived from chitin.[217-220] The crosslinked chitosan, which could have tunable structures and porous networks, is considered to be an excellent candidate for drug delivery applications. Cross-linking chitosan and glutaraldehyde (GA) via Schiff base reaction has been widely

investigated and could have desirable physicochemical properties in biological and biomedical fields.[221, 222] Since the pK_a of GA-crosslinked chitosan is approximately 6.5 depending on the different degrees of crosslinking, the covalent bonding between the GA and chitosan could be destabilized in response to a weakly acidic pH and the drug release could be achieved in such systems as well.

Adenosine triphosphate (ATP) plays indispensable roles in many metabolic pathways, such as cellular respiration and enzyme catalysis etc.[223-226] Also, ATP acted as 'star molecule' by far has been widely investigated, which can be served as a novel trigger for the controlled release of anticancer drugs both *in vitro* and *in vivo*.[227] Compared with the low concentrations of ATP (< 0.4mM) in the extracellular environment, the intracellular concentration of ATP is relatively high between 1 and 10mM.[228] With such a high concentration of ATP in the cytosol of cancer cells, multidrug resistance proteins, which belong to ATP-binding cassette transporter family, can use ATP molecules extensively to promote drug efflux and confer resistance to many anticancer drugs.[229] Therefore, lower the concentration of ATP in the cytosol of cancer cells could enhance the activities of anticancer drugs. What is more, previous report displayed that ATP can be assembled with chitosan to form supramolecular amphiphiles.[230] Based on these ideas to improve the drug targeting efficacy into tumor cells and combat the multidrug resistance to chemotherapy, we aimed to develop pH- and ATP-responsive drug delivery nanosystems and directly promote the release of preloaded anticancer drugs. On

a combination of pH and ATP targeting effects, such system presents a significant improvement in the chemotherapeutic killing of tumor cells.

Here, we developed chitosan-based supramolecular nanogels for chemotherapeutic drug delivery targeting the tumor cells (HepG2). Such supramolecular nanogels were prepared by crosslinking chitosan with glutaraldehyde as a cross-linker via Schiff base reaction. Subsequently, the model anticancer drug, doxorubicin-hydrochloride (Dox-HCl), was loaded into the supramolecular nanogels. Moreover, the as prepared supramolecular nanogels were further investigated for pH and ATP-responsive release properties of Dox-HCl. The schematic illustration was shown in Scheme 5-1(a). Following, the Dox-loaded supramolecular nanogels exhibited the abilities of killing the cancer cells efficiently. Since the Dox could be released in a pH controlled manner of chitosan-based supramolecular nanogels and the pH-degraded nanogels exhibits selectively assemble towards ATP under physiological conditions in cells, which could slow down the efflux of the anticancer drug Dox, resulting in long cellular retention of Dox, thus enhancing the anticancer activity of Dox against Dox-resistant cancer cells. Such schematic illustration was displayed in Scheme 5-1(b). Finally, the CCK-8 assay also demonstrated that such chitosan-based supramolecular nanogels were not cytotoxic at a low concentration in human hepatic normal cells (L02).

5.2 Experimental Sections

5.2.1 Materials

Chitosan was analytical grade with a deactylation degree greater than 90%, obtained from Tokyo Chemical Industry CO., LTD. Glutaraldehyde (GA) was purchased from Sigma-Aldrich with 50 wt. % in H_2O. HEPES was bioperformance certified, $\geqslant$99.5% (titration), cell culture tested which was obtained from Sigma-Aldrich. Sodium hydroxide (NaOH), hydrochloric acid (HCl) and acetic acid with analytical agents were all purchased from the Beijing Chemical Reagents Company and were used as received. Deionized (DI) water, with 18.2 MΩ·cm resistivity, was obtained from a Millipore Milli-Q-Plus system. Doxorubicin hydrochloride (Dox-HCl) was purchased from Aladdin Industrial Corperation. Adenosine triphosphate disodium was purchased from Sinopharm Reagent Company. Dulbecco's modified Eagle's medium (DMEM) and trypsin were both obtained from Gibco Technology (Shanghai, China). Cell Counting Kit-8 (CCK-8) was acquired from Dojindo Molecular Technology Inc. (Shanghai, China). All other reagents and solvents were obtained from commercial suppliers and used without further purification unless specified.

5.2.2 Synthesis of Chitosan-Based Supramolecular Nanogels

Glutaraldehyde cross-linked chitosan supramolecular nanogels were synthesized as

follows: Initially, 0.5 g chitosan was dissolved in 100 mL DI water with 0.5 % (v/v) acetic acid with filtration through a 20-mL syringe affixed to 0.8 μm filter. Subsequently, 1 mL resultant chitosan solution (31 mM) was mingled with pH 7.4 HEPES buffer solution (50 mM, 4.8 mL), followed by dropwise the addition of 0.4 mL glutaraldehyde solution (50%) under the condition of ultrasonication 1 hour and vigorous stirring 4 hours. Finally, the glutaraldehyde cross-linked chitosan supramolecular nanogels were successfully synthesized where the ratio of chitosan to glutaraldehyde is 5:2, accompanying by an apparent Tyndall effect. The supernatant of homogeneous nanogels was separated and purified by centrifugation for 5 minutes in order to remove the large aggregates (~4000 rpm, 25 °C).

5.2.3 Characterization of Chitosan-Based Supramolecular Nanogels

The hydrodynamic diameter of the supramolecular nanogels in HEPES buffer was obtained by dynamic light scattering (DLS), and zeta potential of the supramolecular nanogels was measured using a Malvern ZS 90 Zetasizer instrument equipped with a light source with wavelength of 633 nm, at 25 °C. Transmission electron microscopy (TEM) images were performed with a Jemo 2010 electron microscope. FTIR spectra were recorded using KBr disks, which supramolecular nanogels were lyophilized first, on an FTIR spectrometer (Bruker IFS55, Germany) at room temperature over the range of

4000-400 cm^{-1}. ^{1}H solid-state NMR spectra were measured on a JEOL JNM-ECZ600R spectrometer (600 MHz), with a commercial JEOL 3.2 mm MAS probe at room temperature. All ^{1}H solid-state NMR spectra were referenced to solid glycine.

5.2.4 Drug Encapsulation Efficiency and in Vitro Release

The Dox-HCl solutions (1mM) and supramolecular nanogels (0.8mg/mL) were isovolumetric mixed in pH 7.4 HEPES buffer solutions, followed by gentle magnetic stirred (500 rpm) for 24 h to allow loading the Dox completely into supramolecular nanogels. Then, the drug-loaded supramolecular nanogels were purified by dialysis in pH 7.4 HEPES buffer solutions (MWCO: 1000 Da) for 24 h. Then, the encapsulation efficiency (EE) of Dox-HCl with the supramolecular nanogels was calculated by the following equation 5-1:

$$EE = M_0\text{-}M/M_0 \times 100\% \qquad\qquad (5\text{-}1)$$

where M_0 represents the initial amount of drug and M is the amount of drug partitioned in dialysis solutions with pH 7.4 HEPES buffer. The amount of Dox-HCl in the supramolecular nanogels was determined by the mass of lyophilized nanogels before and after drug-loaded. In general, the encapsulation efficiency (EE) of Dox-HCl with the supramolecular nanogels was approximately 85%.

For the Dox-HCl release measurements, the drug loaded supramolecular nanogels was added to a dialysis membrane tube again, which was then incubated in 40 ml HEPES

buffer solutions with pH 5.0 only and pH 5.0 with different concentrations of ATP at 0.5 mmol, 1 mmol or 2 mmol at 37 °C in a water bath with shaking rate at 200 rpm. At predetermined frequencies, 2 ml incubated solution was taken out and refilled into the initial incubation solution. All fluorescence spectrometric experiments were carried out with excitation and emission wavelengths at 485 nm and 590 nm, respectively, at room temperature (25 °C). Dox-HCl release profiles were determined by measuring the fluorescence of the dialysis solutions at 590 nm. The fluorescent spectra of our samples were used the Cary Eclipse Fluorescence spectrophotometer, Agilent Technologies.

5.2.5 Cell Culture

Human hepatic cancer cells (HepG2) and human hepatic normal cells (L02) were cultivated in the dulbecco's modified eagle's medium (DMEM) medium containing 10% (v/v) fetal bovine serum (FBS) (Hyclone) and 1% (v/v) penicillin/streptomycin. Cell culture was carried out in an incubator with a humidified atmosphere of 5 % CO_2 at 37 °C.

5.2.6 Cell Viability and in Vitro Efficacy Assay

To analyze the cytotoxicity of supramolecular nanogels, the cells were seeded into 96-well plates at a density of 5000 cells/well and cultured with 100 μL of complete medium for 24 h; Certain amount of varying concentrations of supramolecular nanogels

and PBS (as negative control) were added into the medium. After incubation of 24 h, the old medium was discarded, and the cells were rinsed with PBS (10 mmol/ L and pH 7.4), followed by the addition of 10 μL of CCK-8 media into each well. After a further 2 h incubation, the absorbance at 450 nm was measured using a microplate reader (EnVision, PerkinElmer) to analyze the cell viability (%). Three independent experiments were performed. The resultant data for the control cells was normalized to be 100% viable for all subsequent measurements. For the drug release in the HepG2 cells experiment, all the procedure was the same as mentioned before except for using different concentrations of Dox-loaded supramolecular nanogels solutions instead of supramolecular nanogels only.
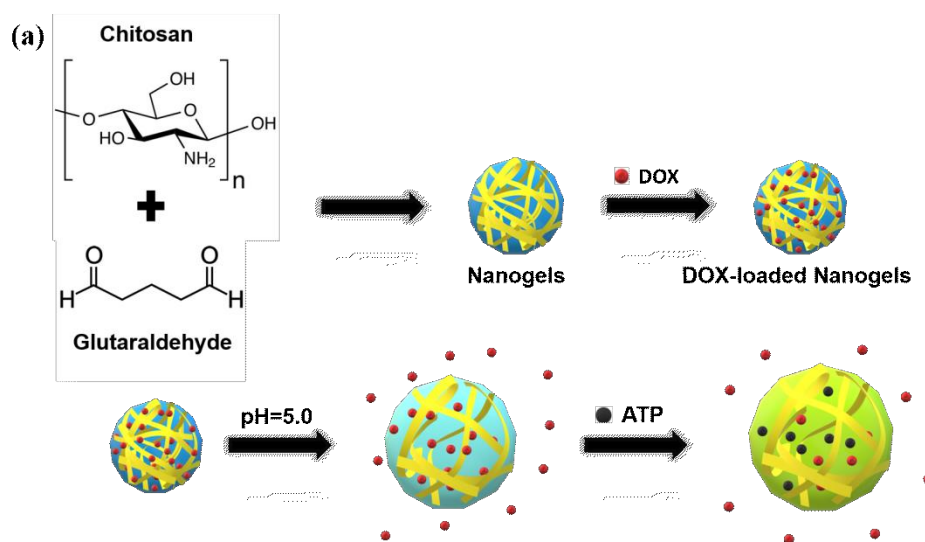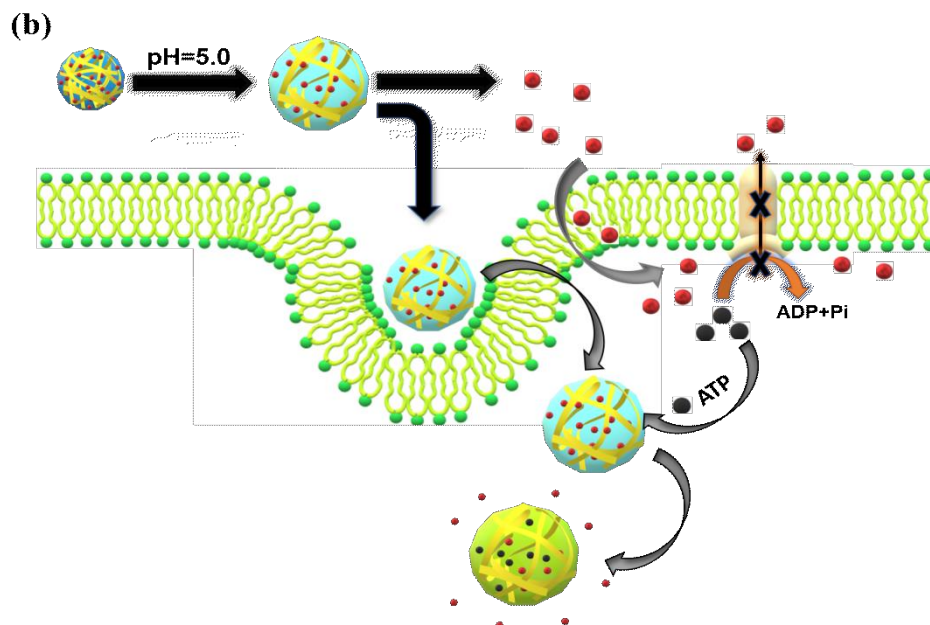
Scheme 5-1. Schematic illustration of chitosan-based supramolecular nanogels for chemotherapeutic drug delivery. (a) Construction of chitosan-based supramolecular nanogels and release mechanisms by pH and ATP. (b) Schematic illustration of *in vitro* drug delivery for chemotherapy

5.3 Results and Discussion

In this work, the ability of chitosan-based supramolecular nanogels for drug delivery was evaluated. The chitosan-based supramolecular nanogels were prepared following a previously published protocol as above. The morphology and hydrodynamic size of glutaraldehyde crosslinked chitosan nanogels were first characterized by TEM and DLS, respectively. As can be seen in Figure 5-1(a), the DLS data indicated that the nanogels

had an average hydrodynamic diameter of 35 nm. Additionally, from the TEM image in

Figure 5-1(b), it could be found that those nanogels were monodisperse and had

round-shape structure with the size of around 25 nm, as expected, which was consistent

with the data obtained by DLS. The zeta potential of chitosan-based supramolecular

nanogels was + 13.6 mV, indicating that supramolecular nanogels possessed positively

charged due to in the presence of amino group.
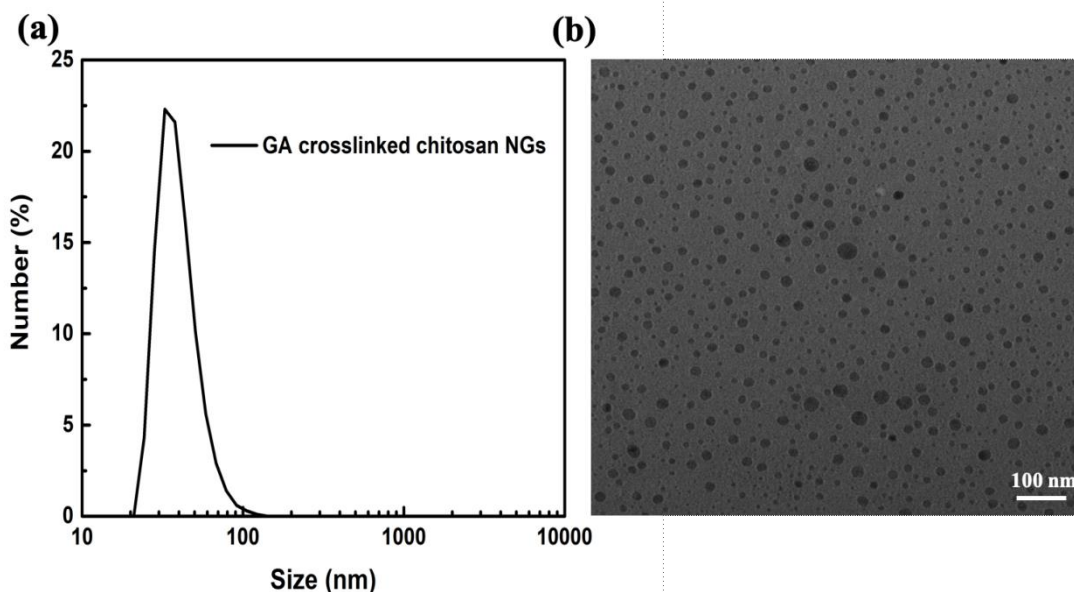
Figure 5-1. DLS measurement (a) and TEM image (b) of glutaraldehyde crosslinked

chitosan nanogels

To further confirm the glutaraldehyde crosslinked chitosan nanogels, the

supramolecular nanogels were characterized by FTIR. The appearance of a peak at a

specific wavenumber indicates a specific chemical bond. Figure 5-2(a) showed the FTIR

spectra of chitosan flake, glutaraldehyde crosslinked chitosan in pH =7.4 and pH = 5.0,

respectively. From the chitosan spectra, the band at 2207 cm^{-1} 1635 cm^{-1} were due to primary ammonium cations and amides group [Vas (C=O)], respectively. The stretching N-H group at 1592 cm^{-1} was due to the combined deformation of amine group [δ(NH$_2$)] and remaining amide group in chitosan. Further, the little signals depicted at 1420 and 1390 cm^{-1} corresponded to the C-N bond stretching and deformation of C-H respectively. In spectrum of glutaraldehyde crosslinked chitosan nanogels at pH 7.4, the peak at 2207 cm^{-1} was disappeared and attenuation due to deprotonation of ammonium cation and cross link with glutaraldehyde. The absorption intensity increasing at 1668 cm^{-1} was contributed to C=O group that belongs to self-polymerization of glutaraldehye in aqueous solution to form a greater crosslinking chain.[231-233] Moreover, there was no peak above 1700 cm^{-1} indicated that there were no free aldehyde groups. The band at 1592 cm^{-1} increasing represented the C=N of imine group [Vas (C=N)] that formed between amine of chitosan and carboxyl of glutaraldehyde by Schiff base reaction. Meanwhile, the IR spectrum of crosslinked chitosan nanogels in pH = 5.0 was rather similar to that of crosslinked chitosan nanogels in pH = 7.4. However, the attenuation of C=N of imine group at 1592 cm^{-1} was obtained due to the amine bond deformation in acid environment. Additionally, the peak at 1665 cm^{-1} was ascribed to degradation of the nanogels and reappearance of amide group and glutaraldehyde of C=O stretching bond, consequently confirmed the imine group formation and pH responsivity of supramolecular nanogels.

Chitosan, glutaraldehyde and crosslinked chitosan nanogels were further

characterized by solid state ^{1}H NMR. As shown in Figure 5-2(b), Chitosan shows typical characteristics resonance in the 2-6 ppm region that are assigned to the hydrogens of amino group and other hydrogens of polysaccharide. The glutaraldehyde spectrum showed obvious peaks of hydrogens of aldehyde unit were found at 10 ppm.[234] For the glutaraldehyde crosslinked chitosan nanogels, there was no characteristics resonance at 10 ppm which meant the absence of hydrogens of aldehyde unit. The spectrum contained some additional peaks between 3-5 ppm which could be ascribed to the hydrogens of amine group and complex structure of crosslinked chitosan nanogels. Based on those data, it was found that the imine group was formed in the supramolecular nanogels.
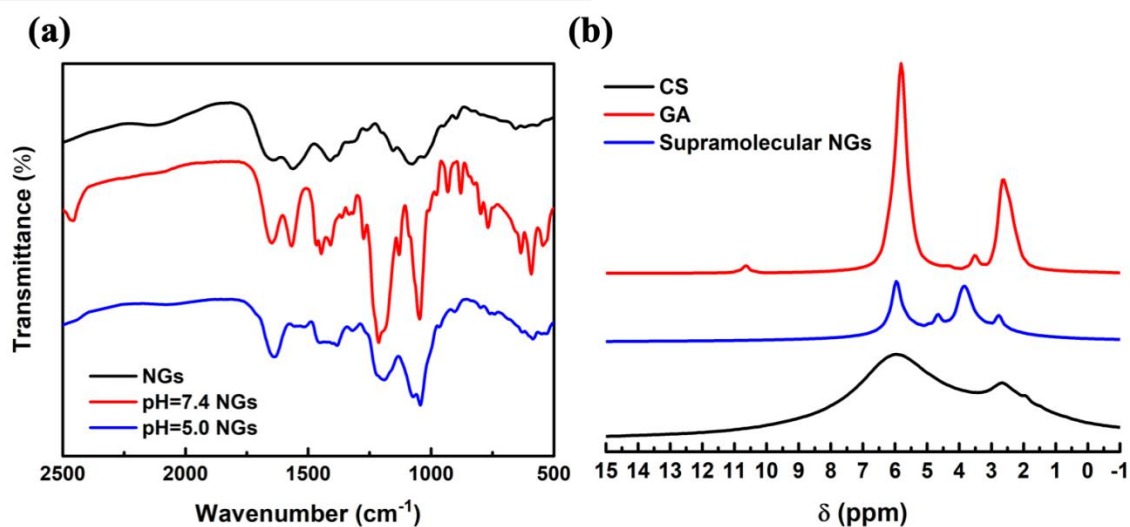
Figure 5-2. FTIR (a) of chitosan (black line), supramolecular nanogels in pH = 5.0 (blue line) and 7.4 (red line), respectively. (b) solid state ^{1}H NMR of chitosan (black line), glutaraldehyde (red line) and supramolecular nanogels (blue line) respectively.

After the characterizations of supramolecular nanogels, in order to confirm the pH

and ATP responsive effect of supramolecular nanogels on the release process, the fluorescence emission spectra of released Dox were measured. The procedure was described as mentioned above. Firstly, the release profile of Dox-loaded GA crosslinked chitosan nanogels with different pH and ATP were recorded at various times. As shown in Figure 5-3(a), in comparison with pH 7.4 solutions, it was found that the release rate and amount of the loaded Dox from the supramolecular nanogels in pH 5.0 solutions increased significantly with the time increasing within 48 hours. This is due to the deformation of supramolecular nanogels in acid environment, resulting in releasing the Dox into the aqueous solutions. Based on the chitosan could be reacted with ATP in the acid environment, we tried to introduce the ATP into our system and enhanced the cumulative release of Dox. From the results, we could clearly observe that the cumulative release of Dox was slightly increasing in the pH 5.0 solutions with 0.5 mM ATP, which is 90% of the loaded Dox released in 2 days, compared with the pH 5.0 solutions only to 75% within the same period. Thus, we believed that both pH and ATP as dual triggers could be effective on the controlled anticancer drugs delivery, which was via a conformational change of supramolecular nanogels in such environment.

Since the concentration of ATP in the cancer cell is in the range from 10 μM to few mM,[235] it is also worthy noticing the cumulative release of Dox as a function of different concentration of ATP. As shown in Figure 5-3(b), the cumulative release of Dox was slightly increased with increasing the concentration of ATP from 0.5 mM to 2mM,

respectively. That is, almost 85% of the loaded Dox released in 2 days by 1 and 2 mM

ATP of acid environment, compared with the 81% in 0.5 mM ATP within the same period.

That is because when the concentration of ATP achieves 1mM, ATP is already in excess

in our system, and the reaction of ATP and the nanogels is at equilibrium at that time.[230,]

[236] Therefore, the concentrations of ATP at mM level have a negligible effect on the

release of Dox in our systems.
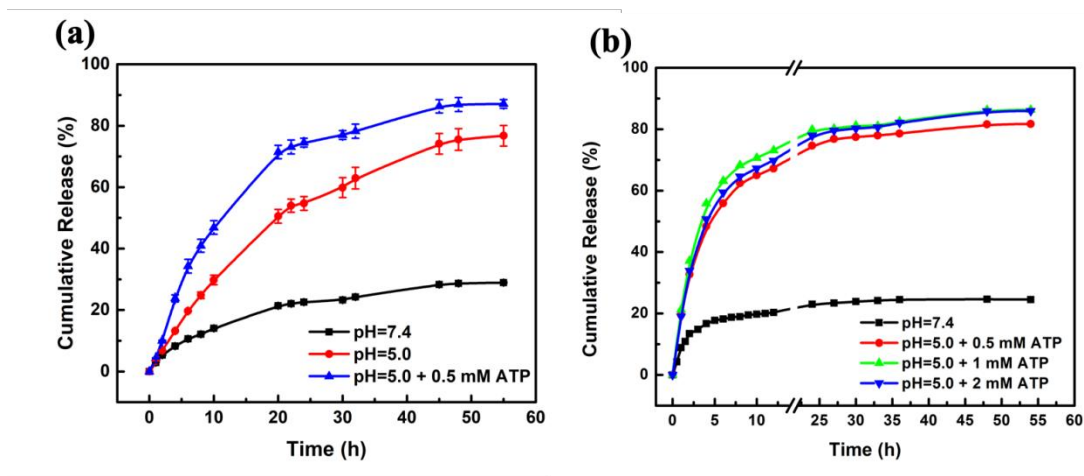
Figure 5-3. Cumulative release profiles of Dox from the prepared supramolecular

nanogels by (a) different pH solutions at different time and (b) different concentration of

ATP at different time. The concentration of the prepared supramolecular nanogels

encapsulated with Dox: 2.5 mg/mL. Error bars represent standard deviation by three

independent measurements.

After, in order to assess the cytotoxicity of the drug-free nanocarriers, human

hepatic normal cells were incubated with as prepared supramolecular nanogels at various

concentrations (0.16, 0.4, 0.8, 1.6, 4, 8, 16 and 24 mg/mL) and their physical mixture

solutions followed by addition of CCK-8 assay reagent. After incubation for 24 h, cell viability was then determined by the CCK-8 assay.[237, 238] Dominant live cells were both obviously shown in experimental group and positive control group. The cells' viability with supramolecular nanogels were above 80% at all the tested concentrations. There was no significant cytotoxicity presented by such different concentrations of nanogels compared with untreated cells as shown in Figure 5-4. These results showed that the as prepared supramolecular nanogels had a negligible effect on the cytotoxicity at low concentrations, and can be employed as safe drug delivery carriers without concerns in terms of cytotoxicity.
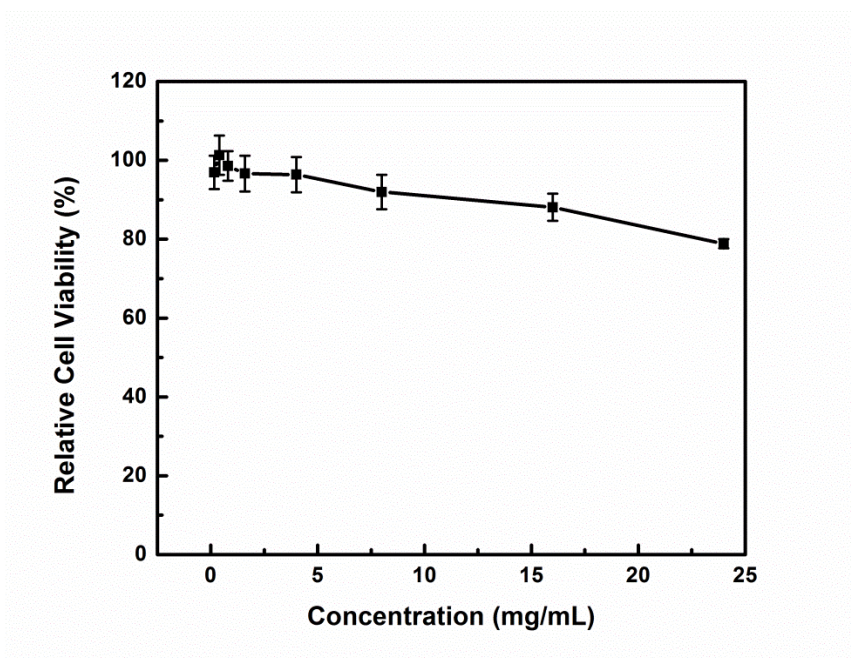
Figure 5-4. Relative cell viability of human hepatic normal cells (L02) in the presence of different concentrations of the supramolecular nanogels. Error bars represent standard deviation by three independent measurements

Ultimately, the anticancer efficiency of Dox-loaded supramolecular nanogels was evaluated using CCK-8 cell survival assay, where HepG2 cells were incubated with free Dox and Dox-loaded supramolecular nanogels for 24 and 48 h, respectively. As indicated in Figure 5-5(a), the relative cell viabilities of HepG2 cells after cultured with different concentration of Dox-loaded supramolecular nanogels were visibly lower by 10-15 % than those of free Dox in the first 24 h. After incubation for 48 h with free Dox and Dox-loaded supramolecular nanogels which was shown in Figure 5-5(b), the results showed relative cell viabilities of HepG2 after cultivated of Dox-loaded supramolecular nanogels with the concentration of 1 µM were significantly lower by 23 % in a comparation with those of free Dox. The reason can be explained that Dox can be released in a pH-controlled fashion by supramolecular nanogels and the degraded nanogels exhibits selectively assemble towards ATP under physiological conditions in cancer cells, which could slow down the efflux of the anticancer drug Dox with long cellular retention of Dox, thus enhancing the anticancer activity of Dox against Dox-resistant cancer cells. However, with increasing concentration of Dox, there is no significantly enhanced the drug anticancer efficiency for HepG2 cells since the side effect of anticancer drug occurred with such high concentration. Another reason could be that the binding effect between degraded nanogels and ATP for decrease of efflux of Dox would be less at the high concentration (e.g. 10 µM). In brief, the results indicated that the encapsulation of Dox by supramolecular nanogels could enhance the drug anticancer

efficiency for HepG2 cells. The obvious in vitro low cytotoxicity to normal cells and high killing efficiency to cancer cells indicates that chitosan-based supramolecular nanogels as multifunctional supramolecular nanoparticles can be used in adjuvant chemotherapy.
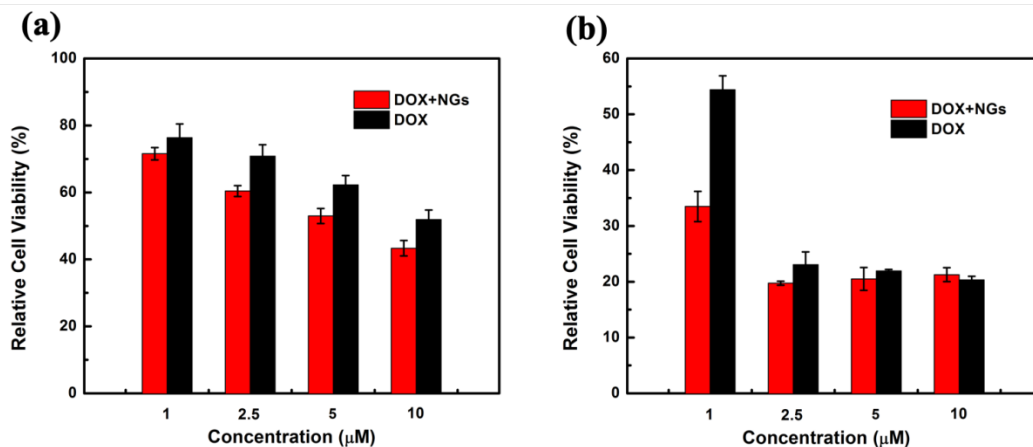
Figure 5-5. In vitro viabilities of HepG2 cells after incubation with different concentrations of free Dox, and Dox-loaded supramolecular nanogels within 24h (a) and 48h (b). Error bars represent standard deviation by three independent measurements

5.4 Conclusions

To sum up, we illustrated the use of assemblies of chitosan-based supramolecular nanogels for drug release in complex conditions (ATP and acid environment). Such chitosan-based supramolecular nanogels were non-toxic at the low concentration (< 24 mg/mL). Moreover, we demonstrated pH and ATP as dual triggers for the controlled anticancer drugs (Dox-HCl) delivery via a conformational change of supramolecular

nanogels in an acid environment in the tumor cell (HepG2). Following, ATP in tumor cells could be directional complexed by the degraded nanogels. With this, the efflux of Dox-HCl could be attenuated, resulting in enhancing the anticancer efficacy of Dox-HCl in vitro. Such pH and ATP-triggered drug release system could provide a sophisticated fashion to modulate the function of ATP in cells, which can facilitate the antitumor efficacy in vitro/vivo.

Chapter 6

Volatile Organic Compound Vapor Detection with Responsive Microgel-Based Etalons

6.1 Introduction

Due to their high vapor pressure, volatile organic compounds (VOCs) are readily transformed to the vapor phase, which subsequently allows them to become easily transported in the environment.[239] Biogenic VOCs produced by a large number of plants play an important role in their communication as well as the plant's communication with insects and animals to attract pollinators, seed dispersers, and as a defense mechanism to prevent their consumption.[240, 241] Moreover, many anthropogenic VOCs produced by human activity are hazardous air pollutants and dangerous to human health;[242] e.g., benzene (a well-known human carcinogen), and chlorofluorocarbons (contributing to ozone depletion).[243]

Some VOCs exhibit significant solubility in water allowing them to endanger aquatic life. Therefore, a number of techniques have been developed and employed to analyze VOC concentration in water and/or in the atmosphere, such as: liquid and gas chromatography, metal oxide sensors, and metal organic framework-based sensors.[244-246]

While these techniques have led to improved monitoring efforts, they each have some deficiencies, e.g., high cost and complex sensor construction and operation. In order to obtain a portable and more cost effective device for VOC quantification, recent attention has been focused on stimuli-responsive polymer-based colorimetric sensors.[247, 248]

Stimuli-responsive polymers are an important class of materials that can be used for various applications, such as: sensors, enzyme encapsulation, and drug delivery.[119, 249, 250] Thermoresponsive poly(N-isopropylacrylamide) (pNIPAm) is one of the most well studied responsive polymers to date, which exhibits a coil to globule transition at the lower critical solution temperature (LCST) of 32 °C. That is, pNIPAm is fully water soluble at temperatures < 32 °C, existing as a random coil, and transitions to a collapsed, "water insoluble" globule when the temperature of the solution is > 32 °C; this transition is fully reversible over many cycles. Like linear pNIPAm, crosslinked pNIPAm hydrogel microparticles (microgels) also exhibit similar behavior. At T < LCST, the pNIPAm-based microgels are water swollen, and expel the water when the temperature exceeds the LCST.[142, 251-253] Using pNIPAm-based microgels, our group has fabricated colorimetric sensors called etalons. As shown schematically in Figure 6-1, our etalons are composed of pNIPAm-based microgels confined between two thin gold (Au) layers (usually 15 nm) to generate the "mirror-dielectric-mirror" configuration of a classic Fabry-Pérot etalon with the pNIPAm-based microgels serving as the dielectric layer.[254, 255] Light striking the surface of the device enters the etalon's microgel layer and undergoes constructive and

destructive interference that leads to specific wavelengths of light being reflected that can be predicted from equation 6-1:

$$m\lambda = 2nd\cos\theta \hspace{3cm} (6\text{-}1)$$

where m is the order of the reflected peak (e.g., 1, 2, 3,...), λ is position of the reflectance peak, n is the refractive index of the dielectric layer, d is the distance between the two Au layers, and θ is the incidence angle. While the wavelength (λ) of light reflected from the etalon (and hence the etalon's color) depends n, θ, and d, we have shown in numerous studies that λ depends primarily on d at a fixed angle.[60] Therefore, any change in the size of the microgels between the two Au layers leads to a change in d, and ultimately λ, and the $\Delta\lambda$ that can be related to the etalon's environment.
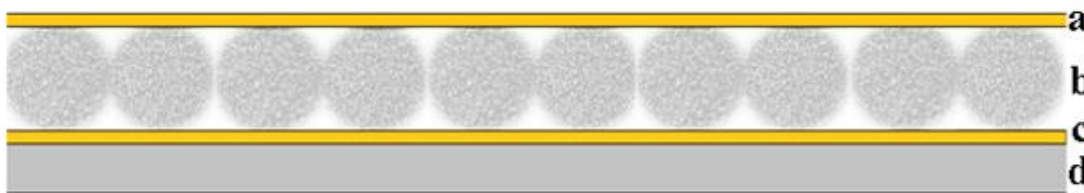
Figure 6-1. Schematic depiction of a microgel-based etalon consisting two 15 nm Au layers (**a** and **c**), sandwiching a single layer of microgels (dielectric, **b**) built on a rigid glass substrate (**d**).

Herein, we show that pNIPAm microgel-based etalons can be used for detecting VOCs. Specifically, the response of the microgel-based etalons to hexane, cyclohexane, petroleum ether, chloroform and tetrahydrofuran (THF) vapors was evaluated. This was accomplished by bubbling their vapor into water containing an etalon, and the position of

the reflectance peak monitored over time. The results obtained here confirm that the microgel-based etalons can detect VOCs bubbled (and hence dissolved) in water, which is related to the microgel solubility in the VOCs and in the case of THF, cononsolvency. The etalons showed high selectivity towards THF compared to the other vapors tested here and a detection time (time to reach the limit of detection (LOD)) of ~4 mins. Also, our devices showed good reversibility over many cycles. Importantly, the etalons provide a new means for VOC sensing, which can lead to new sensors for environmental monitoring.

6.2 Experimental Section

6.2.1 Materials

N-isopropylacrylamide (NIPAm) was purchased from TCI (Portland, Oregon) and purified by recrystallization from hexane (ACS reagent grade, EMD, Gibbstown, NJ) prior to use. *N,N'*-methylenebisacrylamide (BIS) (~ 99%) ammonium persulfate (APS) (~ 98%), hexane ($\geq$ 99%), cyclohexane ($\geq$ 99.5%), chloroform ($\geq$ 99.8%), tetrahydrofuran (THF) ($\geq$ 99.9%), and petroleum ether ($\geq$ 90%) were obtained from Sigma-Aldrich (Oakville, Ontario) and were used as received. Glass substrates (25 mm x 25 mm) were from Fisher Scientific (Ottawa, Ontario). Deionized (DI) water with 18.2 MΩ·cm resistivity was from a Millipore Milli-Q-Plus system (Billerica, MA). Cr (99.999%) and

Au (99.99%) were purchased from ESPI Company and MRCS Canada (Edmonton), respectively.

6.2.2 Synthesis of pNIPAm-Based Microgels

Free radical precipitation polymerization was used to synthesize poly N-isopropylacrylamide (pNIPAm)-based microgels with NIPAm as the monomer and N,N'-methylenebisacrylamide (BIS) as the crosslinker, following our previously published protocol.[150] NIPAm monomer (13.3 mmol) and BIS crosslinker (0.703 mmol) were dissolved in 99 mL deionized water and stirred for 10 min. Then using a 25-mL syringe affixed with a 0.2 µL filter, the resultant solution was transferred into a 3-neck round bottom flask equipped with a nitrogen gas inlet, a reflux condenser, and a thermometer. Afterwards, the temperature of the solution was slowly increased to 70 °C within 1 h and the initiator ammonium persulfate (APS) was introduced into the reaction solution. The reaction was allowed to proceed for 4 h at 70 °C under nitrogen gas atmosphere. The resultant microgel solution was allowed to cool overnight to ambient temperature, and then filtered through glass wool to remove large aggregates that may have formed during polymerization. Finally, microgels solution was purified via centrifugation and resuspension in water six times and the microgels collected.

6.2.3 Etalon Fabrication

Etalons were generated using our previously published paint-on protocol.[151] Initially, 2 nm Cr and 15 nm Au was deposited on a clean glass substrate using a thermal metal evaporator (Torr International Inc., New Windsor, NY). Then, 40 μL of a concentrated pNIPAm-based microgel solution (concentrated via centrifugation) was transferred to the Au-coated glass slide and spread using a micropipet tip. Subsequently, the microgel layer was allowed to dry on a hot plate set to 35 °C for 1h. The excess microgels that were not directly attached to the Au surface were washed away with DI water, resulting in an microgel-coated Au slide with a homogenous, highly packed microgel monolayer. Finally, another 2 nm Cr and 15 nm of Au was deposited on the microgel layer. After the top Au-layer deposition, etalons were immersed in DI water for at least 2 h before being used for the vapor phase experiments. Surface morphology of the etalons was characterized by scanning electron microscopy (SEM).

6.2.4 Characterization

Scanning electron microscope (SEM) images of etalons were collected using a Zeiss Sigma FESEM (Jena, Germany), operated at 20 kV. The hydrodynamic diameter of the microgels in both DI water and the resultant solutions after the VOC bubbling experiment was obtained by dynamic light scattering (DLS) measurements using a Zetasizer Nano ZS - Malvern Instrument (Westborough, MA, USA) equipped with a light source with

wavelength of 633 nm, at 25 °C. A JEOL JEM-2100 EX/S transmission electron microscope (TEM) (JEOL USA, Inc.) was used to determine the morphology of the pNIPAm microgels.

6.2.5 Vapor Sensing Experiment Setup

The setup of the experiment can be seen in Scheme 6-1. An etalon was adhered to the bottom of a glass vessel and 2.5 mL of DI water added, then a reflectance probe and needle was inserted into this vessel. The respective solvents were added to a 2-neck round bottom flask and nitrogen gas pumped in at a rate of 500 cc/min (measured by a Set-A-Flo Precision Analog Flow Meter, Rose Scientific Ltd.) to transfer the solvent vapor into the glass vessel containing the etalon. The solvent vapor was bubbled into the water, and the etalon's reflectance spectrum collected as a function of time.
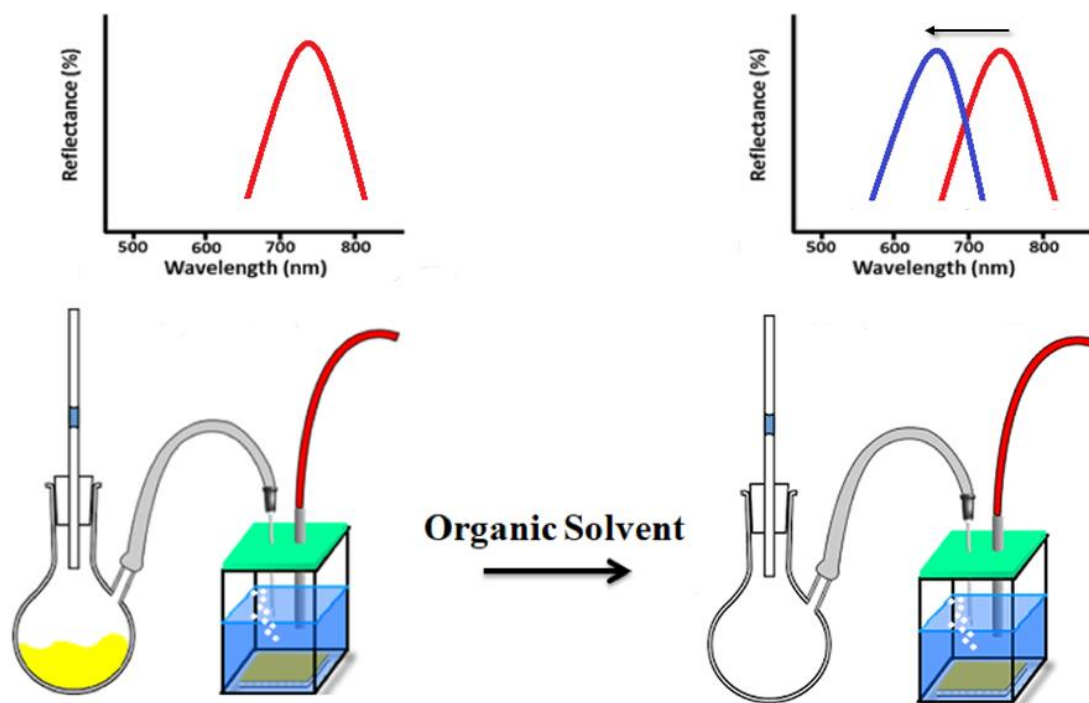
Scheme 6-1. Experimental setup for vapor phase studies.

6.3 Results and Discussion

In this work, the ability of microgel based-etalons to respond to volatile non-polar organic solvent vapor was evaluated.   pNIPAm-based microgels were prepared following a previously published protocol and were characterized by TEM and DLS. As can be seen in Figure 6-2, the TEM image showed that the microgels had a dry diameter of ~500 nm (Figure 6-2(a)) while the DLS revealed an average solvated hydrodynamic diameter of 710 ± 70 nm (Figure 6-2(b)).
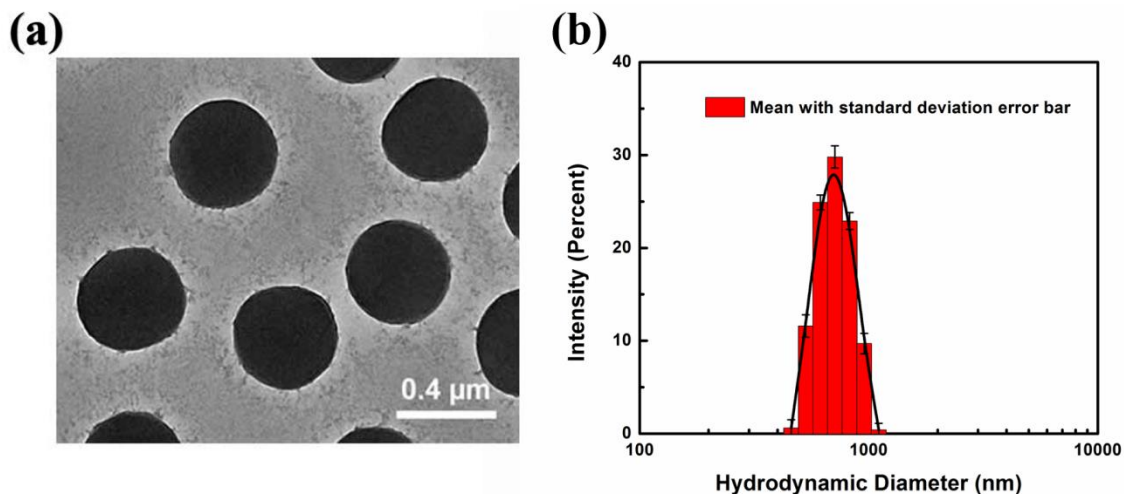
Figure 6-2. (a) TEM image and (b) DLS data of pNIPAm-based microgels. The data in the (b) were obtained by averaging 3 measurements of the solution, while the error bars indicate the standard deviation.

After characterization of the pNIPAm-based microgels, microgel-based etalons were fabricated by depositing pNIPAm-based microgels on a glass substrate that was previously coated with 15 nm layer of Au (via thermal evaporation). Then, an additional 15 nm layer of Au was deposited on top of the microgel layer to yield the etalon's sandwich structure. The resultant etalons were imaged by SEM, as shown in Figure 6-3, and exhibited a morphology that is typical of microgel-based etalons. The fabricated etalons were then incubated overnight in DI water prior to use, and exhibited a red color to the naked eye (Figure 6-5(a)) indicating that the microgels were swollen and the etalons structure was indeed intact and functioning properly. The etalons were then exposed to different organic solvent vapors (hexane, cyclohexane, petroleum ether,

chloroform and THF) as described in the Experimental Section, and shown in Scheme 6-1. In each case, the solvent was completely evaporated and bubbled into the glass vessel containing the etalon, and a reflectance spectrum collected before and after the exposure. The various solvents used have the physical properties shown in Table 6-1.[256]
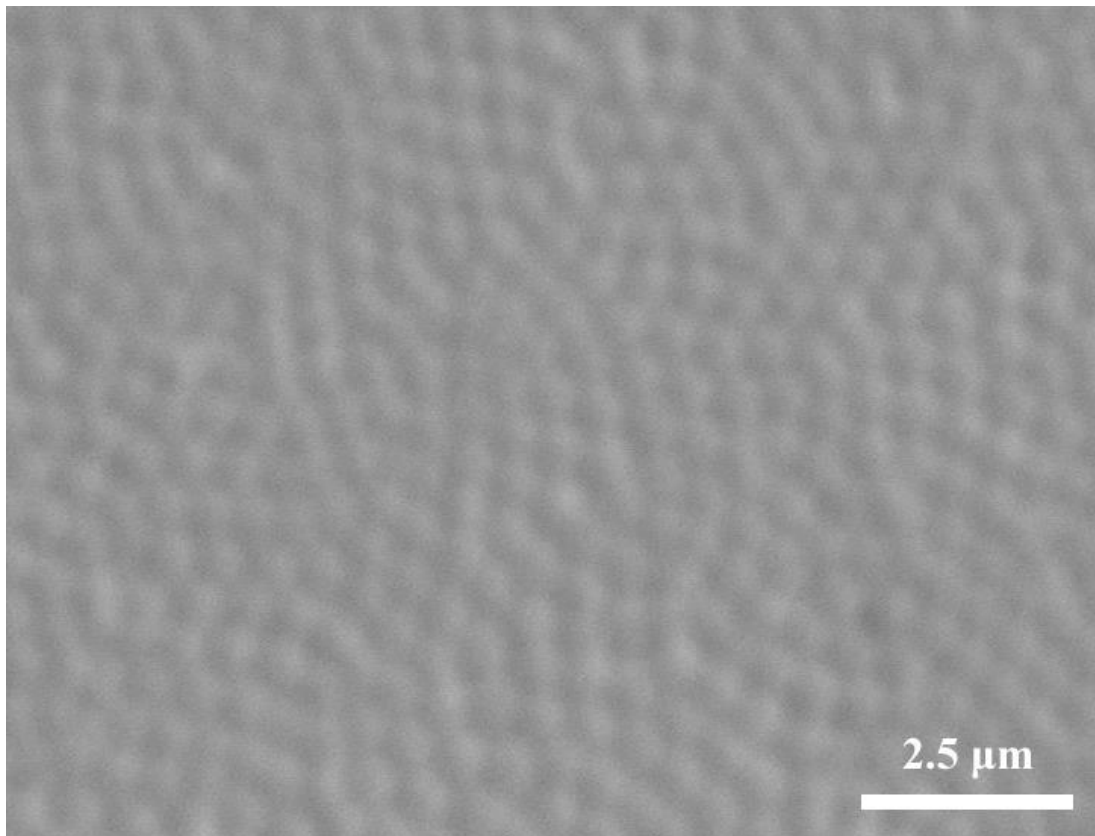
Figure 6-3. SEM image of the surface of a microgel-based etalon.

Initially, we examined the time it took the etalons to stabilize at their maximum response after exposure to the respective vapors, which we refer to as the response time. We saw that etalons stabilized the fastest upon exposure to petroleum ether, which was stable after 30 mins; followed by THF, hexane and chloroform, which took approximately 80 mins to stabilize; and finally the slowest was cyclohexane, which took

almost 100 mins for the etalons to stabilize, as detailed in Table 6-1. In addition to investigating the signal stabilization kinetics, we also quantified the total response of the etalons to the various solvent vapors. To assess this we calculated the total peak shift once the etalons' reflectance spectra were stable compared to the initial peak position; we assigned negative numbers to reflectance peaks that shifted to lower wavelengths (blue shifted), while positive numbers were given to those that shifted to higher wavelengths (red shifted). As can be seen in Table 6-1 and Figure 6-4(a), THF yielded the most significant response out of all the solvent vapors investigated. Specifically, THF yielded a total blue-shift of -238 nm, while hexane, cyclohexene, chloroform and petroleum ether yielded red shifts of 22 nm, 10 nm, 15 nm and 5 nm, respectively.

To understand these results, we considered the physical properties of the solvents used such as boiling point, solubility in water, and polarity index. We hypothesized that solvents with lower boiling points would give faster response times than those with higher boiling points, as they were expected to be bubbled into the water relatively fast making the etalons respond to them faster. As predicted, the results obtained show that the boiling point appears to influence the detection time but not the total peak shift. For example, petroleum ether evaporates faster and required less time to detect (~30 mins) compared to cyclohexane (~80 mins) but the total peak shifts for both of them were statistically similar. These results suggest that solvent boiling point alone cannot explain the etalon response, and other factors also dictate the overall response. Concomitantly,

the polarity index of the organic solvents was considered. Surprisingly, the results showed that the polarity index was not a major factor affecting the etalon response. For instance, we expected hexane to give a higher response than THF as its polarity index is 0.1 p, lower than for THF, and would affect the polarity of water-solvent mixture more than THF. However, THF resulted in a higher peak shift than hexane. Instead, we found the solubility of the organic solvents in water plays the most significant role in determining the etalon's response. The peak shift for THF vapor was found to be the largest of all solvents tested. In this case, the visual color of the etalon changed from pink to green after the exposure to THF vapor as shown in Figure 6-5. However, the response to hexane, cyclohexane, petroleum ether, and chloroform vapors are all relatively small compared to THF and showed no visible color change. Further explanation of these results is provided below.

Table 6-1. Physical properties for the organic solvents used here and the etalon response.

Organic Solvent	Polarity Index (p)	Solubility in water (g/100g)	Boiling point (°C)	Response time (min)	Peak shift (nm)
Hexane	0.1	Insoluble	69.0	~80	22
Cyclohexane	0.1	0.0052	80.7	~100	10
Petroleum ether	0.1	Immiscible	42.0	~30	5
Tetrahydrofuran	4.0	Miscible	66.0	~80	-238

Chloroform	4.0	0.87	61.5	~80	15

In order to further confirm that the results obtained with the etalons are a result of the microgels changing solvation state due to the bubbled vapor dissolving in water, we determined the hydrodynamic diameter of the microgels exposed to the aqueous solution that were generated from the above vapor bubbling experiments. That is, after the respective solvents were fully evaporated and bubbled into the water containing the etalons, the microgels were dissolved in the resultant vapor bubbled water and their diameter measured by DLS. As can be seen in Figure 6-4(b), the hydrodynamic diameter of microgels in the hexane and petroleum ether solution were found to be 720.4 nm, 711.1 nm, respectively, which is slightly larger than in DI water (709.1 nm). However, in the resultant solution from THF vapor bubbling, the hydrodynamic diameter of microgels was 620.8 nm, which is significant smaller than that in DI water. Therefore, the DLS-measured diameters were consistent with the responses obtained from the etalon devices. That is, the etalons that showed a blue shift upon exposure to THF vapor had a dramatically smaller DLS-measured diameter relative to their diameter in water.
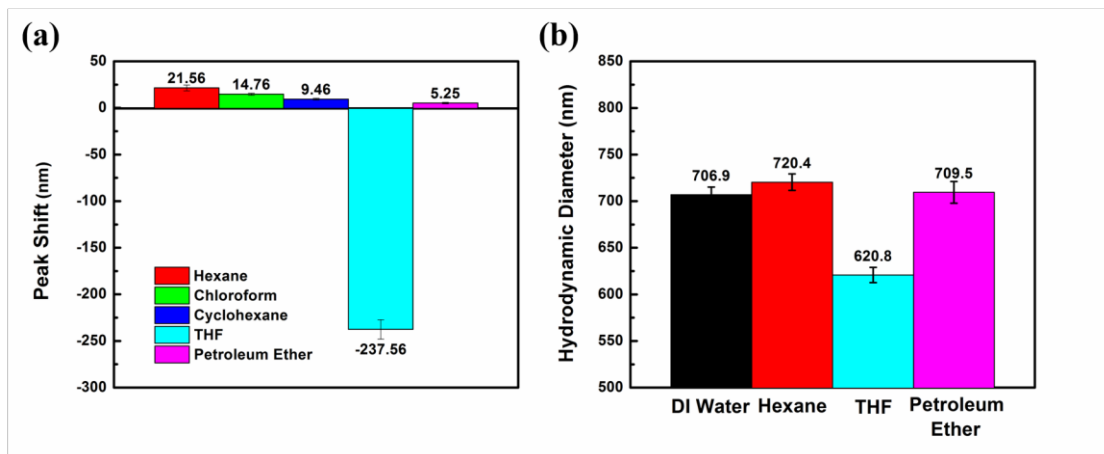
Figure 6-4. (a) Peak shifts for the etalons after exposure to the respective solvent vapors, and (b) hydrodynamic diameter of microgels water previously used in the vapor bubbling experiments measured by DLS. All the data in (a) and (b) were obtained by averaging the response obtained from three different etalons by optical probe and DLS experiments, respectively, while the error bars indicate the standard deviation.
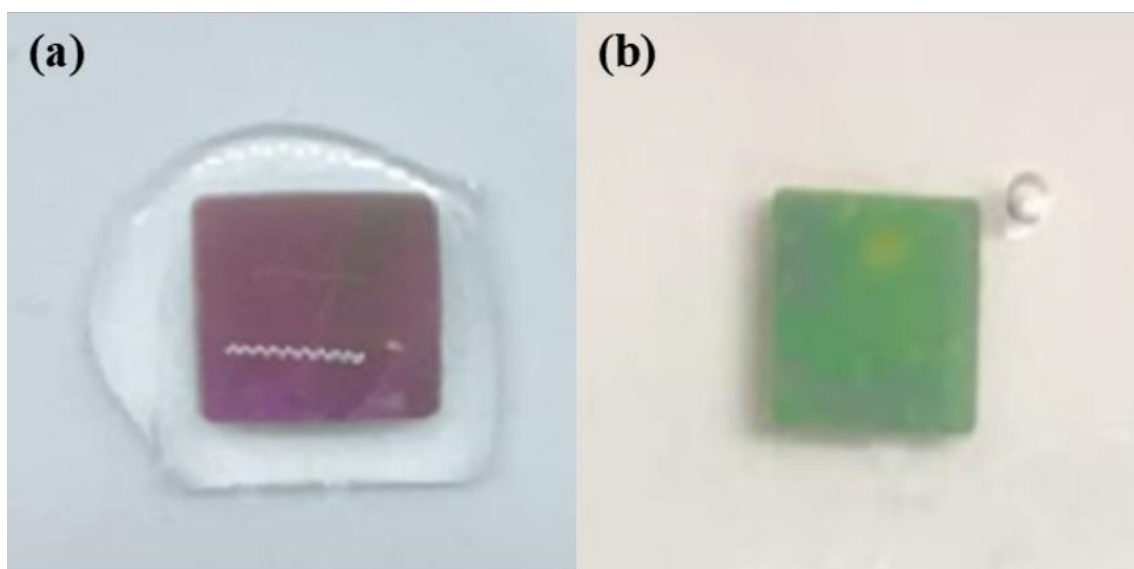
Figure 6-5. Photographs of an etalon (0.6 cm × 0.6 cm) in (a) DI water and (b) after exposure to THF vapor.

In order to explain the relatively high sensitivity of the etalons towards THF, cononsolvency needs to be considered. It is known that H_2O and THF themselves are highly miscible and are both good solvents for pNIPAm (and pNIPAm-based microgels) making pNIPAm swollen and in its extended conformation. Although, mixtures of the two in certain proportions can render pNIPAm insoluble and cause it to collapse and contract. From previous reports,[257, 258] the cononsolvency effect of THF is observed when the THF molar fraction in water (X) is between 0.012 and 0.13, and in this range the LCST of pNIPAm decreases sharply from 32 °C in pure water to -1 °C. Thus, when the fraction of THF overcomes this threshold, the size of the pNIPAm-based microgels sharply decreases at room temperature. Moreover, studies have revealed that hexane can cause pNIPAm polymer chains to expand, which is consistent with our results where the hydrodynamic diameter of microgels slightly increases when exposed to the hexane bubbled water.[259] Hexane is not a particularly good solvent for pNIPAm, so the adsorption of the hexane molecules at the hydrophobic regions of the polymer might occur. Since the polymer structure in the water is the same before and after exposure to hexane vapor, the replacement of water molecules by hexane molecules within the polymer network will lead to a slight swelling due to a larger size of hexane molecules compared to water. Hence, our microgels would appear to swell upon exposure to hexane.[260, 261] This reasoning can also be used to explain the responses to cyclohexane, chloroform and petroleum ether. This effect is slightly different for different organic

solvents due to their solubility and polarity index in water, which are consistent with the obtained peak shift.

Since THF vapor gave us the highest response among all the solvent vapors tested, we decided to use THF to determine other figures of merit for our sensors, e.g., response kinetics, and sensitivity. We first carried out experiments to investigate the rate of color change of our etalon upon exposure to THF vapor, by bubbling a fixed amount of THF (2 mL and 5 mL) into water and recording the absolute peak shift (difference from initial peak position and peak position at a given time) at different time points. The result is shown in Figure 6-6(a). It was found that the rate of reflectance peak shift is independent of the volume of THF used; the rate of reflectance peak shift is approximately 3 nm/min for both volumes of THF. However, what is determined by the amount of THF bubbled into the water is the total response time and the maximum peak shift. As can be seen from Figure 6-6(a), for the etalon to achieve its own maximum response when exposed to 2 mL and 5 mL of THF, roughly 30 mins and 75 mins are required, respectively. The maximum responses for 2 mL and 5 mL of THF are about 91 nm and 194 nm, respectively. It is also worth mentioning here that after the etalon achieves its maximum peak shift, the peak maximum tends to return to its initial position after remaining at the maximum position for several minutes.

154
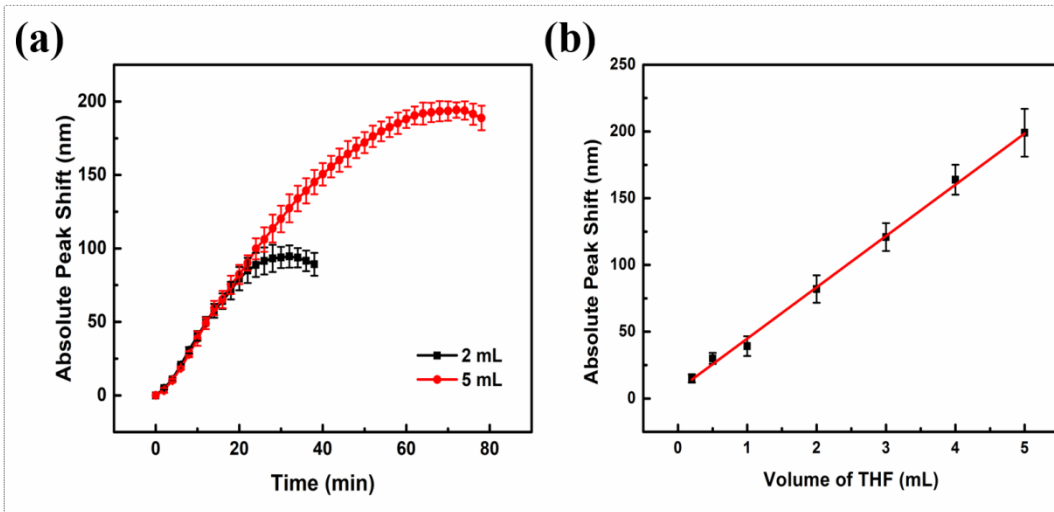
Figure 6-6. (a) Peak shift kinetics of the etalon upon exposure to THF vapor, and (b) total response of etalons to bubbling different amounts of THF. All the data in (a) and (b) were obtained by averaging measurements obtained from three different etalons, while the error bars indicate the standard deviation.

We went on to further investigate the sensitivity of our devices to THF vapor, and conducted a series of experiments to investigate the relationship between the etalon's response and different amount of THF vapor bubbled into the water. Initially, we did the experiments by varying the volume (ranging from 1 mL to 5 mL) of THF solvent in the 2-neck round bottom flask and recorded the shift in the position of the reflectance peak (λ) as the complete THF volume was bubbled through the water, as detailed in the Experimental Section and Scheme 6-1. A calibration curve was constructed and shown in Figure 6-6(b). The calibration curve shows a linear relationship between the etalon's response and amount of THF vapor bubbled into the water yielding the following linear

equation 6-2:

$$y = (40.74 \pm 0.63)\, x - (0.87 \pm 1.68)\; (R^2 = 0.999) \qquad (6\text{-}2)$$

The LOD was calculated using the parameters from the calibration curve and was determined to be 0.12 mL (three standard deviations of the intercept divided by slope). However, this LOD is calculated from the results found in Figure 6-6(b), and is not the LOD for THF vapor, and is simply the LOD for the amount of THF dissolved in the water as a result of bubbling. This is because only a portion of the THF in the vapor is transferred to, and remains dissolved in, the water when it is bubbled through the water. In order to determine the LOD for the THF vapor, we obtained the LOD for the etalon exposed to specific concentrations of liquid THF directly dissolved in water. As can be seen in Figure 6-7, the etalons also exhibit a linear response to direct addition of THF to water, and the response can be described by the equation 6-3 below

$$y = (319.45 \pm 30.21)\, x - (27.39 \pm 3.77)\; (R^2 = 0.974) \qquad (6\text{-}3)$$

From these data the LOD was calculated to be 0.035 mL (1.38% w/w). This LOD reflects the actual concentration of THF in 2.5 mL water that the sensor can detect. However, as mentioned before, not all of the THF in the vapor is dissolved in the water when bubbling. Based on these two calibration curves, the amount of vapor that can be transferred to the water (transfer factor) was calculated to be 21%, which was calculated based on the ratio between the volume of liquid THF and the volume of bubbled THF that resulted in the same etalon response. As such, when bubbling 1 mL THF, only 0.21 mL of THF was

transferred into the water. In order to achieve a lower LOD and make our sensor more relevant for environmental monitoring, we tried to increase the transfer factor by tuning the flow rate of the carrier gas and the size of the bubble being exposed to the water. In the first case, we kept the bubble size the same as before and decreased the flow rate to 10 and 20 cc/min. In the second case, we kept the same flow rate as before (100 cc/min) and decreased the vapor bubble size. From the results, which can be found in the Figure 6-8, we could see a significant increase in the transfer factor by decreasing the bubble size (25% increase) and the flow rate (37.5% increase).
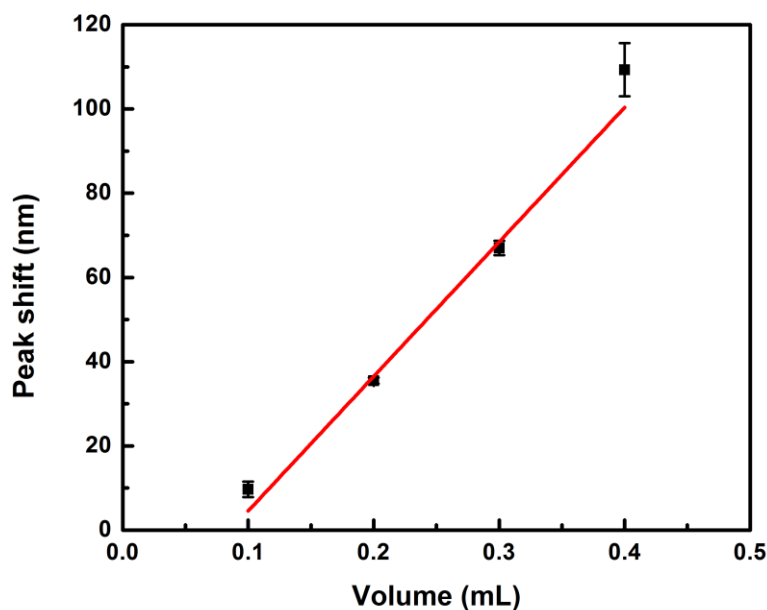
Figure 6-7. Calibration curve of total peak shifts with different amount of liquid THF. All the data points were obtained by averaging measurements obtained from three different etalons, while the error bars indicate the standard deviation.
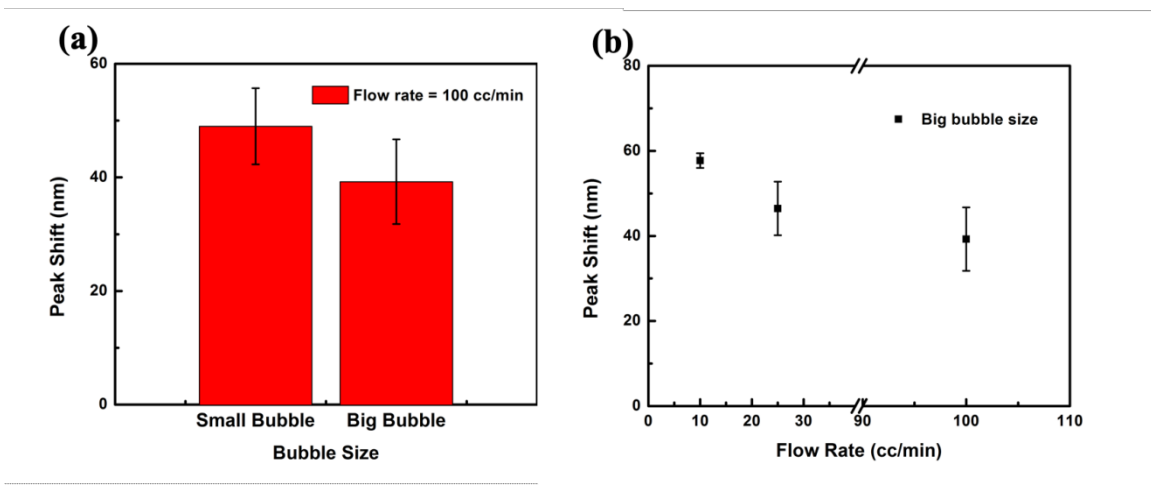
Figure 6-8. The response of our sensor with different (a) bubble size and (b) flow rate

Finally, we aim to determine the LOD for the THF vapor that is being bubbled through the water. From above, we know that our sensors can detect 0.035 mL THF in 2.5 mL water. Therefore, the moles (n) of THF that can be detected can be calculated using Equation 4:

$$n = \rho * V/Mw \qquad (6\text{-}4)$$

where ρ is the density of THF and Mw is the molecular weight of THF, which is 0.43 mmol. Based on the transfer factor of 21%, we can calculate that the amount of vapor THF that is being bubbled into the water is ~2.0 mmol. In order to obtain the concentration of THF vapor, we need to determine the total volume of the carrier gas required to bubble 2 mmol of THF through the water. We know that the liquid THF 2 mmol (0.167 mL) can be vaporized by N_2 carrier gas with 4 minutes (the response time) at a carrier gas flow rate of 0.5 L/min. Hence, the total volume of the carrier gas is 2 L.

Based on these values, we are able to obtain the concentration of the THF vapor is 1.27 mM. We note that this LOD can be decreased dramatically by decreasing the amount of water the THF vapor is bubbled into. Additionally, we can also tune other parameters such as flow rate of carrier gas and bubble size to increase the transfer factor, resulting in improved LOD. Finally, the THF vapor exiting the water can be rebubbled into the water multiple times to improve the transfer efficiency.

Next, we investigated the ability of the etalons to return to their initial state after exposure to THF vapor, and if they can be used again to detect THF vapor. This was accomplished by bubbling N_2 into the water previous exposed to THF vapor overnight to remove the THF that was dissolved in the water. Following rinsing the etalon with water multiple times, we performed the same THF bubbling experiments described above. The results can be seen in Figure 6-9, and show that the etalon's response is robust over at least 3 THF vapor exposure and resetting cycles. The data do not show any degradation of the etalon response, hence we believe that the etalon's can be reused over many cycles.
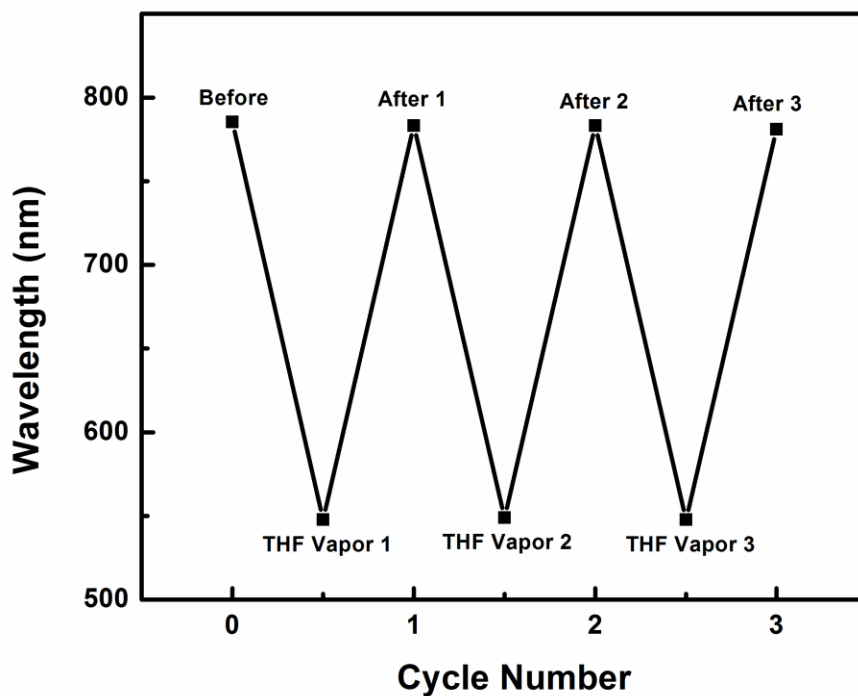
Figure 6-9. Final peak positions before and after exposure of etalons to THF vapor phase over three cycles.

6.4 Conclusions

We demonstrated that pNIPAm microgel-based etalons can be used to detect various VOC vapors by bubbling them through water containing an etalon. From the results, we saw that the devices were able to detect all of the vapors investigated, although the response of the etalons to THF vapor was significantly enhanced compared to the other vapors. We concluded that this was a result of the cononsolvency effect of the microgels

in THF/water mixtures, which makes the microgels respond dramatically to the presence of THF dissolved in water leading to a dramatic response from the etalon. From the results, we demonstrated that 1.27 mM THF vapor could be detected within 4 min, but show that the LOD can be decreased (i.e., improved) by changing the conditions that are used to expose the etalon to the vapors, e.g., reducing the water volume, changing flow rate, and varying bubble dimensions. We showed that the etalon response is reversible over at least 3 cycles without a loss in etalon function, which suggests that the etalons can be used multiple times for detecting VOC vapor. The results taken together suggest that a portable and robust VOC vapor sensing system could be possible, and could find use for quantifying VOC vapors in the field.

Chapter 7

Conclusion and Future Outlook

7.1 Conclusions

In this dissertation, we successfully developed several novel microgels, nanogels and their assemblies based platforms for the use of controlled drug delivery and sensing systems, which can be beneficial to our daily human health.

In Chapter 2, a stretchable pNIPAm-*co*-10%AAc microgel-based etalon immobilized on PDMS was fabricated, and elongation used to control the CV release rate to an aqueous solution. Specifically, when the devices were exposed to pH 3.0 solution, CV could be release from the device and release rates determined at different device elongations of (1 mm, 3 mm, and 5 mm) and Au overlayer thickness (50 nm and 120 nm). The release rate of CV was high for devices with thin Au overlayers and high elongation, while thick Au overlayers, and low elongation slowed the release rate. We also proposed that the release was dominated by the Au pores at low elongations, while release through the stretching-induced cracks was dominant when elongations are high. Finally, we showed that the release can be turned "on" and "off "by stretching and relaxation, respectively. Hence, this behavior can be used to achieve release via ubiquitous daily

motion that induces device stretching and small molecule release.

In Chapter 3, a novel light/temperature responsive pNIPAm-*co*-NBMA microgels were designed and synthesized by a facile free radical precipitation polymerization method. The prepared pNIPAm-*co*-NBMA microgels are monodisperse and possess a uniform morphology with a size of approximately 320 nm. Subsequently, the model drug, fluorescein, was loaded by exploiting hydrophobic interactions between hydrophobic moiety (*o*-nitrobenzyl methacrylate) of microgels and fluorescein. Due to conformational changes or photodegradation on exposure to either heat or UV irradiation, the fluorescein can be explosively released from pNIPAm-*co*-NBMA microgels into the aqueous solution. Importantly, it is known that the stimuli-responsive polymer of pNIPAm and the photodegradation products of *o*-nitrobenzyl-ester derivatives are biocompatible thus the prepared dual-stimuli responsive pNIPAm-*co*-NBMA microgels can possess great potential for biomedical applications in controlled drug delivery.

Followed by the work of Chapter 3, Chapter 4 described the study by using DEX incorporated photo-responsive pNIPAm-*co*-NBMA microgels for photo-controlled osteogenic differentiation of hMSCs. The *in vitro* results showed that our microgels were not toxic to hMSC, and DEX could be released in a light-controlled fashion, which induced osteogenic differentiation of hMSCs, as evaluated by the increased level of normalized alkaline phosphatase activity as well as increased calcium deposition detected by Alizarin Red S staining. Notably, we also indicated that the osteogenic differentiation

of hMSCs in our system could be tuned by turning on/off UV light source. Such DEX loaded photo-responsive microgels were able to control the induction of hMSCs osteogenic differentiation upon light exposure, which has promising applications in bone tissue engineering.

In Chapter 5, we illustrated the use of assemblies of chitosan-based supramolecular nanogels for drug release in complex conditions (ATP and acid environment). Such chitosan-based supramolecular nanogels were non-toxic at the low concentration (< 24 mg/mL) with the hydrodynamic diameter of 35 nm. Moreover, we demonstrated pH and ATP as dual triggers for the controlled anticancer drugs (Dox-HCl) delivery via a conformational change of supramolecular nanogels in an acid environment in the tumor cell (HepG2). Following, ATP in tumor cells could be directional complexed by the degraded nanogels. With this, the efflux of Dox-HCl could be attenuated, resulting in enhancing the anticancer efficacy of Dox-HCl in vitro. Such pH and ATP-triggered drug release system could provide a sophisticated fashion to modulate the function of ATP in cells, which can facilitate the antitumour efficacy in vitro/vivo.

Besides all of the smart drug delivery systems, Chapter 6 described the ability of the pNIPAm based colorimetric etalon sensors to detect the volatile organic compounds of hexane, cyclohexane, petroleum ether, chloroform and THF. Among these vapors, the etalons showed high selectivity and sensitivity towards THF with the limit of detection (LOD) 1.27 mM and a short response time, and the LOD can be improved by reducing

the water volume, changing flow rate, and varying bubble dimensions that are used to expose the etalon to the vapors. Ultimately, we showed our colorimetric sensors were robust with good reversibility for at least three times. The results reported suggests that such portable and robust analytic sensors can be tested/used against biogenic and anthropogenic VOCs found in the environment for in field application.

7.2 Future outlook

There are various possible extensions of the current studies. As mentioned in Chapter 3 and 4, we developed novel light/temperature responsive pNIPAm-*co*-NBMA microgels in the application of drug release and light-controlled osteogenic differentiation of hMSCs. However, most of the existing O-NBE based light-responsive systems rely on using ultraviolet (UV) light, which have several drawbacks such as cytotoxicity and limited tissue penetration. This may hinder the applications of light-responsive systems in real world applications. Therefore, in the future, we will focus on the development of near infrared light (NIR)-responsive micro/nanogels-based systems for triggered biomolecule delivery-based biomedical applications. For example, we aim to develop a NIR-responsive microgel system for triggered DEX release and thus achieving hMSCs differentiation in a NIR-controlled manner. We will propose to synthesize $NaYF_4$:Yb,Tm upconversion nanoparticles (UCNP) and UCNP will be incorporated into UV-responsive pNIPAm-co-NBMA microgels (UCNP@microgels). Upon NIR irradiation, UCNP will

absorb NIR and emit UV, thus triggering degradation of UV-responsive NBMA moiety in microgels; NIR overcomes the drawbacks of UV by offering relatively deep tissue penetration and high cytocompatibility, which will allow for ready in vivo experimentation in the future. The NIR-responsive behavior, size and morphology of the nanogels, will be characterized by fluorescence spectroscopy, dynamic light scattering (DLS) and transmission electron microscopy (TEM), respectively. We will then conjugate DEX onto the UCNP@nanogels. Once BMP-2 loaded NIR-sensitive microgels are successfully synthesized, the NIR-triggered release of DEX from those microgels will be verified via LC-MS. Furthermore, the cytotoxicity of our microgels and the NIR-controlled hMSC differentiation using such system will be evaluated by alamar blue assay and normalized alkaline phosphatase (ALP) activity assay, respectively.

In addition, we aim to develop a photo-responsive microgel system for triggered cytokines (TNF or IL-4) release and followed by controlled macrophage M1-M2 polarization in a photo-responsive manner. The photo-responsive monomer, 4-(4-(1-(acryloyloxy)ethyl)-2-methoxy-5-nitrophenoxy) butanoic acid (AEMNPBA) will be synthesized via a multi-step reaction using acetovanillone as the starting material. Following, microgels composed of poly(N-isopropylacrylamide-co-4-(4-(1-(acryloyloxy)ethyl)-2-methoxy-5-nitrophenoxy) butanoic acid) (pNIPAm-co-AEMNPBA) will be synthesized via free radical precipitation polymerization similarly to our previously published protocols with minor

modification. After, we will propose to conjugate streptavidin onto AEMNPBA moiety on the microgels by carbodiimide chemistry, and then use commercially available biotinylation kits to conjugate biotin onto TNF or IL-4, followed by incorporation of biotinylated TNF or IL-4 onto our streptavidin-based light responsive microgels by biotin-streptavidin interaction. Lastly, when we gain the human acute monocytic leukemia cell line (THP-1) derived macrophages, we will evaluate the cytotoxicity of our sample via measuring the cell viability of THP-1 derived macrophages, and plan to culture macrophages with the addition of our sample, releasing TNF or IL-4 upon exposure to external UV irradiation (365 nm) for only 5 min so that the TNF-loaded sample will induce the macrophages towards M1 polarization whereas the IL-4-loaded sample will induce the macrophages towards M2 polarization, achieving to regulate the polarization state of macrophages using external UV light. The assessment of macrophage polarization will be performed through flow cytometry, phagocytosis capabilities measurements, gene expression by real-time quantitative polymerase chain reaction (RT-qPCR) and immunofluorescent staining etc. Finally, we aim to apply our sample into the mice and evaluate our experimental approaches for in vivo applications.

Reference

1. Schild, H. G., Poly (N-isopropylacrylamide): experiment, theory and application. *Progress in polymer science* **1992,** *17* (2), 163-249.

2. Teyssier, J.; Saenko, S. V.; Van Der Marel, D.; Milinkovitch, M. C., Photonic crystals cause active colour change in chameleons. *Nature communications* **2015,** *6,* 6368.

3. Amador-Vargas, S.; Dominguez, M.; León, G.; Maldonado, B.; Murillo, J.; Vides, G. L., Leaf-folding response of a sensitive plant shows context-dependent behavioral plasticity. *Plant ecology* **2014,** *215* (12), 1445-1454.

4. Dai, S.; Ravi, P.; Tam, K. C., pH-Responsive polymers: synthesis, properties and applications. *Soft Matter* **2008,** *4* (3), 435-449.

5. Gandhi, M. V.; Thompson, B., *Smart materials and structures*. Springer Science & Business Media: 1992.

6. Hosomi, T.; Masai, H.; Fujihara, T.; Tsuji, Y.; Terao, J., A Typical Metal-Ion-Responsive Color-Tunable Emitting Insulated π-Conjugated Polymer Film. *Angewandte Chemie International Edition* **2016,** *55* (43), 13427-13431.

7. Hu, J.; Zhang, G.; Liu, S., Enzyme-responsive polymeric assemblies, nanoparticles and hydrogels. *Chemical Society Reviews* **2012,** *41* (18), 5933-5949.

8. Jiang, X. C.; Xiang, J. J.; Wu, H. H.; Zhang, T. Y.; Zhang, D. P.; Xu, Q. H.; Huang, X. L.; Kong, X. L.; Sun, J. H.; Hu, Y. L., Neural Stem Cells Transfected with Reactive Oxygen Species–Responsive Polyplexes for Effective Treatment of Ischemic Stroke. *Advanced Materials* **2019,** *31* (10), 1807591.

9. Katsuno, C.; Konda, A.; Urayama, K.; Takigawa, T.; Kidowaki, M.; Ito, K., Pressure-Responsive Polymer Membranes of Slide-Ring Gels with Movable Cross-Links. *Advanced Materials* **2013,** *25* (33), 4636-4640.

10. Kwon, I. C.; Bae, Y. H.; Kim, S. W., Electrically erodible polymer gel for controlled release of drugs. *Nature* **1991,** *354* (6351), 291-293.

11. Miyata, T.; Asami, N.; Uragami, T., A reversibly antigen-responsive hydrogel. *Nature* **1999,** *399* (6738), 766-769.

12. Stoychev, G.; Kirillova, A.; Ionov, L., Light-responsive shape-changing polymers. *Advanced Optical Materials* **2019,** *7* (16), 1900067.

13. Tanaka, T.; Nishio, I.; Sun, S.-T.; Ueno-Nishio, S., Collapse of gels in an electric field. *Science* **1982,** *218* (4571), 467-469.

14. Thévenot, J.; Oliveira, H.; Sandre, O.; Lecommandoux, S., Magnetic responsive polymer composite materials. *Chemical Society Reviews* **2013,** *42* (17), 7099-7116.

15. Aguilar, M. R.; San Román, J., Introduction to smart polymers and their applications. In *Smart polymers and their applications*, Elsevier: 2019; pp 1-11.

16. Bordat, A.; Boissenot, T.; Nicolas, J.; Tsapis, N., Thermoresponsive polymer nanocarriers for biomedical applications. *Advanced drug delivery reviews* **2019,** *138*, 167-192.

17. Lu, Y.; Sun, W.; Gu, Z., Stimuli-responsive nanomaterials for therapeutic protein delivery. *Journal of controlled release* **2014,** *194*, 1-19.

18. Yang, H.; Zhu, H.; Hendrix, M. M.; Lousberg, N. J.; de With, G.; Esteves, A. C. C.; Xin, J. H., Temperature-Triggered Collection and Release of Water from Fogs by a Sponge-Like Cotton Fabric. *Advanced materials* **2013,** *25* (8), 1150-1154.

19. Echeverria, C.; Peppas, N. A.; Mijangos, C., Novel strategy for the determination of UCST-like microgels network structure: effect on swelling behavior and rheology. *Soft Matter* **2012,** *8* (2), 337-346.

20. Liu, F.; Urban, M. W., Recent advances and challenges in designing stimuli-responsive polymers. *Progress in polymer science* **2010,** *35* (1-2), 3-23.

21. Cho, E. C.; Lee, J.; Cho, K., Role of bound water and hydrophobic interaction in phase transition of poly (N-isopropylacrylamide) aqueous solution. *Macromolecules* **2003,** *36* (26), 9929-9934.

22. Kirsh, Y. E., *Water soluble poly-N-vinylamides: synthesis and physicochemical properties*. John Wiley & Sons: 1998.

23. Cortez-Lemus, N. A.; Licea-Claverie, A., Poly (N-vinylcaprolactam), a comprehensive review on a thermoresponsive polymer becoming popular. *Progress in Polymer Science* **2016,** *53*, 1-51.

24. Meeussen, F.; Nies, E.; Berghmans, H.; Verbrugghe, S.; Goethals, E.; Du Prez,

F., Phase behaviour of poly (N-vinyl caprolactam) in water. *Polymer* **2000,** *41* (24), 8597-8602.

25. Maeda, Y.;   Nakamura, T.; Ikeda, I., Hydration and phase behavior of poly (N-vinylcaprolactam) and poly (N-vinylpyrrolidone) in water. *Macromolecules* **2002,** *35* (1), 217-222.

26. Aoshima, S.; Kanaoka, S., Synthesis of stimuli-responsive polymers by living polymerization: poly (N-isopropylacrylamide) and poly (vinyl ether) s. In *Wax crystal control· nanocomposites· stimuli-responsive polymers*, Springer: 2007; pp 169-208.

27. Hoogenboom, R.;   Thijs, H. M.;   Jochems, M. J.;   van Lankvelt, B. M.;   Fijten, M. W.; Schubert, U. S., Tuning the LCST of poly (2-oxazoline) s by varying composition and molecular weight: alternatives to poly (N-isopropylacrylamide)? *Chemical communications* **2008,**   (44), 5758-5760.

28. Iwasaki, Y.;   Yamaguchi, E., Synthesis of well-defined thermoresponsive polyphosphoester macroinitiators using organocatalysts. *Macromolecules* **2010,** *43* (6), 2664-2666.

29. Pietsch, C.;   Hoogenboom, R.; Schubert, U. S., PMMA based soluble polymeric temperature sensors based on UCST transition and solvatochromic dyes. *Polymer Chemistry* **2010,** *1* (7), 1005-1008.

30. Zhang, Q.; Hoogenboom, R., Polymers with upper critical solution temperature behavior in alcohol/water solvent mixtures. *Progress in Polymer Science* **2015,** *48*, 122-142.

31. Bertrand, O.;   Vlad, A.;   Hoogenboom, R.; Gohy, J.-F., Redox-controlled upper critical solution temperature behaviour of a nitroxide containing polymer in alcohol–water mixtures. *Polymer Chemistry* **2016,** *7* (5), 1088-1095.

32. Zhang, Q.;   Schattling, P.;   Theato, P.; Hoogenboom, R., UV-tunable upper critical solution temperature behavior of azobenzene containing poly (methyl methacrylate) in aqueous ethanol. *European Polymer Journal* **2015,** *62*, 435-441.

33. Pang, X.;   Jiang, Y.;   Xiao, Q.;   Leung, A. W.;   Hua, H.; Xu, C., pH-responsive polymer–drug conjugates: design and progress. *Journal of controlled release* **2016,** *222*, 116-129.

34. Pang, X.; Yang, X.; Zhai, G., Polymer-drug conjugates: recent progress on administration routes. *Expert opinion on drug delivery* **2014,** *11* (7), 1075-1086.

35. Zhang, X.; Achazi, K.; Haag, R., Boronate Cross-linked ATP-and pH-Responsive Nanogels for Intracellular Delivery of Anticancer Drugs. *Advanced healthcare materials* **2015,** *4* (4), 585-592.

36. Wang, Y.; Shi, Y.; Xu, M.; Wu, L.; Jia, X.; Wei, T.; Zhang, S.; Guo, X., Smart flocculant with temperature and pH response derived from starch. *RSC advances* **2016,** *6* (50), 44383-44391.

37. Gu, Y.; Zhong, Y.; Meng, F.; Cheng, R.; Deng, C.; Zhong, Z., Acetal-linked paclitaxel prodrug micellar nanoparticles as a versatile and potent platform for cancer therapy. *Biomacromolecules* **2013,** *14* (8), 2772-2780.

38. Gao, Y.; Zago, G. P.; Jia, Z.; Serpe, M. J., Controlled and triggered small molecule release from a confined polymer film. *ACS applied materials & interfaces* **2013,** *5* (19), 9803-9808.

39. Gabaston, L.; Furlong, S.; Jackson, R.; Armes, S., Direct synthesis of novel acidic and zwitterionic block copolymers via TEMPO-mediated living free-radical polymerization. *Polymer* **1999,** *40* (16), 4505-4514.

40. Bingöl, B.; Strandberg, C.; Szabo, A.; Wegner, G., Copolymers and hydrogels based on vinylphosphonic acid. *Macromolecules* **2008,** *41* (8), 2785-2790.

41. Guan, Y.; Zhang, Y., Boronic acid-containing hydrogels: synthesis and their applications. *Chemical Society Reviews* **2013,** *42* (20), 8106-8121.

42. Schmalz, A.; Hanisch, M.; Schmalz, H.; Müller, A. H., Double stimuli-responsive behavior of linear and star-shaped poly (N, N-diethylaminoethyl methacrylate) in aqueous solution. *Polymer* **2010,** *51* (6), 1213-1217.

43. Samal, S. K.; Dash, M.; Van Vlierberghe, S.; Kaplan, D. L.; Chiellini, E.; Van Blitterswijk, C.; Moroni, L.; Dubruel, P., Cationic polymers and their therapeutic potential. *Chemical Society Reviews* **2012,** *41* (21), 7147-7194.

44. Jochum, F. D.; Theato, P., Temperature-and light-responsive smart polymer materials. *Chemical Society Reviews* **2013,** *42* (17), 7468-7483.

45. Mutter, N. L.; Volarić, J.; Szymanski, W.; Feringa, B. L.; Maglia, G.,

Reversible Photocontrolled Nanopore Assembly. *Journal of the American Chemical Society* **2019**, *141* (36), 14356-14363.

46. Klajn, R., Spiropyran-based dynamic materials. *Chemical Society Reviews* **2014**, *43* (1), 148-184.

47. Ruskowitz, E. R.; DeForest, C. A., Photoresponsive biomaterials for targeted drug delivery and 4D cell culture. *Nature Reviews Materials* **2018**, *3* (2), 1-17.

48. Kloxin, A. M.; Kasko, A. M.; Salinas, C. N.; Anseth, K. S., Photodegradable hydrogels for dynamic tuning of physical and chemical properties. *Science* **2009**, *324* (5923), 59-63.

49. Graham, N. B.; Cameron, A., Nanogels and microgels: The new polymeric materials playground. *Pure and Applied chemistry* **1998**, *70* (6), 1271-1275.

50. Tanaka, T.; Fillmore, D.; Sun, S.-T.; Nishio, I.; Swislow, G.; Shah, A., Phase transitions in ionic gels. *Physical Review Letters* **1980**, *45* (20), 1636.

51. Pelton, R.; Chibante, P., Preparation of aqueous latices with N-isopropylacrylamide. *Colloids and Surfaces* **1986**, *20* (3), 247-256.

52. Pelton, R.; Pelton, H.; Morphesis, A.; Rowell, R., Particle sizes and electrophoretic mobilities of poly (N-isopropylacrylamide) latex. *Langmuir* **1989**, *5* (3), 816-818.

53. Wu, X.; Pelton, R.; Hamielec, A.; Woods, D.; McPhee, W., The kinetics of poly (N-isopropylacrylamide) microgel latex formation. *Colloid and polymer science* **1994**, *272* (4), 467-477.

54. Goodwin, J. W.; Ottewill, R. H.; Pelton, R.; Vianello, G.; Yates, D. E., Control of particle size in the formation of polymer latices. *British Polymer Journal* **1978**, *10* (3), 173-180.

55. Lyon, L. A.; Meng, Z.; Singh, N.; Sorrell, C. D.; John, A. S., Thermoresponsive microgel-based materials. *Chemical Society Reviews* **2009**, *38* (4), 865-874.

56. Scotti, A.; Bochenek, S.; Brugnoni, M.; Fernandez-Rodriguez, M.-A.; Schulte, M. F.; Houston, J.; Gelissen, A. P.; Potemkin, I. I.; Isa, L.; Richtering, W., Exploring the colloid-to-polymer transition for ultra-low crosslinked microgels from three to two dimensions. *Nature communications* **2019**, *10* (1), 1-8.

57. Sorrell, C. D.; Carter, M. C.; Serpe, M. J., Color Tunable Poly (N-Isopropylacrylamide)-co-Acrylic Acid Microgel–Au Hybrid Assemblies. *Advanced Functional Materials* **2011,** *21* (3), 425-433.

58. Islam, M. R.; Gao, Y.; Li, X.; Serpe, M. J., Responsive polymers for biosensing and protein delivery. *Journal of Materials Chemistry B* **2014,** *2* (17), 2444-2451.

59. Wen, B.; Xue, J.; Zhou, X.; Wu, Q.; Nie, J.; Xu, J.; Du, B., Highly selective and sensitive detection of Pb2+ in aqueous solution using tetra (4-pyridyl) porphyrin-functionalized Thermosensitive ionic microgels. *ACS applied materials & interfaces* **2018,** *10* (30), 25706-25716.

60. Zhang, Q. M.; Ahiabu, A.; Gao, Y.; Serpe, M. J., CO 2-switchable poly (N-isopropylacrylamide) microgel-based etalons. *Journal of Materials Chemistry C* **2015,** *3* (3), 495-498.

61. Di, J.; Yao, S.; Ye, Y.; Cui, Z.; Yu, J.; Ghosh, T. K.; Zhu, Y.; Gu, Z., Stretch-triggered drug delivery from wearable elastomer films containing therapeutic depots. *ACS nano* **2015,** *9* (9), 9407-9415.

62. Gao, Y.; Wong, K. Y.; Ahiabu, A.; Serpe, M. J., Sequential and controlled release of small molecules from poly (N-isopropylacrylamide) microgel-based reservoir devices. *Journal of Materials Chemistry B* **2016,** *4* (30), 5144-5150.

63. Parsons, S. A.; Jefferson, B., *Introduction to potable water treatment processes*. Blackwell publishing: 2006.

64. Hall, R. J.; Pinkrah, V. T.; Chowdhry, B. Z.; Snowden, M. J., Heteroaggregation studies of mixed cationic co-polymer/anionic homopolymer microgel dispersions. *Colloids and Surfaces A: Physicochemical and Engineering Aspects* **2004,** *233* (1-3), 25-38.

65. Parasuraman, D.; Serpe, M. J., Poly (N-isopropylacrylamide) microgels for organic dye removal from water. *ACS Applied Materials & Interfaces* **2011,** *3* (7), 2732-2737.

66. Zhang, F.; Braun, G. B.; Pallaoro, A.; Zhang, Y.; Shi, Y.; Cui, D.; Moskovits, M.; Zhao, D.; Stucky, G. D., Mesoporous multifunctional upconversion luminescent and magnetic "nanorattle" materials for targeted chemotherapy. *Nano letters* **2012,** *12* (1), 61-67.

67. Skirtach, A. G.; Munoz Javier, A.; Kreft, O.; Köhler, K.; Piera Alberola, A.; Möhwald, H.; Parak, W. J.; Sukhorukov, G. B., Laser-induced release of encapsulated materials inside living cells. *Angewandte Chemie International Edition* **2006,** *45* (28), 4612-4617.

68. Yatvin, M. B.; Weinstein, J. N.; Dennis, W. H.; Blumenthal, R., Design of liposomes for enhanced local release of drugs by hyperthermia. *Science* **1978,** *202* (4374), 1290-1293.

69. Chen, K.-J.; Liang, H.-F.; Chen, H.-L.; Wang, Y.; Cheng, P.-Y.; Liu, H.-L.; Xia, Y.; Sung, H.-W., A thermoresponsive bubble-generating liposomal system for triggering localized extracellular drug delivery. *ACS nano* **2013,** *7* (1), 438-446.

70. Park, K., Controlled drug delivery systems: past forward and future back. *Journal of Controlled Release* **2014,** *190*, 3-8.

71. Bertrand, N.; Leroux, J.-C., The journey of a drug-carrier in the body: an anatomo-physiological perspective. *Journal of controlled release* **2012,** *161* (2), 152-163.

72. Marschall, A. L.; Zhang, C.; Frenzel, A.; Schirrmann, T.; Hust, M.; Perez, F.; Dübel, S. In *Delivery of antibodies to the cytosol: debunking the myths*, MAbs, Taylor & Francis: 2014; pp 943-956.

73. Jeong, B.; Bae, Y. H.; Lee, D. S.; Kim, S. W., Biodegradable block copolymers as injectable drug-delivery systems. *Nature* **1997,** *388* (6645), 860-862.

74. Paul, A.; Hasan, A.; Kindi, H. A.; Gaharwar, A. K.; Rao, V. T.; Nikkhah, M.; Shin, S. R.; Krafft, D.; Dokmeci, M. R.; Shum-Tim, D., Injectable graphene oxide/hydrogel-based angiogenic gene delivery system for vasculogenesis and cardiac repair. *ACS nano* **2014,** *8* (8), 8050-8062.

75. Yang, S. Y.; O'Cearbhaill, E. D.; Sisk, G. C.; Park, K. M.; Cho, W. K.; Villiger, M.; Bouma, B. E.; Pomahac, B.; Karp, J. M., A bio-inspired swellable microneedle adhesive for mechanical interlocking with tissue. *Nature communications* **2013,** *4* (1), 1-10.

76. Freed, L. E.; Vunjak-Novakovic, G.; Biron, R. J.; Eagles, D. B.; Lesnoy, D. C.; Barlow, S. K.; Langer, R., Biodegradable polymer scaffolds for tissue engineering. *Bio/technology* **1994,** *12* (7), 689-693.

77. Gu, Z.; Aimetti, A. A.; Wang, Q.; Dang, T. T.; Zhang, Y.; Veiseh, O.; Cheng, H.; Langer, R. S.; Anderson, D. G., Injectable nano-network for glucose-mediated insulin delivery. *ACS nano* **2013,** *7* (5), 4194-4201.

78. He, Y.; Hong, C.; Li, J.; Howard, M. T.; Li, Y.; Turvey, M. E.; Uppu, D. S.; Martin, J. R.; Zhang, K.; Irvine, D. J., Synthetic charge-invertible polymer for rapid and complete implantation of layer-by-layer microneedle drug films for enhanced transdermal vaccination. *ACS nano* **2018,** *12* (10), 10272-10280.

79. Glenn, G. M.; Kenney, R. T.; Ellingsworth, L. R.; Frech, S. A.; Hammond, S. A.; Zoeteweij, J. P., Transcutaneous immunization and immunostimulant strategies: capitalizing on the immunocompetence of the skin. *Expert review of vaccines* **2003,** *2* (2), 253-267.

80. Yun, Y. H.; Lee, B. K.; Park, K., Controlled drug delivery: historical perspective for the next generation. *Journal of Controlled Release* **2015,** *219*, 2-7.

81. Langer, R., Polymer implants for drug delivery in the brain. *Journal of Controlled Release* **1991,** *16* (1-2), 53-59.

82. Dong, Y.; Chin, S.-F.; Blanco, E.; Bey, E. A.; Kabbani, W.; Xie, X.-J.; Bornmann, W. G.; Boothman, D. A.; Gao, J., Intratumoral delivery of β-lapachone via polymer implants for prostate cancer therapy. *Clinical Cancer Research* **2009,** *15* (1), 131-139.

83. Vollenhoven, B.; Lawrence, A.; Healy, D., Uterine fibroids: a clinical review. *BJOG: An International Journal of Obstetrics & Gynaecology* **1990,** *97* (4), 285-298.

84. Blum, A. P.; Kammeyer, J. K.; Rush, A. M.; Callmann, C. E.; Hahn, M. E.; Gianneschi, N. C., Stimuli-responsive nanomaterials for biomedical applications. *Journal of the american chemical society* **2015,** *137* (6), 2140-2154.

85. Peer, D.; Karp, J. M.; Hong, S.; Farokhzad, O. C.; Margalit, R.; Langer, R., Nanocarriers as an emerging platform for cancer therapy. *Nature nanotechnology* **2007,** *2* (12), 751.

86. Gong, J.; Chen, M.; Zheng, Y.; Wang, S.; Wang, Y., Polymeric micelles drug delivery system in oncology. *Journal of Controlled Release* **2012,** *159* (3), 312-323.

87. Deng, C.; Jiang, Y.; Cheng, R.; Meng, F.; Zhong, Z., Biodegradable polymeric

micelles for targeted and controlled anticancer drug delivery: promises, progress and prospects. *Nano Today* **2012,** *7* (5), 467-480.

88. Gabizon, A.; Martin, F., Polyethylene glycol-coated (pegylated) liposomal doxorubicin. *Drugs* **1997,** *54* (4), 15-21.

89. Kratz, F., Albumin as a drug carrier: design of prodrugs, drug conjugates and nanoparticles. *Journal of controlled release* **2008,** *132* (3), 171-183.

90. Chen, W.; Meng, F.; Li, F.; Ji, S.-J.; Zhong, Z., pH-responsive biodegradable micelles based on acid-labile polycarbonate hydrophobe: synthesis and triggered drug release. *Biomacromolecules* **2009,** *10* (7), 1727-1735.

91. Langer, R.; Peppas, N., Chemical and physical structure of polymers as carriers for controlled release of bioactive agents: a review. *Journal of Macromolecular Science-Reviews in Macromolecular Chemistry and Physics* **1983,** *23* (1), 61-126.

92. Varelas, C. G.; Dixon, D. G.; Steiner, C. A., Zero-order release from biphasic polymer hydrogels. *Journal of controlled release* **1995,** *34* (3), 185-192.

93. Costa, P.; Lobo, J. M. S., Modeling and comparison of dissolution profiles. *European journal of pharmaceutical sciences* **2001,** *13* (2), 123-133.

94. Washington, C., Drug release from microdisperse systems: a critical review. *International Journal of Pharmaceutics* **1990,** *58* (1), 1-12.

95. Peppas, N. A.; Narasimhan, B., Mathematical models in drug delivery: How modeling has shaped the way we design new drug delivery systems. *Journal of Controlled Release* **2014,** *190*, 75-81.

96. Grassi, M.; Grassi, G., Mathematical modelling and controlled drug delivery: matrix systems. *Current drug delivery* **2005,** *2* (1), 97-116.

97. Ramteke, K.; Dighe, P.; Kharat, A.; Patil, S., Mathematical models of drug dissolution: a review. *Sch. Acad. J. Pharm* **2014,** *3* (5), 388-396.

98. Bruschi, M. L., *Strategies to modify the drug release from pharmaceutical systems*. Woodhead Publishing: 2015.

99. Higuchi, T., Rate of release of medicaments from ointment bases containing drugs in suspension. *Journal of pharmaceutical sciences* **1961,** *50* (10), 874-875.

100. Higuchi, T., Mechanism of sustained-action medication. Theoretical analysis of

rate of release of solid drugs dispersed in solid matrices. *Journal of pharmaceutical sciences* **1963,** *52* (12), 1145-1149.

101.   Shaikh, H. K.;   Kshirsagar, R.; Patil, S., Mathematical models for drug release characterization: a review. *World J. Pharm. Pharm. Sci* **2015,** *4* (4), 324-338.

102.   Dash, S.;   Murthy, P. N.;   Nath, L.; Chowdhury, P., Kinetic modeling on drug release from controlled drug delivery systems. *Acta Pol Pharm* **2010,** *67* (3), 217-23.

103.   Hixson, A.; Crowell, J., Dependence of reaction velocity upon surface and agitation. *Industrial & Engineering Chemistry* **1931,** *23* (8), 923-931.

104.   Costa, P., An alternative method to the evaluation of similarity factor in dissolution testing. *International journal of pharmaceutics* **2001,** *220* (1-2), 77-83.

105.   Karimi, M.;   Sahandi Zangabad, P.;   Ghasemi, A.;   Amiri, M.;   Bahrami, M.;   Malekzad, H.;   Ghahramanzadeh Asl, H.;   Mahdieh, Z.;   Bozorgomid, M.; Ghasemi, A., Temperature-responsive smart nanocarriers for delivery of therapeutic agents: applications and recent advances. *ACS applied materials & interfaces* **2016,** *8* (33), 21107-21133.

106.   Nakayama, M.;   Okano, T.;   Miyazaki, T.;   Kohori, F.;   Sakai, K.;   Yokoyama, M., Molecular design of biodegradable polymeric micelles for temperature-responsive drug release. *Journal of Controlled Release* **2006,** *115* (1), 46-56.

107.   Sun, J. T.;   Yu, Z. Q.;   Hong, C. Y.; Pan, C. Y., Biocompatible zwitterionic sulfobetaine copolymer-coated mesoporous silica nanoparticles for temperature-responsive drug release. *Macromolecular rapid communications* **2012,** *33* (9), 811-818.

108.   Forgac, M., Vacuolar ATPases: rotary proton pumps in physiology and pathophysiology. *Nature reviews Molecular cell biology* **2007,** *8* (11), 917-929.

109.   Felber, A. E.;   Dufresne, M.-H.; Leroux, J.-C., pH-sensitive vesicles, polymeric micelles, and nanospheres prepared with polycarboxylates. *Advanced drug delivery reviews* **2012,** *64* (11), 979-992.

110. Gillies, R. J.;   Schomack, P. A.;   Secomb, T. W.; Raghunand, N., Causes and effects of heterogeneous perfusion in tumors. *Neoplasia* **1999,** *1* (3), 197-207.

111. Liu, Y.;   Wang, W.;   Yang, J.;   Zhou, C.; Sun, J., pH-sensitive polymeric micelles triggered drug release for extracellular and intracellular drug targeting delivery. *asian*

journal of pharmaceutical sciences **2013,** *8* (3), 159-167.

112. Kanamala, M.; Wilson, W. R.; Yang, M.; Palmer, B. D.; Wu, Z., Mechanisms and biomaterials in pH-responsive tumour targeted drug delivery: a review. *Biomaterials* **2016,** *85*, 152-167.

113. Zhou, Z.; Li, L.; Yang, Y.; Xu, X.; Huang, Y., Tumor targeting by pH-sensitive, biodegradable, cross-linked N-(2-hydroxypropyl) methacrylamide copolymer micelles. *Biomaterials* **2014,** *35* (24), 6622-6635.

114. Cao, Z.; Li, Q.; Wang, G., Photodegradable polymer nanocapsules fabricated from dimethyldiethoxysilane emulsion templates for controlled release. *Polymer Chemistry* **2017,** *8* (44), 6817-6823.

115. Wajs, E.; Nielsen, T. T.; Larsen, K. L.; Fragoso, A., Preparation of stimuli-responsive nano-sized capsules based on cyclodextrin polymers with redox or light switching properties. *Nano Research* **2016,** *9* (7), 2070-2078.

116. Jiang, J.; Tong, X.; Morris, D.; Zhao, Y., Toward photocontrolled release using light-dissociable block copolymer micelles. *Macromolecules* **2006,** *39* (13), 4633-4640.

117. Kawano, T.; Niidome, Y.; Mori, T.; Katayama, Y.; Niidome, T., PNIPAM gel-coated gold nanorods for targeted delivery responding to a near-infrared laser. *Bioconjugate chemistry* **2009,** *20* (2), 209-212.

118. Bawa, P.; Pillay, V.; Choonara, Y. E.; Du Toit, L. C., Stimuli-responsive polymers and their applications in drug delivery. *Biomedical materials* **2009,** *4* (2), 022001.

119. Wei, M.; Gao, Y.; Li, X.; Serpe, M. J., Stimuli-responsive polymers and their applications. *Polymer Chemistry* **2017,** *8* (1), 127-143.

120. Hwang, G. H.; Min, K. H.; Lee, H. J.; Nam, H. Y.; Choi, G. H.; Kim, B. J.; Jeong, S. Y.; Lee, S. C., pH-Responsive robust polymer micelles with metal–ligand coordinated core cross-links. *Chemical Communications* **2014,** *50* (33), 4351-4353.

121. Heskins, M.; Guillet, J. E., Solution properties of poly (N-isopropylacrylamide). *Journal of Macromolecular Science—Chemistry* **1968,** *2* (8), 1441-1455.

122. Mura, S.; Nicolas, J.; Couvreur, P., Stimuli-responsive nanocarriers for drug delivery. *Nature materials* **2013,** *12* (11), 991-1003.

123. Zhang, Y.; Carvalho, W. S.; Fang, C.; Serpe, M. J., Volatile organic

compound vapor detection with responsive microgel-based etalons. *Sensors and Actuators B: Chemical* **2019,** *290*, 520-526.

124.   Kim, H. J.; Matsuda, H.; Zhou, H.; Honma, I., Ultrasound-triggered smart drug release from a poly (dimethylsiloxane)–mesoporous silica composite. *Advanced Materials* **2006,** *18* (23), 3083-3088.

125.   Sahoo, B.; Devi, K. S. P.; Banerjee, R.; Maiti, T. K.; Pramanik, P.; Dhara, D., Thermal and pH responsive polymer-tethered multifunctional magnetic nanoparticles for targeted delivery of anticancer drug. *ACS applied materials & interfaces* **2013,** *5* (9), 3884-3893.

126.   Ge, J.; Neofytou, E.; Cahill III, T. J.; Beygui, R. E.; Zare, R. N., Drug release from electric-field-responsive nanoparticles. *ACS nano* **2012,** *6* (1), 227-233.

127.   Dong, L.; Agarwal, A. K.; Beebe, D. J.; Jiang, H., Adaptive liquid microlenses activated by stimuli-responsive hydrogels. *Nature* **2006,** *442* (7102), 551-554.

128.   Zhang, J.; Yuan, Z.-F.; Wang, Y.; Chen, W.-H.; Luo, G.-F.; Cheng, S.-X.; Zhuo, R.-X.; Zhang, X.-Z., Multifunctional envelope-type mesoporous silica nanoparticles for tumor-triggered targeting drug delivery. *Journal of the American Chemical Society* **2013,** *135* (13), 5068-5073.

129.   Horcajada, P.; Serre, C.; Vallet-Regí, M.; Sebban, M.; Taulelle, F.; Férey, G., Metal–organic frameworks as efficient materials for drug delivery. *Angewandte Chemie International Edition* **2006,** *45* (36), 5974-5978.

130.   Nadrah, P.; Maver, U.; Jemec, A.; Tišler, T.; Bele, M.; Dražić, G.; Benčina, M.; Pintar, A.; Planinšek, O.; Gaberšček, M., Hindered disulfide bonds to regulate release rate of model drug from mesoporous silica. *ACS applied materials & interfaces* **2013,** *5* (9), 3908-3915.

131.   Zhang, J.; Pelton, R., Poly (N-isopropylacrylamide) microgels at the air− water interface. *Langmuir* **1999,** *15* (23), 8032-8036.

132.   Li, J.; Nagamani, C.; Moore, J. S., Polymer mechanochemistry: from destructive to productive. *Accounts of chemical research* **2015,** *48* (8), 2181-2190.

133.   Caruso, M. M.; Davis, D. A.; Shen, Q.; Odom, S. A.; Sottos, N. R.;

White, S. R.; Moore, J. S., Mechanically-induced chemical changes in polymeric materials. *Chemical reviews* **2009,** *109* (11), 5755-5798.

134. May, P. A.; Munaretto, N. F.; Hamoy, M. B.; Robb, M. J.; Moore, J. S., Is molecular weight or degree of polymerization a better descriptor of ultrasound-induced mechanochemical transduction? *ACS Macro Letters* **2016,** *5* (2), 177-180.

135. Davis, D. A.; Hamilton, A.; Yang, J.; Cremar, L. D.; Van Gough, D.; Potisek, S. L.; Ong, M. T.; Braun, P. V.; Martínez, T. J.; White, S. R., Force-induced activation of covalent bonds in mechanoresponsive polymeric materials. *Nature* **2009,** *459* (7243), 68-72.

136. Zhang, Y.; Yu, J.; Bomba, H. N.; Zhu, Y.; Gu, Z., Mechanical force-triggered drug delivery. *Chemical reviews* **2016,** *116* (19), 12536-12563.

137. Xiong, B.; Huang, Z.; Zou, H.; Qiao, C.; He, Y.; Yeung, E. S., Single plasmonic nanosprings for visualizing reactive-oxygen-species-activated localized mechanical force transduction in live cells. *ACS nano* **2017,** *11* (1), 541-548.

138. González-Domínguez, J. M.; Martín, C.; Durá, O. s. J.; Merino, S.; Vázquez, E., Smart hybrid graphene hydrogels: A study of the different responses to mechanical stretching stimulus. *ACS applied materials & interfaces* **2018,** *10* (2), 1987-1995.

139. Wang, J.; Kaplan, J. A.; Colson, Y. L.; Grinstaff, M. W., Stretch-induced drug delivery from superhydrophobic polymer composites: use of crack propagation failure modes for controlling release rates. *Angewandte Chemie International Edition* **2016,** *55* (8), 2796-2800.

140. Okada, Y.; Tanaka, F., Cooperative hydration, chain collapse, and flat LCST behavior in aqueous poly (N-isopropylacrylamide) solutions. *Macromolecules* **2005,** *38* (10), 4465-4471.

141. Kujawa, P.; Winnik, F. M., Volumetric studies of aqueous polymer solutions using pressure perturbation calorimetry: A new look at the temperature-induced phase transition of poly (N-isopropylacrylamide) in water and D2O. *Macromolecules* **2001,** *34* (12), 4130-4135.

142. Gao, Y.; Xu, W.; Serpe, M. J., Free-standing poly (N-isopropylacrylamide)

microgel-based etalons. *Journal of Materials Chemistry C* **2014,** *2* (29), 5878-5884.

143.   Karg, M.;   Lu, Y.;   Carbó-Argibay, E.;   Pastoriza-Santos, I.;   Pérez-Juste, J.; Liz-Marzán, L. M.; Hellweg, T., Multiresponsive hybrid colloids based on gold nanorods and poly (NIPAM-co-allylacetic acid) microgels: temperature-and pH-tunable plasmon resonance. *Langmuir* **2009,** *25* (5), 3163-3167.

144.   Guo, S.;   Gao, Y.;   Wei, M.;   Zhang, Q. M.; Serpe, M. J., Controlled release kinetics from a surface modified microgel-based reservoir device. *Journal of Materials Chemistry B* **2015,** *3* (12), 2516-2521.

145.   Islam, M. R.; Serpe, M. J., Polyelectrolyte mediated intra and intermolecular crosslinking in microgel-based etalons for sensing protein concentration in solution. *Chemical Communications* **2013,** *49* (26), 2646-2648.

146.   Hu, L.; Serpe, M. J., Controlling the response of color tunable poly (N-isopropylacrylamide)   microgel-based   etalons   with   hysteresis.   *Chemical Communications* **2013,** *49* (26), 2649-2651.

147.   Wang, J.;   Rivas, G.;   Jiang, M.; Zhang, X., Electrochemically induced release of DNA from gold ultramicroelectrodes. *Langmuir* **1999,** *15* (19), 6541-6545.

148.   Wang, J.;   Jiang, M.; Mukherjee, B., On-demand electrochemical release of DNA from gold surfaces. *Bioelectrochemistry* **2000,** *52* (1), 111-114.

149.   Xu, W.;   Zhang, Y.;   Gao, Y.; Serpe, M. J., Electrically triggered small molecule release from poly (n-isopropylacrylamide-co-acrylic acid) microgel-modified electrodes. *ACS applied materials & interfaces* **2018,** *10* (15), 13124-13129.

150.   Sorrell, C. D.; Serpe, M. J., Reflection order selectivity of color-tunable poly (N-isopropylacrylamide) microgel based etalons. *Advanced materials* **2011,** *23* (35), 4088-4092.

151.   Sorrell, C. D.;   Carter, M. C.; Serpe, M. J., A "paint-on" protocol for the facile assembly of uniform microgel coatings for color tunable etalon fabrication. *ACS applied materials & interfaces* **2011,** *3* (4), 1140-1147.

152.   Li, X.; Serpe, M. J., Understanding the Shape Memory Behavior of Self-Bending Materials and Their Use as Sensors. *Advanced Functional Materials* **2016,** *26* (19), 3282-3290.

153.   Wong, W. S.; Gutruf, P.; Sriram, S.; Bhaskaran, M.; Wang, Z.; Tricoli, A., Strain Engineering of Wave-like Nanofibers for Dynamically Switchable Adhesive/Repulsive Surfaces. *Advanced Functional Materials* **2016,** *26* (3), 399-407.

154.   Carter, M. C.; Sorrell, C. D.; Serpe, M. J., Deswelling kinetics of color tunable poly (N-isopropylacrylamide) microgel-based etalons. *The Journal of Physical Chemistry B* **2011,** *115* (49), 14359-14368.

155.   Karimi, M.; Ghasemi, A.; Zangabad, P. S.; Rahighi, R.; Basri, S. M. M.; Mirshekari, H.; Amiri, M.; Pishabad, Z. S.; Aslani, A.; Bozorgomid, M., Smart micro/nanoparticles in stimulus-responsive drug/gene delivery systems. *Chemical Society Reviews* **2016,** *45* (5), 1457-1501.

156.   Stuart, M. A. C.; Huck, W. T.; Genzer, J.; Müller, M.; Ober, C.; Stamm, M.; Sukhorukov, G. B.; Szleifer, I.; Tsukruk, V. V.; Urban, M., Emerging applications of stimuli-responsive polymer materials. *Nature materials* **2010,** *9* (2), 101-113.

157.   Shen, Y.; Fu, X.; Fu, W.; Li, Z., Biodegradable stimuli-responsive polypeptide materials prepared by ring opening polymerization. *Chemical Society Reviews* **2015,** *44* (3), 612-622.

158.   Zhang, Q. M.; Wang, W.; Su, Y.-Q.; Hensen, E. J.; Serpe, M. J., Biological imaging and sensing with multiresponsive microgels. *Chemistry of Materials* **2016,** *28* (1), 259-265.

159.   Carling, C.-J.; Viger, M. L.; Huu, V. A. N.; Garcia, A. V.; Almutairi, A., In vivo visible light-triggered drug release from an implanted depot. *Chemical science* **2015,** *6* (1), 335-341.

160.   De Koker, S.; Hoogenboom, R.; De Geest, B. G., Polymeric multilayer capsules for drug delivery. *Chemical Society Reviews* **2012,** *41* (7), 2867-2884.

161.   Zhao, Y.; Lv, L.-P.; Jiang, S.; Landfester, K.; Crespy, D., Advanced stimuli-responsive polymer nanocapsules with enhanced capabilities for payloads delivery. *Polymer Chemistry* **2015,** *6* (23), 4197-4205.

162.   Zhao, Z.; Zhu, F.; Qu, X.; Wu, Q.; Wang, Q.; Zhang, G.; Liang, F., pH-Responsive polymeric Janus containers for controlled drug delivery. *Polymer*

Chemistry **2015,** *6* (22), 4144-4153.

163.   Liu, F.;   Kozlovskaya, V.;   Medipelli, S.;   Xue, B.;   Ahmad, F.;   Saeed, M.; Cropek, D.; Kharlampieva, E., Temperature-sensitive polymersomes for controlled delivery of anticancer drugs. *Chemistry of Materials* **2015,** *27* (23), 7945-7956.

164.   Islam, M. R.;   Irvine, J.; Serpe, M. J., Photothermally induced optical property changes of poly (N-isopropylacrylamide) microgel-based etalons. *ACS applied materials & interfaces* **2015,** *7* (43), 24370-24376.

165.   Lv, L.-P.;   Zhao, Y.;   Vilbrandt, N.;   Gallei, M.;   Vimalanandan, A.; Rohwerder, M.;   Landfester, K.; Crespy, D., Redox responsive release of hydrophobic self-healing agents from polyaniline capsules. *Journal of the American Chemical Society* **2013,** *135* (38), 14198-14205.

166.   Huang, F.;   Liao, W.-C.;   Sohn, Y. S.;   Nechushtai, R.;   Lu, C.-H.; Willner, I., Light-responsive and pH-responsive DNA microcapsules for controlled release of loads. *Journal of the American Chemical Society* **2016,** *138* (28), 8936-8945.

167.   Smeets, N. M.; Hoare, T., Designing responsive microgels for drug delivery applications. *Journal of Polymer Science Part A: Polymer Chemistry* **2013,** *51* (14), 3027-3043.

168.   Oh, J. K.;   Drumright, R.;   Siegwart, D. J.; Matyjaszewski, K., The development of microgels/nanogels for drug delivery applications. *Progress in Polymer Science* **2008,** *33* (4), 448-477.

169.   Guan, Y.; Zhang, Y., PNIPAM microgels for biomedical applications: from dispersed particles to 3D assemblies. *Soft Matter* **2011,** *7* (14), 6375-6384.

170.   Jiang, J.;   Tong, X.; Zhao, Y., A new design for light-breakable polymer micelles. *Journal of the American Chemical Society* **2005,** *127* (23), 8290-8291.

171.   Yang, L.;   Sun, H.;   Liu, Y.;   Hou, W.;   Yang, Y.;   Cai, R.;   Cui, C.; Zhang, P.;   Pan, X.; Li, X., Self-Assembled Aptamer-Grafted Hyperbranched Polymer Nanocarrier for Targeted and Photoresponsive Drug Delivery. *Angewandte Chemie* **2018,** *130* (52), 17294-17298.

172.   Otto, P.;   Bergmann, S.;   Sandmeyer, A.;   Dirksen, M.;   Wrede, O.; Hellweg, T.; Huser, T., Resolving the internal morphology of core–shell microgels with

super-resolution fluorescence microscopy. *Nanoscale Advances* **2020**.

173.   Fomina, N.; McFearin, C.; Sermsakdi, M.; Edigin, O.; Almutairi, A., UV and near-IR triggered release from polymeric nanoparticles. *Journal of the American Chemical Society* **2010,** *132* (28), 9540-9542.

174.   Yan, B.; Boyer, J.-C.; Branda, N. R.; Zhao, Y., Near-infrared light-triggered dissociation of block copolymer micelles using upconverting nanoparticles. *Journal of the American Chemical Society* **2011,** *133* (49), 19714-19717.

175.   Dong, H.; Du, H.; Qian, X., Theoretical prediction of p K a values for methacrylic acid oligomers using combined quantum mechanical and continuum solvation methods. *The Journal of Physical Chemistry A* **2008,** *112* (49), 12687-12694.

176.   Ma, X.; Xi, J.; Huang, X.; Zhao, X.; Tang, X., Novel hydrophobically modified temperature-sensitive microgels with tunable volume-phase transition temperature. *Materials Letters* **2004,** *58* (27-28), 3400-3404.

177.   WooáLee, C.; JunáPark, B., Sweat pore mapping using a fluorescein–polymer composite film for fingerprint analysis. *Chemical Communications* **2015,** *51* (15), 3177-3180.

178.   Wang, L.-T.; Ting, C.-H.; Yen, M.-L.; Liu, K.-J.; Sytwu, H.-K.; Wu, K. K.; Yen, B. L., Human mesenchymal stem cells (MSCs) for treatment towards immune-and inflammation-mediated diseases: review of current clinical trials. *Journal of biomedical science* **2016,** *23* (1), 76.

179.   Bruder, S. P.; Kurth, A. A.; Shea, M.; Hayes, W. C.; Jaiswal, N.; Kadiyala, S., Bone regeneration by implantation of purified, culture-expanded human mesenchymal stem cells. *Journal of orthopaedic research* **1998,** *16* (2), 155-162.

180.   Reichert, J. C.; Epari, D. R.; Wullschleger, M. E.; Saifzadeh, S.; Steck, R.; Lienau, J.; Sommerville, S.; Dickinson, I. C.; Schütz, M. A.; Duda, G. N., Establishment of a preclinical ovine model for tibial segmental bone defect repair by applying bone tissue engineering strategies. *Tissue Engineering Part B: Reviews* **2010,** *16* (1), 93-104.

181.   Huang, G.; Li, F.; Zhao, X.; Ma, Y.; Li, Y.; Lin, M.; Jin, G.; Lu, T. J.; Genin, G. M.; Xu, F., Functional and biomimetic materials for engineering of the

three-dimensional cell microenvironment. *Chemical reviews* **2017,** *117* (20), 12764-12850.

182. Santo, V. E.; Gomes, M. E.; Mano, J. F.; Reis, R. L., Controlled release strategies for bone, cartilage, and osteochondral engineering—part I: recapitulation of native tissue healing and variables for the design of delivery systems. *Tissue Engineering Part B: Reviews* **2013,** *19* (4), 308-326.

183. Shimer, A. L.; Öner, F. C.; Vaccaro, A. R., Spinal reconstruction and bone morphogenetic proteins: open questions. *Injury* **2009,** *40*, S32-S38.

184. Urist, M. R.; DeLange, R. J.; Finerman, G., Bone cell differentiation and growth factors. *Science* **1983,** *220* (4598), 680-686.

185. Comer, G. C.; Smith, M. W.; Hurwitz, E. L.; Mitsunaga, K. A.; Kessler, R.; Carragee, E. J., Retrograde ejaculation after anterior lumbar interbody fusion with and without bone morphogenetic protein-2 augmentation: a 10-year cohort controlled study. *The Spine Journal* **2012,** *12* (10), 881-890.

186. Chen, Y.; Li, J.; Kawazoe, N.; Chen, G., Preparation of dexamethasone-loaded calcium phosphate nanoparticles for the osteogenic differentiation of human mesenchymal stem cells. *Journal of Materials Chemistry B* **2017,** *5* (33), 6801-6810.

187. Raida, M.; Clement, J. H.; Leek, R. D.; Ameri, K.; Bicknell, R.; Niederwieser, D.; Harris, A. L., Bone morphogenetic protein 2 (BMP-2) and induction of tumor angiogenesis. *Journal of cancer research and clinical oncology* **2005,** *131* (11), 741-750.

188. Kim, M.-J.; Lee, B.; Yang, K.; Park, J.; Jeon, S.; Um, S. H.; Kim, D.-I.; Im, S. G.; Cho, S.-W., BMP-2 peptide-functionalized nanopatterned substrates for enhanced osteogenic differentiation of human mesenchymal stem cells. *Biomaterials* **2013,** *34* (30), 7236-7246.

189. Beauvais, S.; Drevelle, O.; Lauzon, M.-A.; Daviau, A.; Faucheux, N., Modulation of MAPK signalling by immobilized adhesive peptides: Effect on stem cell response to BMP-9-derived peptides. *Acta biomaterialia* **2016,** *31*, 241-251.

190. Koehler, K. C.; Alge, D. L.; Anseth, K. S.; Bowman, C. N., A Diels–Alder

modulated approach to control and sustain the release of dexamethasone and induce osteogenic differentiation of human mesenchymal stem cells. *Biomaterials* **2013,** *34* (16), 4150-4158.

191.   Ghali, O.;   Broux, O.;   Falgayrac, G.;   Haren, N.;   van Leeuwen, J. P.; Penel, G.;   Hardouin, P.; Chauveau, C., Dexamethasone in osteogenic medium strongly induces adipocyte differentiation of mouse bone marrow stromal cells and increases osteoblast differentiation. *BMC cell biology* **2015,** *16* (1), 9.

192.   Kiefer, R.; Kreutzberg, G. W., Effects of dexamethasone on microglial activation in vivo: selective downregulation of major histocompatibility complex class II expression in regenerating facial nucleus. *Journal of neuroimmunology* **1991,** *34* (2-3), 99-108.

193.   Bensiamar, F.;   Olalde, B.;   Cifuentes, S. C.;   Argarate, N.;   Atorrasagasti, G.;   González-Carrasco, J. L.;   García-Rey, E.;   Vilaboa, N.; Saldaña, L., Bioactivity of dexamethasone-releasing coatings on polymer/magnesium composites. *Biomedical Materials* **2016,** *11* (5), 055011.

194.   Wadhwa, R.;   Lagenaur, C. F.; Cui, X. T., Electrochemically controlled release of dexamethasone from conducting polymer polypyrrole coated electrode. *Journal of controlled release* **2006,** *110* (3), 531-541.

195.   Nanda, H. S.;   Nakamoto, T.;   Chen, S.;   Cai, R.;   Kawazoe, N.; Chen, G., Collagen microgel-assisted dexamethasone release from PLLA-collagen hybrid scaffolds of controlled pore structure for osteogenic differentiation of mesenchymal stem cells. *Journal of Biomaterials Science, Polymer Edition* **2014,** *25* (13), 1374-1386.

196.   Qi, H.;   Chen, Q.;   Ren, H.;   Wu, X.;   Liu, X.; Lu, T., Electrophoretic deposition of dexamethasone-loaded gelatin nanospheres/chitosan coating and its dual function in anti-inflammation and osteogenesis. *Colloids and Surfaces B: Biointerfaces* **2018,** *169*, 249-256.

197.   Wang, Q.;   Wang, J.;   Lu, Q.;   Detamore, M. S.; Berkland, C., Injectable PLGA based colloidal gels for zero-order dexamethasone release in cranial defects. *Biomaterials* **2010,** *31* (18), 4980-4986.

198.   Qiu, K.;   Chen, B.;   Nie, W.;   Zhou, X.;   Feng, W.;   Wang, W.;   Chen, L.; Mo, X.;   Wei, Y.; He, C., Electrophoretic deposition of dexamethasone-loaded

mesoporous silica nanoparticles onto poly (L-lactic acid)/poly (ε-caprolactone) composite scaffold for bone tissue engineering. *ACS applied materials & interfaces* **2016,** *8* (6), 4137-4148.

199.　Lin, Z.-Y.;　Duan, Z.-X.;　Guo, X.-D.;　Li, J.-F.;　Lu, H.-W.;　Zheng, Q.-X.; Quan, D.-P.; Yang, S.-H., Bone induction by biomimetic PLGA-(PEG-ASP) n copolymer loaded with a novel synthetic BMP-2-related peptide in vitro and in vivo. *Journal of Controlled Release* **2010,** *144* (2), 190-195.

200.　Zhang, Y.;　Gao, Y.;　Carvalho, W. S.;　Fang, C.; Serpe, M. J., Microgel-Based Stretchable Reservoir Devices for Elongation Enhanced Small Molecule Release Rate. *ACS Applied Materials & Interfaces* **2020,** *12* (16), 19062-19068.

201.　Klinger, D.; Landfester, K., Dual stimuli-responsive poly (2-hydroxyethyl methacrylate-co-methacrylic acid) microgels based on photo-cleavable cross-linkers: pH-dependent swelling and light-induced degradation. *Macromolecules* **2011,** *44* (24), 9758-9772.

202.　Rejman, J.;　Oberle, V.;　Zuhorn, I. S.; Hoekstra, D., Size-dependent internalization of particles via the pathways of clathrin-and caveolae-mediated endocytosis. *Biochemical journal* **2004,** *377* (1), 159-169.

203.　Sahay, G.;　Alakhova, D. Y.; Kabanov, A. V., Endocytosis of nanomedicines. *Journal of controlled release* **2010,** *145* (3), 182-195.

204.　Il'ichev, Y. V.;　Schwörer, M. A.; Wirz, J., Photochemical reaction mechanisms of 2-nitrobenzyl compounds: methyl ethers and caged ATP. *Journal of the American Chemical Society* **2004,** *126* (14), 4581-4595.

205.　Griffin, D. R.; Kasko, A. M., Photodegradable macromers and hydrogels for live cell encapsulation and release. *Journal of the American chemical society* **2012,** *134* (31), 13103-13107.

206.　Ruskowitz, E. R.; DeForest, C. A., Proteome-wide analysis of cellular response to ultraviolet light for biomaterial synthesis and modification. *ACS Biomaterials Science & Engineering* **2019,** *5* (5), 2111-2116.

207.　Pittenger, M. F.;　Mackay, A. M.;　Beck, S. C.;　Jaiswal, R. K.;　Douglas, R.; Mosca, J. D.;　Moorman, M. A.;　Simonetti, D. W.;　Craig, S.; Marshak, D. R.,

Multilineage potential of adult human mesenchymal stem cells. *science* **1999,** *284* (5411), 143-147.

208.   Zhou, X.; Feng, W.; Qiu, K.; Chen, L.; Wang, W.; Nie, W.; Mo, X.; He, C., BMP-2 derived peptide and dexamethasone incorporated mesoporous silica nanoparticles for enhanced osteogenic differentiation of bone mesenchymal stem cells. *ACS applied materials & interfaces* **2015,** *7* (29), 15777-15789.

209.   Langenbach, F.; Handschel, J., Effects of dexamethasone, ascorbic acid and β-glycerophosphate on the osteogenic differentiation of stem cells in vitro. *Stem cell research & therapy* **2013,** *4* (5), 117.

210.   Colson, Y. L.; Grinstaff, M. W., Biologically responsive polymeric nanoparticles for drug delivery. *Advanced Materials* **2012,** *24* (28), 3878-3886.

211. Zhai, L., Stimuli-responsive polymer films. *Chemical Society Reviews* **2013,** *42* (17), 7148-7160.

212.   Liu, G.;   Liu, W.; Dong, C.-M., UV-and NIR-responsive polymeric nanomedicines for on-demand drug delivery. *Polymer Chemistry* **2013,** *4* (12), 3431-3443.

213.   Cheng, R.;   Meng, F.;   Deng, C.;   Klok, H.-A.; Zhong, Z., Dual and multi-stimuli responsive polymeric nanoparticles for programmed site-specific drug delivery. *Biomaterials* **2013,** *34* (14), 3647-3657.

214.   El-Sawy, H. S.;   Al-Abd, A. M.;   Ahmed, T. A.;   El-Say, K. M.; Torchilin, V. P., Stimuli-responsive nano-architecture drug-delivery systems to solid tumor micromilieu: past, present, and future perspectives. *ACS nano* **2018,** *12* (11), 10636-10664.

215.   Lu, C.; Urban, M. W., Stimuli-responsive polymer nano-science: Shape anisotropy, responsiveness, applications. *Progress in Polymer Science* **2018,** *78*, 24-46.

216.   Qu, Y.;   Chu, B.;   Wei, X.;   Lei, M.;   Hu, D.;   Zha, R.;   Zhong, L.; Wang, M.;   Wang, F.; Qian, Z., Redox/pH dual-stimuli responsive camptothecin prodrug nanogels for "on-demand" drug delivery. *Journal of controlled release* **2019,** *296*, 93-106.

217.   Dash, M.;   Chiellini, F.;   Ottenbrite, R. M.; Chiellini, E., Chitosan—A

versatile semi-synthetic polymer in biomedical applications. *Progress in polymer science* **2011,** *36* (8), 981-1014.

218. Rodrigues, S.; Dionísio, M.; López, C. R.; Grenha, A., Biocompatibility of chitosan carriers with application in drug delivery. *Journal of functional biomaterials* **2012,** *3* (3), 615-641.

219. Ghosh, B.; Urban, M. W., Self-repairing oxetane-substituted chitosan polyurethane networks. *Science* **2009,** *323* (5920), 1458-1460.

220. Grenha, A., Chitosan nanoparticles: a survey of preparation methods. *Journal of drug targeting* **2012,** *20* (4), 291-300.

221. Yu, S.; Zhang, X.; Tan, G.; Tian, L.; Liu, D.; Liu, Y.; Yang, X.; Pan, W., A novel pH-induced thermosensitive hydrogel composed of carboxymethyl chitosan and poloxamer cross-linked by glutaraldehyde for ophthalmic drug delivery. *Carbohydrate polymers* **2017,** *155*, 208-217.

222. Poon, L.; Wilson, L. D.; Headley, J. V., Chitosan-glutaraldehyde copolymers and their sorption properties. *Carbohydrate polymers* **2014,** *109*, 92-101.

223. Warburg, O., On the origin of cancer cells. *Science* **1956,** *123* (3191), 309-314.

224. Bours, M.; Swennen, E.; Di Virgilio, F.; Cronstein, B.; Dagnelie, P., Adenosine 5′-triphosphate and adenosine as endogenous signaling molecules in immunity and inflammation. *Pharmacology & therapeutics* **2006,** *112* (2), 358-404.

225. Mo, R.; Jiang, T.; Gu, Z., Enhanced anticancer efficacy by ATP-mediated liposomal drug delivery. *Angewandte Chemie International Edition* **2014,** *53* (23), 5815-5820.

226. Chen, W. H.; Liao, W. C.; Sohn, Y. S.; Fadeev, M.; Cecconello, A.; Nechushtai, R.; Willner, I., Stimuli-Responsive Nucleic Acid-Based Polyacrylamide Hydrogel-Coated Metal–Organic Framework Nanoparticles for Controlled Drug Release. *Advanced Functional Materials* **2018,** *28* (8), 1705137.

227. Knowles, J. R., Enzyme-catalyzed phosphoryl transfer reactions. *Annual review of biochemistry* **1980,** *49* (1), 877-919.

228. Gorman, M. W.; Feigl, E. O.; Buffington, C. W., Human plasma ATP concentration. *Clinical chemistry* **2007,** *53* (2), 318-325.

229.   Wang, H.;   Feng, Z.;   Qin, Y.;   Wang, J.; Xu, B., Nucleopeptide assemblies selectively sequester ATP in cancer cells to increase the efficacy of doxorubicin. *Angewandte Chemie* **2018,** *130* (18), 5025-5029.

230.   Kang, Y.;   Wang, C.;   Liu, K.;   Wang, Z.; Zhang, X., Enzyme-responsive polymeric supra-amphiphiles formed by the complexation of chitosan and ATP. *Langmuir* **2012,** *28* (41), 14562-14566.

231.   Sutirman, Z. A.;   Sanagi, M. M.;   Karim, K. J. A.; Ibrahim, W. A. W., Preparation of methacrylamide-functionalized crosslinked chitosan by free radical polymerization for the removal of lead ions. *Carbohydrate polymers* **2016,** *151*, 1091-1099.

232.   Unsoy, G.;   Khodadust, R.;   Yalcin, S.;   Mutlu, P.; Gunduz, U., Synthesis of Doxorubicin loaded magnetic chitosan nanoparticles for pH responsive targeted drug delivery. *European Journal of Pharmaceutical Sciences* **2014,** *62*, 243-250.

233.   Wang, X.;   Chen, Y.;   Dahmani, F. Z.;   Yin, L.;   Zhou, J.; Yao, J., Amphiphilic carboxymethyl chitosan-quercetin conjugate with P-gp inhibitory properties for oral delivery of paclitaxel. *Biomaterials* **2014,** *35* (26), 7654-7665.

234.   Ye, Z.;   Guo, J.;   Wu, D.;   Tan, M.;   Xiong, X.;   Yin, Y.; He, G., Photo-responsive shell cross-linked micelles based on carboxymethyl chitosan and their application in controlled release of pesticide. *Carbohydrate polymers* **2015,** *132*, 520-528.

235.   Mo, R.;   Jiang, T.;   DiSanto, R.;   Tai, W.; Gu, Z., ATP-triggered anticancer drug delivery. *Nature communications* **2014,** *5* (1), 1-10.

236.   Biswas, S.;   Kinbara, K.;   Niwa, T.;   Taguchi, H.;   Ishii, N.;   Watanabe, S.;   Miyata, K.;   Kataoka, K.; Aida, T., Biomolecular robotics for chemomechanically driven guest delivery fuelled by intracellular ATP. *Nature chemistry* **2013,** *5* (7), 613.

237.   Bell, O. A.;   Wu, G.;   Haataja, J. S.;   Brömmel, F.;   Fey, N.;   Seddon, A. M.;   Harniman, R. L.;   Richardson, R. M.;   Ikkala, O.; Zhang, X., Self-assembly of a functional oligo (aniline)-based amphiphile into helical conductive nanowires. *Journal of the American Chemical Society* **2015,** *137* (45), 14288-14294.

238.   Maman, S.; Witz, I. P., A history of exploring cancer in context. *Nature Reviews*

Drug Discovery **2018,** *17* (3), 13-30.

239. Bailey, R. C.; Hupp, J. T., Micropatterned polymeric gratings as chemoresponsive volatile organic compound sensors: implications for analyte detection and identification via diffraction-based sensor arrays. *Analytical chemistry* **2003,** *75* (10), 2392-2398.

240. Kesselmeier, J.; Staudt, M., Biogenic volatile organic compounds (VOC): an overview on emission, physiology and ecology. *Journal of atmospheric chemistry* **1999,** *33* (1), 23-88.

241. Tuet, W. Y.; Chen, Y.; Xu, L.; Fok, S.; Gao, D.; Weber, R. J.; Ng, N. L., Chemical oxidative potential of secondary organic aerosol (SOA) generated from the photooxidation of biogenic and anthropogenic volatile organic compounds. *Atmospheric Chemistry & Physics* **2017,** *17* (2).

242. Atkinson, R.; Arey, J., Gas-phase tropospheric chemistry of biogenic volatile organic compounds: a review. *Atmospheric Environment* **2003,** *37*, 197-219.

243. Duan, J.; Tan, J.; Yang, L.; Wu, S.; Hao, J., Concentration, sources and ozone formation potential of volatile organic compounds (VOCs) during ozone episode in Beijing. *Atmospheric Research* **2008,** *88* (1), 25-35.

244. Elosua, C.; Matias, I. R.; Bariain, C.; Arregui, F. J., Volatile organic compound optical fiber sensors: A review. *Sensors* **2006,** *6* (11), 1440-1465.

245. Kida, T.; Harano, H.; Minami, T.; Kishi, S.; Morinaga, N.; Yamazoe, N.; Shimanoe, K., Control of electrode reactions in a mixed-potential-type gas sensor based on a BiCuVOx solid electrolyte. *The Journal of Physical Chemistry C* **2010,** *114* (35), 15141-15148.

246. Tian, K.; Hu, D.; Hu, R.; Wang, S.; Li, S.; Li, Y.; Yang, G., Multiple fluorescence ΔCIE and ΔRGB codes for sensing volatile organic compounds with a wide range of responses. *Chemical Communications* **2011,** *47* (36), 10052-10054.

247. Yoon, J.; Chae, S. K.; Kim, J.-M., Colorimetric sensors for volatile organic compounds (VOCs) based on conjugated polymer-embedded electrospun fibers. *Journal of the American Chemical Society* **2007,** *129* (11), 3038-3039.

248. Wang, X.; Sun, X.; Hu, P. A.; Zhang, J.; Wang, L.; Feng, W.; Lei, S.;

Yang, B.; Cao, W., Colorimetric sensor based on self-assembled Polydiacetylene/graphene-stacked composite film for vapor-phase volatile organic compounds. *Advanced Functional Materials* **2013,** *23* (48), 6044-6050.

249.   Wang, Q.; Yang, Z.; Zhang, X.; Xiao, X.; Chang, C. K.; Xu, B., A supramolecular-hydrogel-encapsulated hemin as an artificial enzyme to mimic peroxidase. *Angewandte Chemie International Edition* **2007,** *46* (23), 4285-4289.

250.   Kim, E.; Kim, D.; Jung, H.; Lee, J.; Paul, S.; Selvapalam, N.; Yang, Y.; Lim, N.; Park, C. G.; Kim, K., Facile, template-free synthesis of stimuli-responsive polymer nanocapsules for targeted drug delivery. *Angewandte Chemie International Edition* **2010,** *49* (26), 4405-4408.

251.   Hoare, T.; Pelton, R., Engineering glucose swelling responses in poly (N-isopropylacrylamide)-based microgels. *Macromolecules* **2007,** *40* (3), 670-678.

252.   Jones, C. D.; Lyon, L. A., Shell-restricted swelling and core compression in poly (N-isopropylacrylamide) core− shell microgels. *Macromolecules* **2003,** *36* (6), 1988-1993.

253.   Brugger, B.; Richtering, W., Magnetic, thermosensitive microgels as stimuli-responsive emulsifiers allowing for remote control of separability and stability of oil in water-emulsions. *Advanced Materials* **2007,** *19* (19), 2973-2978.

254.   Xu, W.; Gao, Y.; Serpe, M. J., Electrochemically color tunable poly (N-isopropylacrylamide) microgel-based etalons. *Journal of Materials Chemistry C* **2014,** *2* (20), 3873-3878.

255.   Gao, Y.; Serpe, M. J., Light-induced color changes of microgel-based etalons. *ACS applied materials & interfaces* **2014,** *6* (11), 8461-8466.

256.   Reichardt, C.; Welton, T., *Solvents and solvent effects in organic chemistry*. John Wiley & Sons: 2011.

257.   Winnik, F. M.; Ottaviani, M. F.; Bossmann, S. H.; Pan, W.; Garcia-Garibay, M.; Turro, N. J., Cononsolvency of poly (N-isopropylacrylamide): a look at spin-labeled polymers in mixtures of water and tetrahydrofuran. *Macromolecules* **1993,** *26* (17), 4577-4585.

258.   Yu, Y.; de la Cruz, R. A. L.; Kieviet, B. D.; Gojzewski, H.; Pons, A.;

Vancso, G. J.; de Beer, S., Pick up, move and release of nanoparticles utilizing co-non-solvency of PNIPAM brushes. *Nanoscale* **2017,** *9* (4), 1670-1675.

259.   Phipps, J.; Richardson, R.; Cosgrove, T.; Eaglesham, A., Neutron reflection studies of copolymers at the hexane/water interface. *Langmuir* **1993,** *9* (12), 3530-3537.

260.   Porter, T. L.; Eastman, M. P.; Pace, D. L.; Bradley, M., Polymer-based materials to be used as the active element in microsensors: A scanning force microscopy study. *Scanning* **2000,** *22* (5), 304-309.

261.   Karthaus, O.; Maruyama, N.; Cieren, X.; Shimomura, M.; Hasegawa, H.; Hashimoto, T., Water-assisted formation of micrometer-size honeycomb patterns of polymers. *Langmuir* **2000,** *16* (15), 6071-6076.

Appendix A: Alkaline Environment Triggered Drug Release from Poly(N-isopropylacrylamide-co-3-(trimethoxysilyl)propyl methacrylate) Microgels

In some body tissues, such as duodenum and intestinal tract, they are in an alkaline environment, and the increased alkalinity can lead to metabolic alkalosis which has severe symptoms, the alkaline environment triggered drug release is of particular interest. However, the utilization of alkaline environment as an external stimulus to control drug release from microgels is less studied. In this project, we synthesized novel alkaline-responsive poly(*N*-isopropylacrylamide-*co*-3-(trimethoxysilyl)propyl methacrylate) (pNIPAm-*co*-TMSPMA) microgels using free radical precipitation polymerization. The morphology, size and alkaline-responsive properties of our microgels were characterized by transmission electron microscopy (TEM) and dynamic light scattering (DLS) respectively. Finally, we showed that our pNIPAm-*co*-TMSPMA microgels can promote the release of preloaded model drug (Rhodamine B) in the alkaline environment.
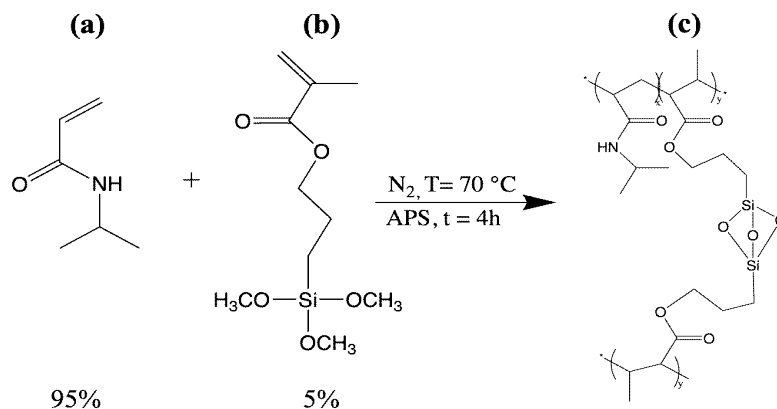
Figure A1. Synthesis of pNIPAm-*co*-TMSPMA microgels. NIPAm (a) and TMSPMA (b), were copolymerized to yield pNIPAm-*co*-TMSPMA microgels (c)
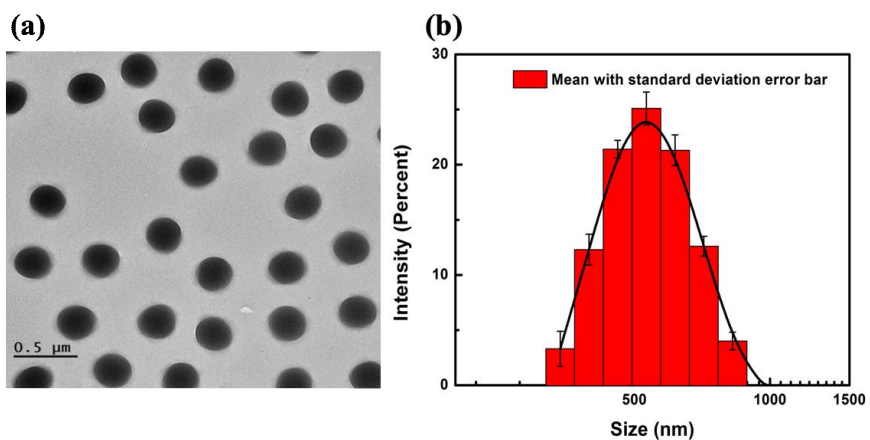

Figure A2. TEM image (a) and DLS measurement (b) of pNIPAm-*co*-TMSPMA microgels

Table A1. Size variation of pNIPAm-*co*-TMSPMA microgels under different concentrations of NaOH

Concentration of NaOH (M)	Size of pNIPAm-*co*-TMSPMA microgels, in average diameter (nm)	Poly dispersity index (PDI)
0	568.7	0.070
0.04	681.6	0.100
0.1	803.4	0.270
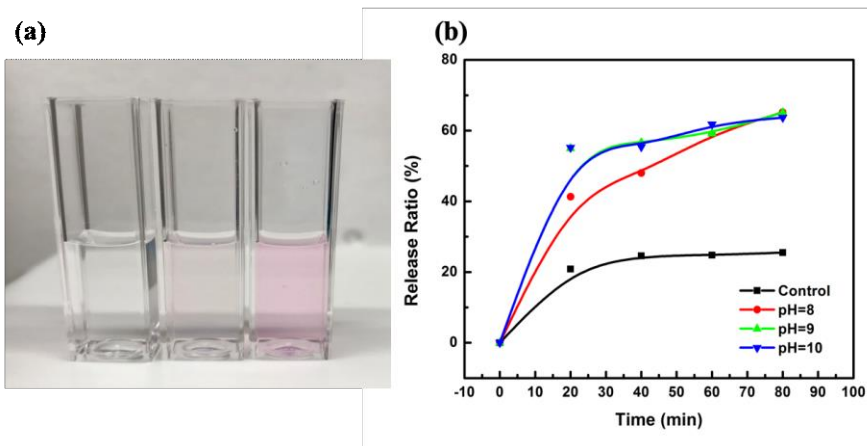
Figure A3. (a) Photographic image of supernatant of the centrifuged RhB-loaded microgel. Left: blank (DI water only). Middle: control (after reaction with DI water). Right: after reaction with pH=8 NaOH solution. (b) Cumulative release profiles of RhB from the pNIPAm-*co*-TMSPMA microgels at different time.

Appendix B: Photo-cleavable crosslinkers based microgels for drug delivery

In light of photo-responsive monomer based polymers, photo-crosslinker based polymers have also attracted considerable interests due to their unique advantages in practical applications such as fast response, well-controlled, and no byproducts formation during the polymerization. In this project, two photo-cleavable crosslinkers that were 1,10-(4,40-(4,40-(Ethane-1,2-diylbis(azanediyl))bis(4-oxobutane-4,1-diyl))bis(oxy)bis(5-methoxy-2-nitro-4,1-phenylene))-bis(ethane-1,1-diyl)bis(acrylate) (PCL-1) and PEG500-methacrylate-4-(4-(1-acryloyloxyethyl)-2-methoxy-5-nitrophenoxy)butanoate (PCL-2) were synthesized, and their corresponding photo-degradable pNIPAm-based microgels were developed using free radical precipitation polymerization. The photo-cleavable behaviors of photo-crosslinkers and thermo-responsive properties were characterized by UV-Visible spectroscopy and dynamic light scattering (DLS), respectively. The size, morphology and structure of the prepared microgels were characterised by transmission electron microscopy (TEM). The model drug fluorescein was loaded into the microgels and the release of loaded drug was investigated by fluorescence spectroscopy. We found that our microgels are dual-stimuli responsive and

the release of fluorescein can be achieved in a controlled manner by either light or heat. Since it is known that the stimuli-responsive polymer of pNIPAm and the photodegradation products of *o*-nitrobenzyl-ester derivatives are biocompatible, we envision that our photo-cleavable pNIPAm-based microgels have a great potential in the field of biomedical applications such as controlled drug delivery.
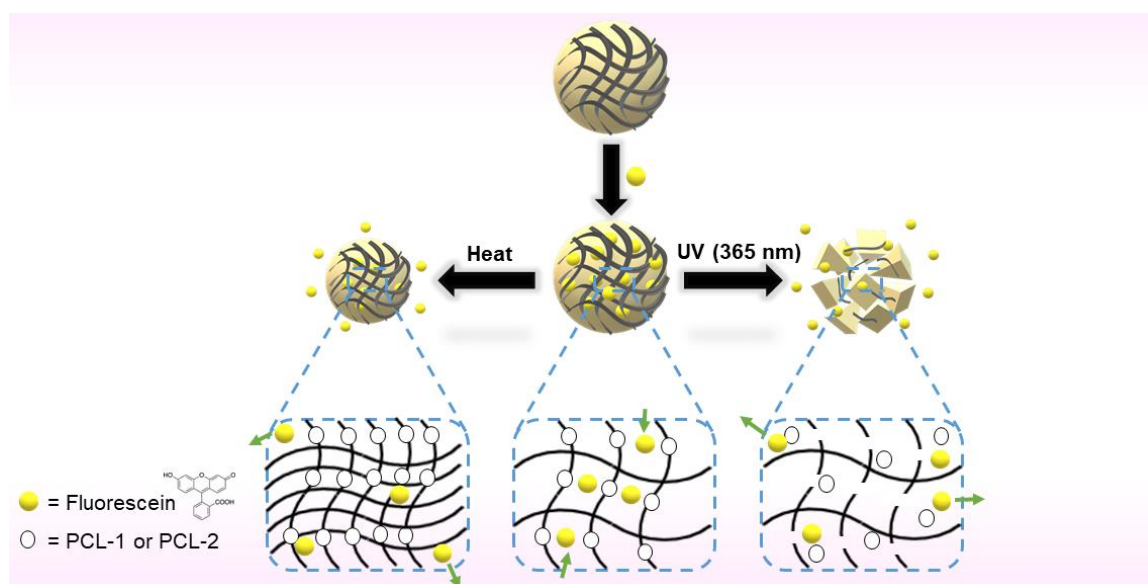
Scheme B1. Schematic of the dual stimuli (UV-light and temperature) triggered release of fluorescein molecules (drug) loaded PCL-1 and PCL-2 based microgels
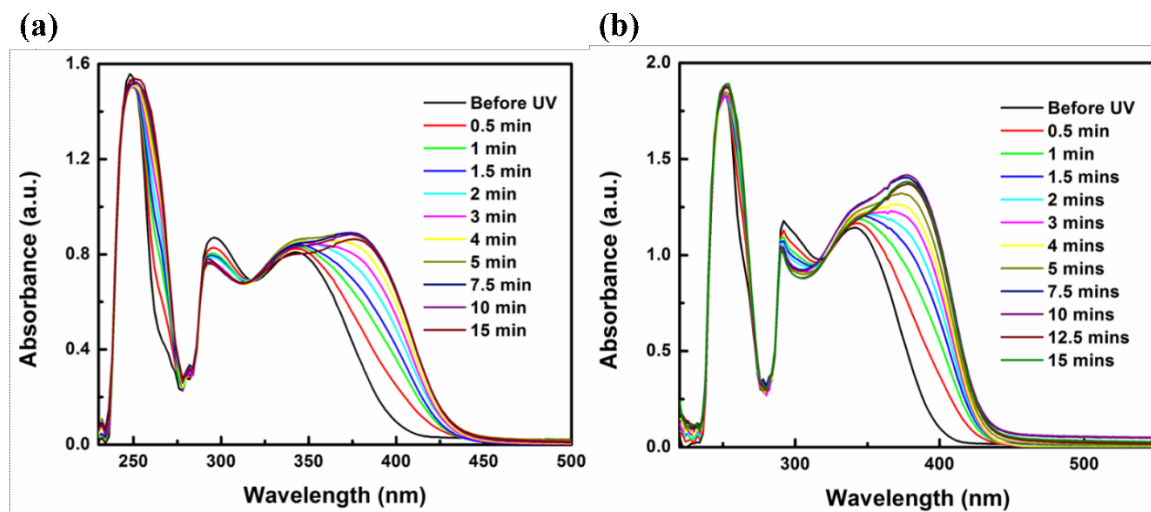
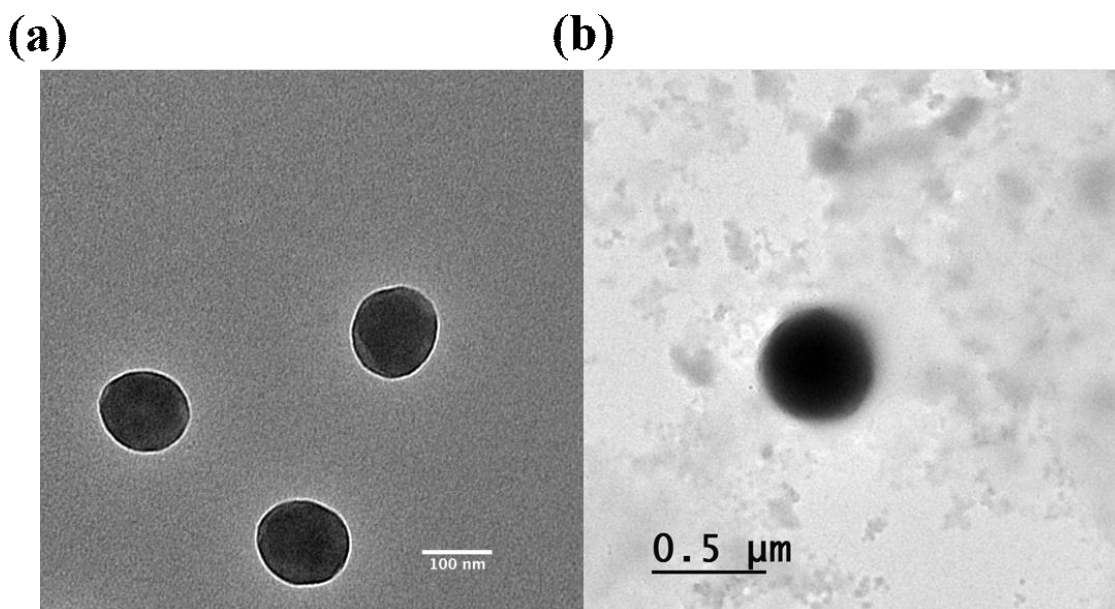**Figure B1**. Photodegradation studies of PCL-1 (a) and PCL-2 (b)

Figure B2. TEM images of PCL-1 based microgels (a) and PCL-2 based microgels (b)
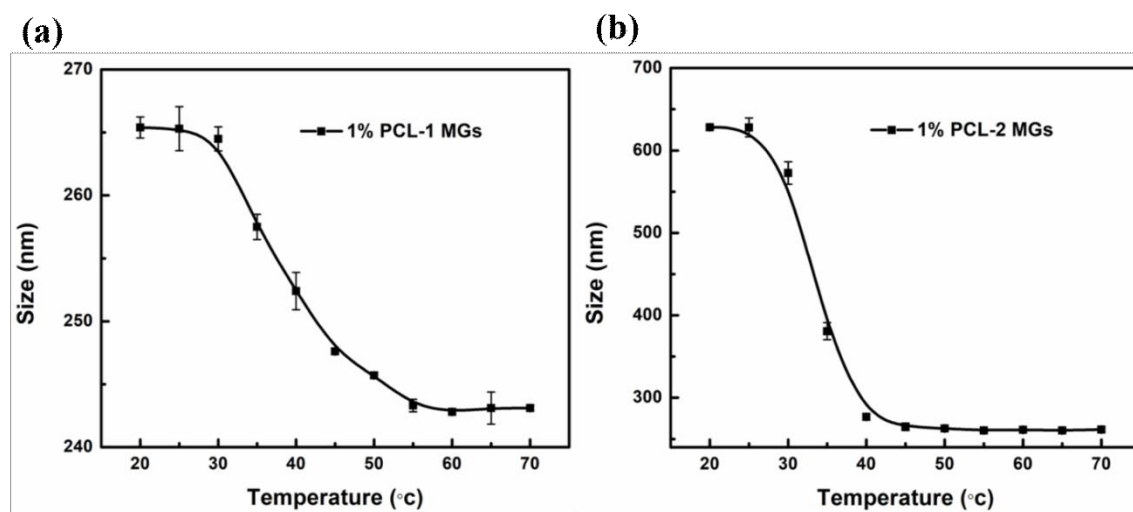
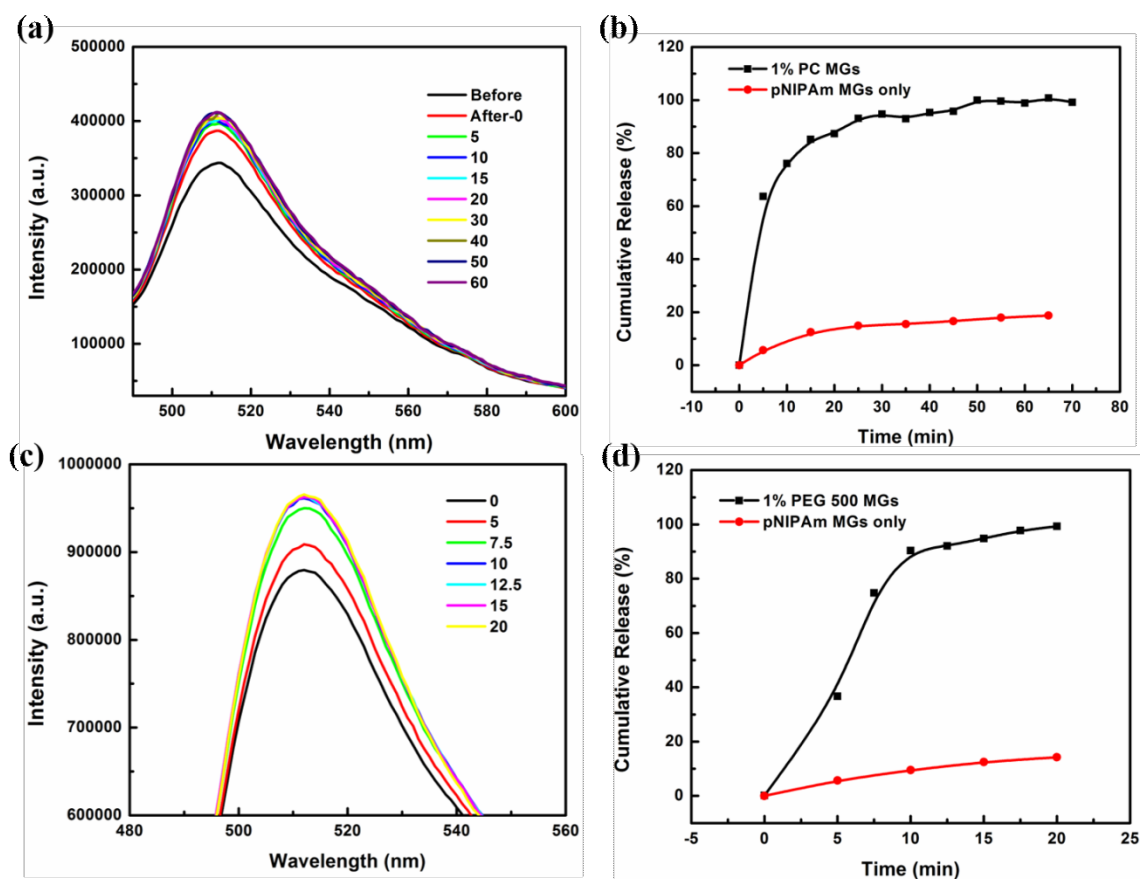**Figure B3.** Temperature-responsive properties of PCL-1 based microgels (a) and PCL-2 based microgels (b)

Figure B4. (a) and (c) Fluorescence emission spectra (λ_{ex} = 510 nm) of fluorescein

loaded in the PCL-1 and PCL-2 based microgels without and with UV irradiation (365 nm), respectively. Each profile was represented by fluorescent intensity of the sample as a function of time. (b) and (d) Cumulative release profiles of fluorescein from the prepared PCL-1 microgels at different time, respectively.
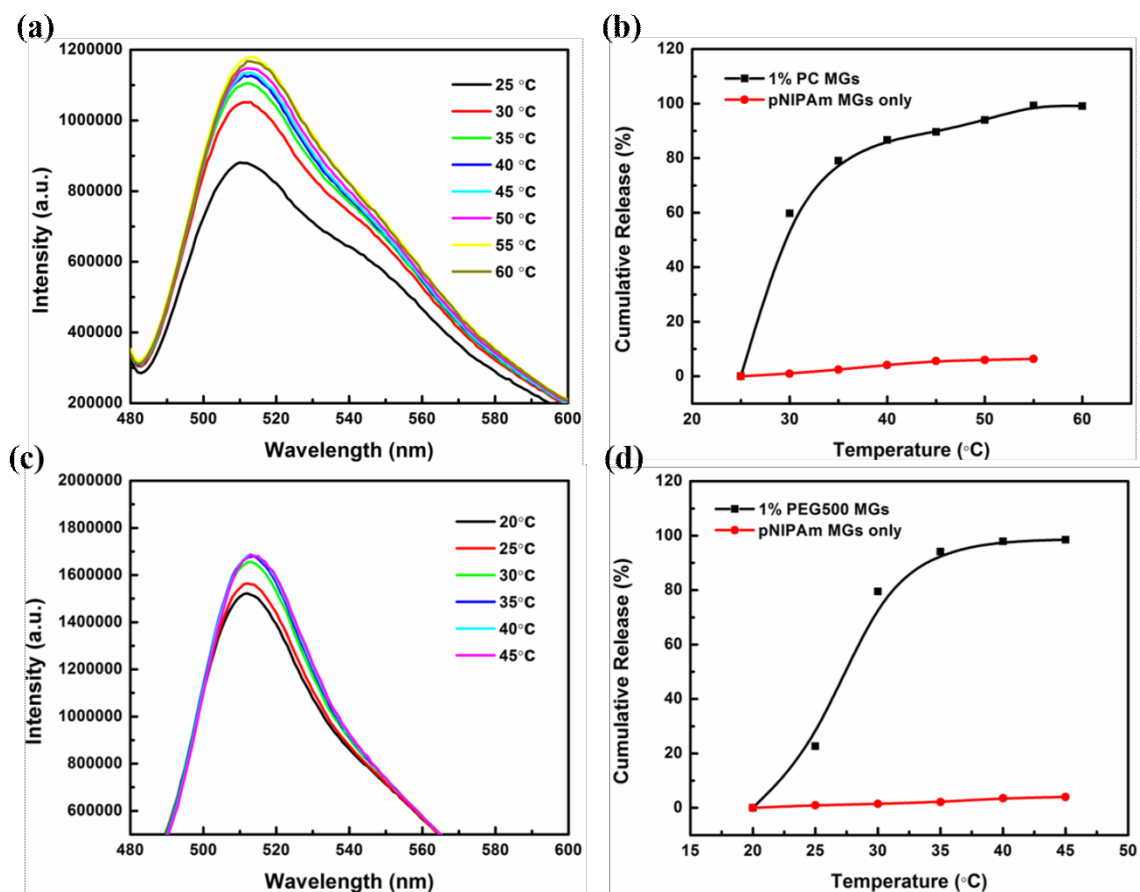

Figure B5. (a) and (c) Fluorescence emission spectra (λ_{ex} = 510 nm) of fluorescein loaded in the PCL-1 and PCL-2 based microgels with different temperatures, respectively. (b) and (d) Cumulative release profiles of fluorescein from the prepared pNIPAm-*co*-NBMA microgels at different temperatures.